Forschungsbericht 2022-27

Determination of the Measurement Errors for the HALO Basic Data System BAHAMAS by Means of Error Propagation

Andreas Giez, Martin Zöger, Christian Mallaun, Vladyslav Nenakhov, Marina Schimpf, Christoph Grad, Andreas Numberger, Kevin Raynor

Deutsches Zentrum für Luft- und Raumfahrt
Flugexperimente
Oberpfaffenhofen

Deutsches Zentrum
DLR für Luft- und Raumfahrt

Forschungsbericht 2022-27

Determination of the Measurement Errors for the HALO Basic Data System BAHAMAS by Means of Error Propagation

Andreas Giez, Martin Zöger, Christian Mallaun, Vladyslav Nenakhov, Marina Schimpf, Christoph Grad, Andreas Numberger, Kevin Raynor

Deutsches Zentrum für Luft- und Raumfahrt
Flugexperimente
Oberpfaffenhofen

97 Seiten
51 Bilder
5 Tabellen
13 Literaturstellen

DLR Deutsches Zentrum für Luft- und Raumfahrt

Herausgeber:

Deutsches Zentrum
für Luft- und Raumfahrt e. V.
Wissenschaftliche Information
Linder Höhe
D-51147 Köln

ISSN 1434-8454
ISRN DLR-FB-2022-27
Erscheinungsjahr 2022

DOI: https://doi.org/10.57676/5rdc-q708

Fehlerrechnung, Fehlerbetrachtung, Forschungsflugzeug, meteorologische Basisdaten, Atmosphärendaten, Flugzeugmessungen, Nasenmast, flugzeuggetragene Windmessung, Druck, Temperatur, Strömungsmessung

Andreas Giez, Martin Zöger, Christian Mallaun, Vladyslav Nenakhov, Marina Schimpf,
Christoph Grad, Andreas Numberger, Kevin Raynor
DLR, Flugexperimente, Oberpfaffenhofen

Determination of the Measurement Errors for the HALO Basic Data System BAHAMAS by Means of Error Propagation

Der Forschungsbericht beschreibt die Bestimmung der Messfehler für die meteorologischen Basisdaten des Atmosphären-Forschungsflugzeugs HALO. Diese Daten werden von der vom DLR entwickelten Basismessanlage BAHAMAS erfasst.

Die Fehleranalyse basiert auf einer Fehlerfortpflanzungs-Methode, bei der auf die originalen Messdaten ein künstliches weißes Rauschsignal aufsetzt wird, das auf diese Weise die gesamte Datenverarbeitung durchläuft. Die Fehlerrechnung umfasst sowohl statistische Messfehler in den originalen Rohdaten als auch systematischen Fehlerbeiträge in der Datenprozessierung, die durch Sensorkalibrierung, ungenaue Parametrisierungen von physikalischen Zusammenhängen oder Unsicherheiten aus Laborergebnissen herrühren. Die präsentierte Methode stellt eine echte Fehlerfortpflanzung da und basiert nicht auf Vereinfachungen oder Linearisierungs-Ansätzen wie bei einer klassischen Fehlerfortpflanzungsbetrachtung.

Das Dokument präsentiert und diskutiert alle bekannten Fehlerquellen für Basismessdaten auf HALO. Abschließend werden Ergebnisse dieser Fehleranalyse für typische Flugszenarien dargestellt und mögliche Ansatzpunkte für eine weitere Minimierung dieser Fehler diskutiert.

Error propagation, error analysis, atmospheric research aircraft, basic meteorological data, airborne wind measurement, aircraft data, nose boom, pressure, temperature, airflow measurement

(Published in English)

Andreas Giez, Martin Zöger, Christian Mallaun, Vladyslav Nenakhov, Marina Schimpf,
Christoph Grad, Andreas Numberger, Kevin Raynor
German Aerospace Center (DLR), Flight Experiments, Oberpfaffenhofen

Determination of the Measurement Errors for the HALO Basic Data System BAHAMAS by Means of Error Propagation

The document determines the measurement errors of basic meteorological data from the German atmospheric research aircraft HALO. The presented results are based on an error propagation method that uses artificial white noise which is added to the original data and which propagates through the complete air data calculation scheme. The error calculation covers statistical noise of the original raw data as well as all possible systematic error sources from sensor calibration, inaccurate parameterizations of physical relations and the uncertainties from laboratory investigations. The method represents a true error propagation which is not based on linearization or approximations in the data calculation scheme.

The document finally presents and analyses all known error sources for HALO aircraft data. It also provides a complete error analysis for typical HALO flight conditions and discusses the potential for further improvements of the data quality.

Abstract

The document determines the measurement errors of basic meteorological data from the German atmospheric research aircraft HALO. The presented results are based on an error propagation method that uses artificial white noise which is added to the original data and which propagates through the complete air data calculation scheme. The error calculation covers statistical noise of the original raw data as well as all possible systematic error sources from sensor calibration, inaccurate parameterizations of physical relations and the uncertainties from laboratory investigations. The method represents a true error propagation which is not based on linearization or approximations in the data calculation scheme.
The document finally presents and analyses all known error sources for HALO aircraft data. It also provides a complete error analysis for typical HALO flight conditions and discusses the potential for further improvements of the data quality.

Content

Abstract 1
Introduction 4
The Atmospheric Research Aircraft HALO 6
Processing of DLR Research Aircraft Data: RAMSES Software 7
Time Series Data 10
  Raw, Primary and Secondary Data 10
  The Undesired Contributions: Random Error and Systematic Errors 12
  Accuracy and Precision 14
  White Noise 17
    Properties of Random Noise 18
    Random Error Investigation: Autocorrelation and Power Spectrum 18
    Example: Real Aircraft Data 25
    Effect of Additional Input Errors on Secondary Data 26
    White Noise Propagation in Data Processing 27
  Systematic Errors 34
    Sensor 36
    Calibration 37
    Data Processing 39
    Error Investigation: Error Propagation Calculation 39
True Error Propagation: White Noise Method 41
  Basic Idea 41
  Possible Error Parameterizations 44
    Absolute Error 44
    Relative Error 45
    Error Dependence on Other Parameters 46
    Correlated Errors 47
  Implementation in RAMSES-II 48
Error Sources for HALO Aircraft Data 50
  Sensor/Instrument Errors 50

Pressure Sensors 50
Temperature Sensors 53
Humidity Sensors 56
Attitude and Speed Measurement 59
Processing/Parameterization Errors 63
Pressure: Static Source Error 63
Pressure: Flow Angle Dependence 64
Flow Angle 65
Flow Angle Dynamic Correction 67
Pressure: Flow Angle Dynamic Pressure Correction 69
Temperature: Recovery Correction and Deicing Error 71
Sensor Random Noise 75
Error Analysis for HALO BAHAMAS Data 76
Low Altitude 78
Mid Altitude 79
High Altitude 80
Influence of Heading Relatively to Wind Direction 81
Discussion 84
Result of error calculation 84
Possible Improvements 87
Pressure 87
Temperature 88
Flow 90
Summary 92
Acknowledgement 95
References 96

Introduction

Research aircraft represent an important contributor to the "toolbox" of atmospheric research. Their ability to access a large portion of the atmosphere in a very controlled manner which allows to precisely determine the exact location, time and in some cases even the desired meteorological conditions for a planned scientific investigation make the aircraft a first choice for many experiments in this field of research. Aircraft platforms allow for "in situ" measurements of atmospheric parameters or specific species with high spatial resolution when compared to a satellite. The possibility to access instruments inside the aircraft cabin during a measurement make the aircraft an ideal platform for testing new technologies and prototype instrumentation.
However, the calculation of air data for the free atmosphere from instrument data which is acquired inside the aircraft requires precise information about the thermodynamic parameters of the free atmosphere. The data processing typically needs temperature, pressure and air density data of the undisturbed air in the vicinity of the aircraft. Furthermore, the interpretation of the acquired data is greatly simplified by information about the associated air motion i.e. speed and direction of the wind with a high temporal resolution. Wind data is also needed to determine transport parameters like the flux of trace gases or kinetic energy.

None of these thermodynamic parameters can be measured directly on an aircraft because aerodynamic effects change air pressure, temperature and the flow field in the vicinity of the fuselage. Therefore, any measurement requires significant corrections in order to determine the desired parameters with an acceptable accuracy [6], [7].
Basic meteorological data is typically provided by the aircraft operator who is therefore also responsible to determine the necessary air data corrections. It is obvious that the quality of this basic data is critical to almost any unit which is measured by other instruments. In other words: the quality of basic meteorological data on a research aircraft limits the accuracy of almost every measurement taken

by the scientific instrument payload inside the cabin. This also means that information about the error of these parameters is an essential input for any instrument onboard.
However, due to the complex data processing scheme of basic meteorological data on an aircraft there is typically no precise (calculated) error data available and the provided information is usually based on rough estimations and major simplifications.

The Atmospheric Research Aircraft HALO

Figure 1*: The German atmospheric research aircraft HALO*

This investigation concerns the German atmospheric research aircraft HALO (High Altitude and LOng range research aircraft) which is shown in Figure 1. The aircraft and its instrumentation are described in detail in [11], [6] and [7].
HALO is operated by the German Aerospace Center (Deutsches Zentrum für Luft- und Raumfahrt, DLR) in the Flight Experiments Facility (FX). HALO home base is the research flight facility in Oberpfaffenhofen (Bavaria), one of two flight facilities (Oberpfaffenhofen and Braunschweig) inside FX. Part of this department is the "Instrumentation and Data Science Group" which is responsible for the basic scientific instrumentation, data acquisition and data processing on this aircraft. The basic aircraft and atmospheric data is measured by the Basic HALO Measurement and Data System (BAHAMAS), which was developed by this group.

Processing of DLR Research Aircraft Data: RAMSES Software

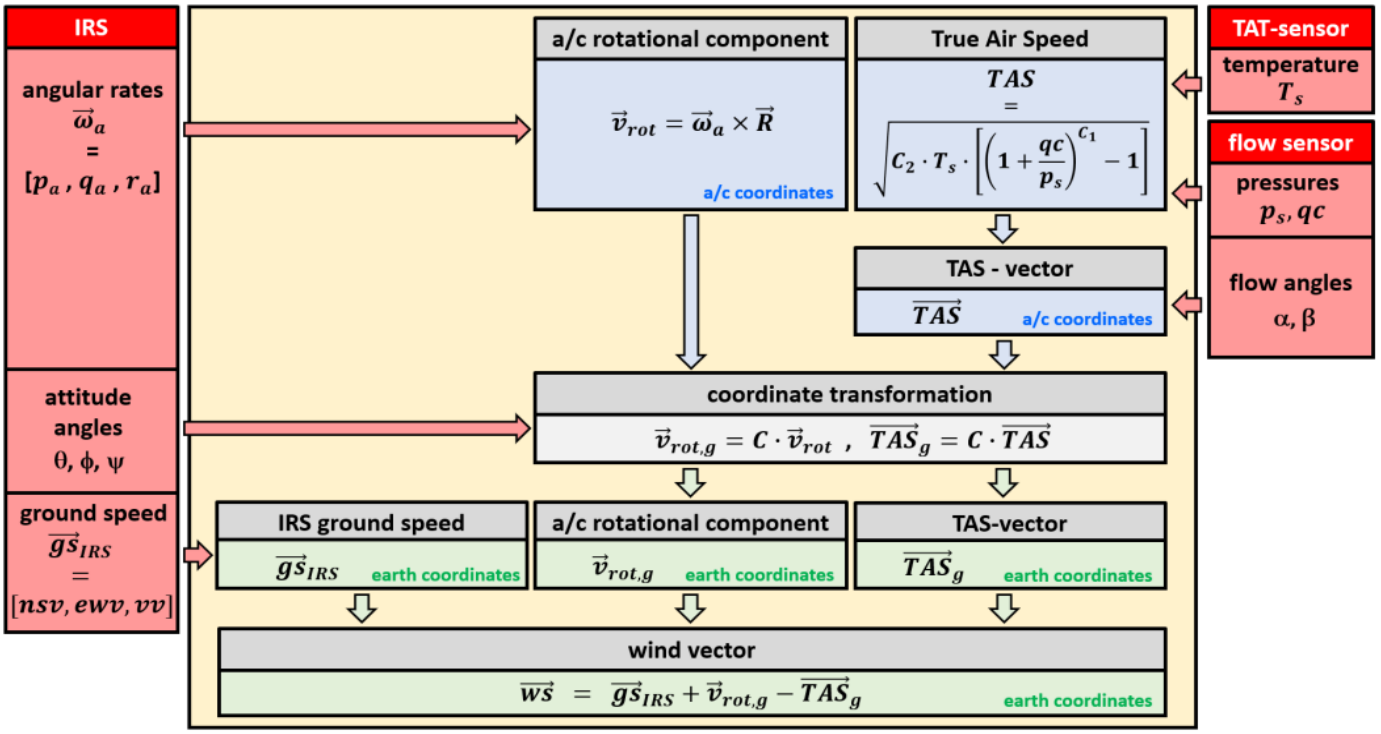

Figure 2*: Processing scheme for a general RAMSES software module which is used for all aircraft: Wind vector calculation (from [7]).*

HALO aircraft data is processed with a software package called RAMSES (Research Aircraft Meteorological Sensor data Evaluation Software) which is based on the programming software IDL (Interactive Data Language).
RAMSES uses data bases, is highly modular and has been developed by FX since 1996. Today, the software is used for all atmospheric research aircraft which are operated by FX in Oberpfaffenhofen.
The data evaluation of a single flight with RAMSES starts with unscaled raw data and uses a calibration data base and a large library of meteorological and thermodynamic routines.
The key processing parameters for each flight are also stored in a data base in order guarantee an identical processing even a long time after the first data evaluation. The data processing always follows a general workflow with specific

modules for each aircraft which consider individual aerodynamic corrections, different sensors or specific instrument configurations.

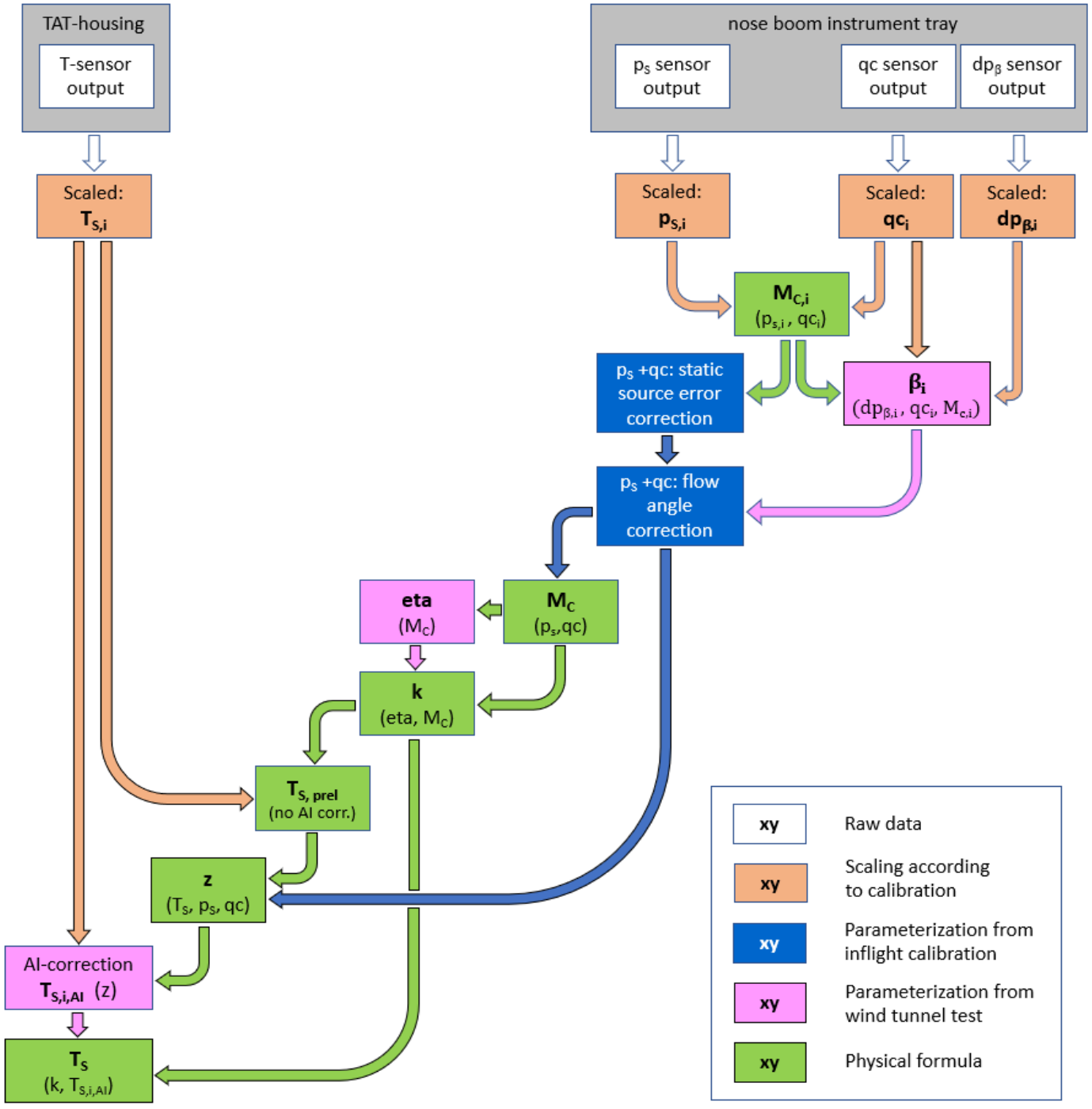

Figure 3: ***RAMSES workflow for the calculation of static air temperature. The blue modules represent aircraft specific routines.***

Figure 2 shows the workflow of a general RAMSES module which is used to calculate the atmospheric wind vector and which applies to all DLR aircraft. In contrast the calculation of static air temperature requires aircraft specific corrections in the pressure determination. Figure 3 shows where these modules appear in the processing of temperature data on HALO.

Time Series Data

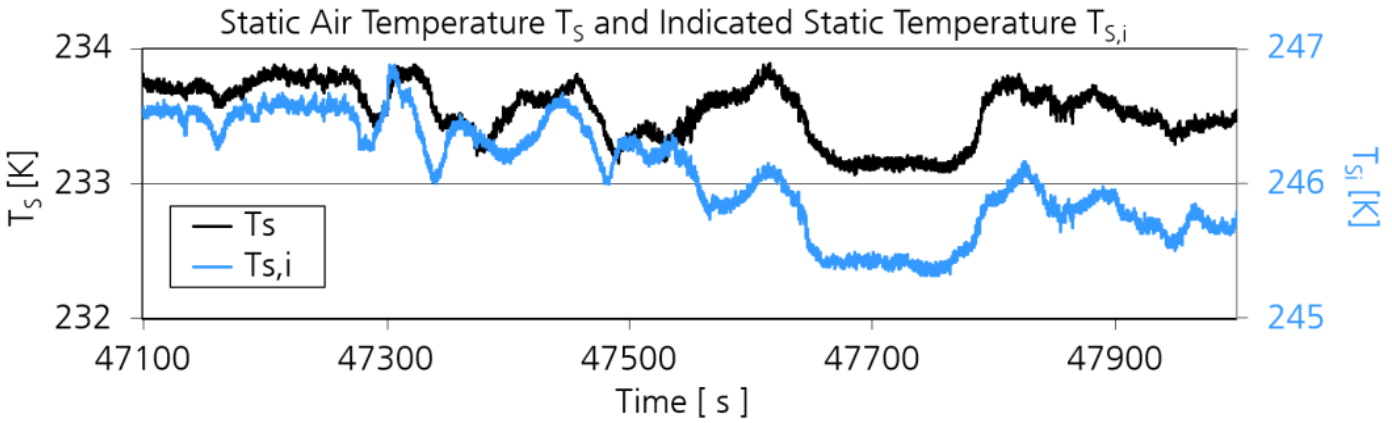

Figure 4*: Static air temperature T_S and indicated static air temperature $T_{S,i}$ time series from a HALO test flight on May 16th 2019. The offset of $T_{S,i}$ accounts for the temperature increase caused by the adiabatic heating in the Total Air Temperature (TAT) housing of the sensor.*

As an example, Figure 4 shows a time series of static air temperature T_S over a time interval of 15 minutes as calculated by RAMSES for a HALO test flight which took place on May 16th 2019 over Germany. The data is taken at a flight altitude (pressure height) of 7934m (359 hPa) and a mean True Air Speed of 163m/s (M_C=0.53). The time series has a time resolution of 10Hz.
From the shown time series it becomes immediately clear that it is impossible to distinguish between real atmospheric variation, statistical noise or the influence of changing flight parameters like aircraft altitude, attitude or speed on the data. The key to this analysis is the quantification of these contributions which requires a proper error analysis and the application of certain statistical tools.

Raw, Primary and Secondary Data

During the acquisition and processing of sensor signals on HALO the respective data is available at different processing levels. Therefore, it is common to use the following classification:

Raw Data

Raw data is the original sensor data, as collected by the data acquisition system. Raw data is not processed or even scaled in any way. Therefore, the unit of raw data in an analog system like BAHAMAS is typically "voltage". In case of the BAHAMAS temperature measurement the raw signal is the output of the analog signal conditioner which converts the resistance of a Platinium resistance temperature element (Pt100) into a DC voltage between 0 and 5 Volts. For digital sensors raw data might not be available at all.

Primary Data

Primary data is raw data which has been converted into physical units using a conversion scheme which was determined by means of a calibration. During the calibration of a temperature sensor the sensing element itself is exposed to an extremely well defined (i.e. homogeneous and very accurately controlled) temperature reference bath. The sensor signal is recorded and then used to generate a precise relation between sensor output and real temperature.

In an analogue system a complete calibration must include the data acquisition (i.e. the analogue to digital conversion). As a consequence, the calibration is very often a two-step process: HALO temperature calibration consists of (1) a temperature versus resistance calibration in the laboratory and (2) a resistance versus voltage calibration on the aircraft which includes the data acquisition system.

Primary data always describes the physical unit as measured directly by the sensor during flight. It represents the "local" or "indicated" value of this unit at the sensor. The indicated static temperature $T_{S,i}$ can also be seen in the example of Figure 4. $T_{S,i}$ is subject to the data processing scheme shown in Figure 3 which determines the T_S for the free atmosphere in the vicinity of the aircraft from the indicated values.

Secondary Data

All data which has been subject to data processing is called secondary data. An example is the static air temperature of the free atmosphere (T_S). It is calculated by RAMSES from the BAHAMAS raw data according to the processing scheme shown in Figure 3. Besides the scaling of raw data this process accounts for the aerodynamic and thermal properties of the sensor housing (Total Air Temperature Housing). It is obvious that every unit which is generated throughout the data processing is also classified as secondary data. Please note that the variance of $T_{S,i}$ in Figure 4 is larger than the variance of the real temperature T_S. This is due to the fact that some of the observed variations of $T_{S,i}$ are caused by changing flight parameters (mainly aircraft speed). This dependency is removed in the data processing.

The Undesired Contributions: Random Error and Systematic Errors

Different factors shape a secondary data time series like the one displayed in Figure 4. The final curve is the result of several inputs:

- The physical signal from the sensor itself is typically the dominant contribution to the final secondary data time series. In case of temperature the sensor raw data represents the real temperature variation as measured directly at the sensing element. It is important to note that raw data does not exclusively describe the atmospheric variance only, but also the influence of external parameters on the indicated unit such as aircraft speed, aircraft altitude or the anti-ice status of the temperature sensor housing. The data processing will later account for theses influences in order to determine the real temperature. Additionally, the raw signal can also be influenced by changes of instrument properties (like electronic drift effects) during the measurement.
- Any physical measurement is subject to statistical effects and a measurement signal always contains electronic random noise. If this noise contribution is in the same order of magnitude as the original raw data

variations the respective contribution will become visible in the data. Therefore, white noise is always part of real data, it only depends on the strength of the atmospheric variability whether it becomes visible or not.

- The raw data time series is subject to a significant data processing effort (as shown in Figure 3) which is necessary to determine the desired secondary data. It is clear that every unit and every formula which is used throughout this calculation will leave its "footprint" in the data and will also have an impact on the final secondary data time series.

The goal of any measurement is "realistic" secondary data i.e. data with minimum deviations from the undisturbed atmospheric values. However, from the above one can see that there are many factors which potentially generate deviations from the desired result.
The total error of secondary data can be divided into two categories which will be analyzed in detail in the following chapters:

Random error

The random error ("rn") is completely uncorrelated and caused by statistical effects. Therefore, this contribution is often referred to as "white noise" or "random noise". For random noise no relation between adjacent data points can be detected.

Systematic error

All other errors are referred to as "systematic errors" because they result from physical effects and can in principle be measured and parameterized. Systematic errors occur along the complete workflow of a measurement and the following data processing. Possible contributions result from changing sensor properties during a measurement caused by drift effects or due to the impact of environmental conditions on sensor sensitivity, from inaccurate scaling of raw data caused by a "bad" calibration, from error contributions during the data processing by other units which are used in the calculation or from inaccurate formulas or

wrong parameterizations of physical effects. Since most of these contributions cannot be precisely parameterized there remains an uncertainty in the final data which leads to systematic deviations of the secondary data from reality.

The total error of a unit is the sum of statistical and systematic errors.

Accuracy and Precision

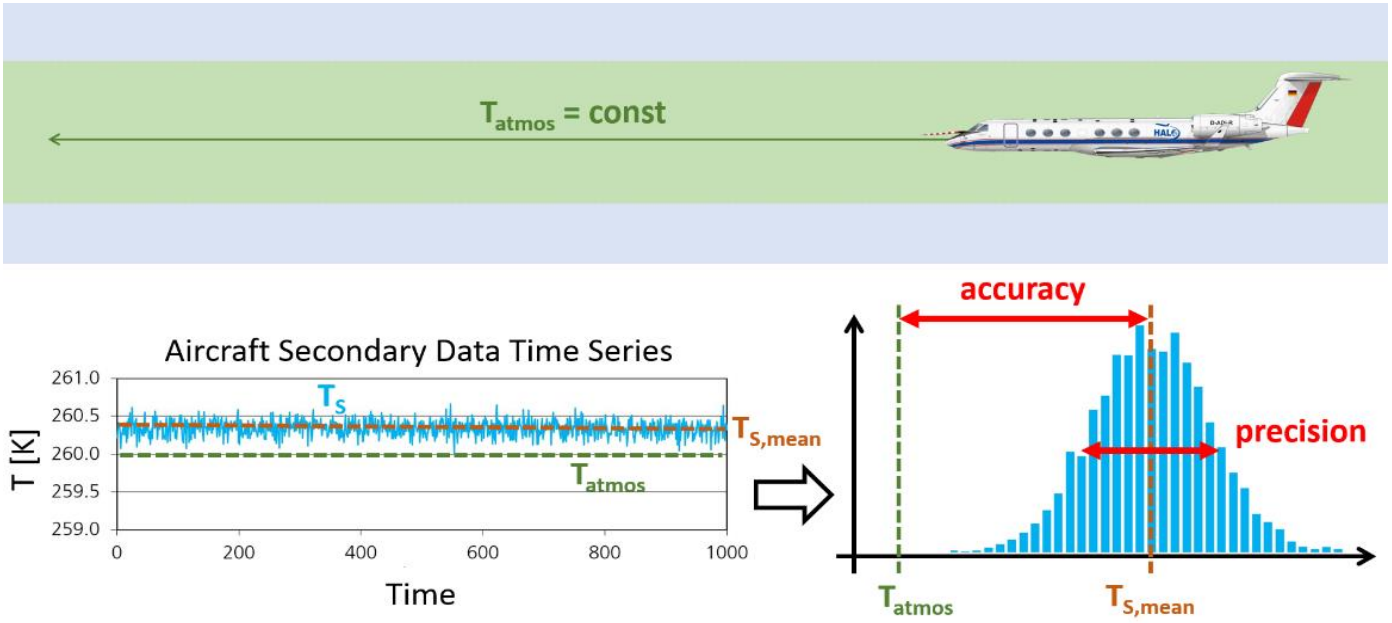

Figure 5*: Accuracy and precision*

Imagine an aircraft flying in an airmass with an absolute homogeneous temperature. How does in this case the time series of the processed static temperature T_S look like? Figure 5 shows the expected result: The secondary data T_S will not only show a time dependent variability but also a potential systematic difference from the real atmospheric temperature T_{atmos}.
The ability to exactly reproduce data which was acquired under identical conditions is described by the "precision" of a data system for the respective unit. As can be seen from Figure 5 precision is the random "scatter" of data around the mean value. The parameter obviously quantifies the total statistical noise in the system caused by white noise contributions from the original data as well as from all parameters which get involved in the data processing. Visible variability in

the data which exceeds this noise level can be attributed to real atmospheric structures.
The offset of the mean processed data from the real atmospheric value is known as the "accuracy" of a measurement system. As an example, the usage of a bad reference sensor in the sensor calibration will result in an erroneous scaling of the raw data which then leads to an error (offset) in the secondary data.
A measurement system with a good precision and bad accuracy can still be used to detect atmospheric structures or to determine statistical units like fluxes or variances from time series.
On the other hand, the calculation of secondary data like the relative humidity requires a very accurate static temperature T_S. This unit is used to determine the saturation water vapor pressure which has an exponential dependence on T_S. Therefore, systematic errors in the temperature can lead to large errors in this humidity unit. For this reason, the measurement of relative humidity requires a very accurate system.
Figure 6 shows an example from [7] which demonstrates the precision of HALO air data. The plot shows the variation of static pressure (secondary data!) during pitch oscillation maneuvers. The pressure data is compared to a reference value which was determined outside (before/after) the α-oscillations.
The pressure data shown had to be corrected for variations caused by aircraft altitude changes during the maneuver. This correction requires information about the air density and the changes of aircraft altitude during the oscillations. The altitude data is determined by an inertial reference system (IRS). Therefore, the data contains uncertainties not only from the static pressure itself (which has already been corrected for static source error) but also from the angle of attack measurement (as calculated from differential α-pressure, dynamic pressure, static pressure), from the air density (temperature, pressure) and from the aircraft altitude (aircraft altitude and attitude). As one can see from Figure 6 the standard deviation of the data with respect to the mean value (i.e. the fit into the data) is less than 1Pa which is significantly better than the absolute accuracy of the static pressure sensor calibration which is shown in Figure 30.

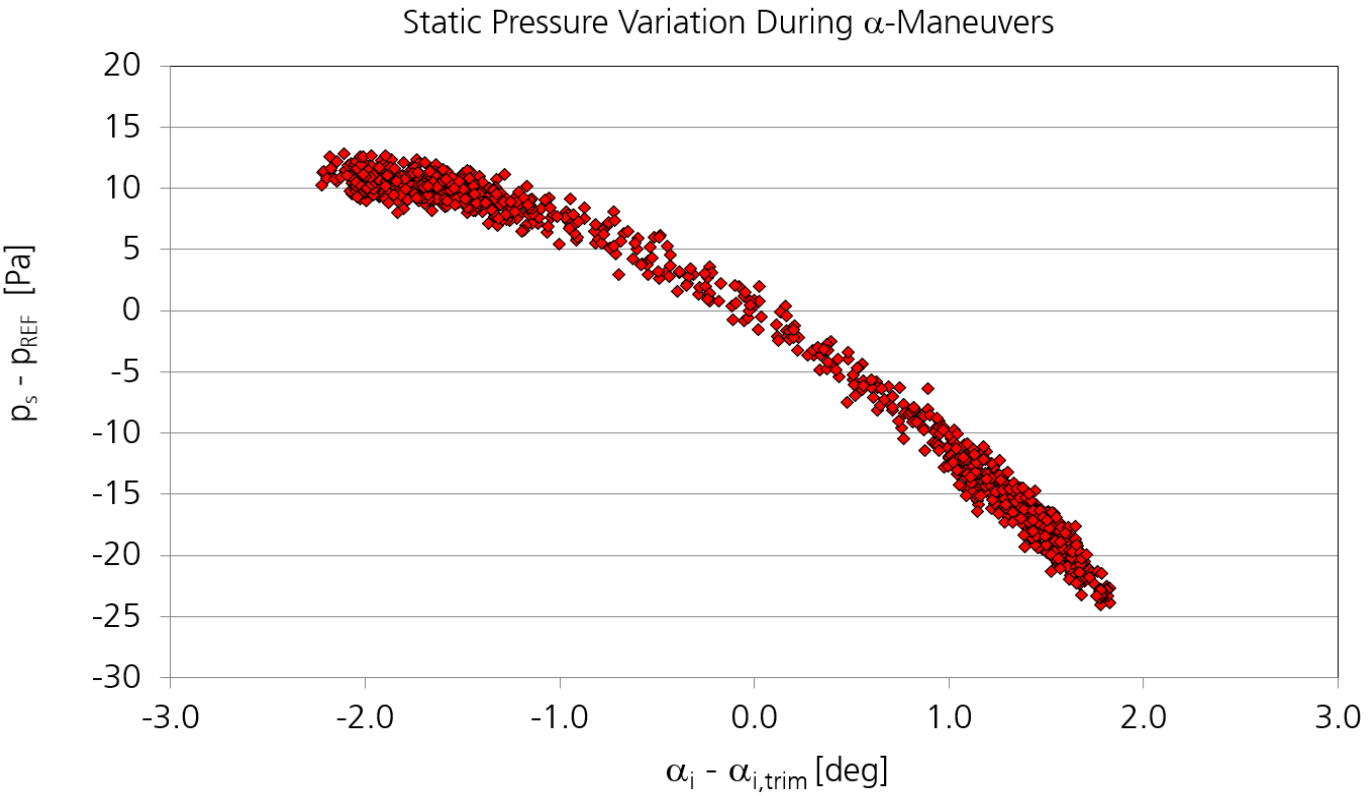

Figure 6*: Dependence of static pressure on dynamic angle of attack variations associated with harmonic pitch maneuvers (from [7]). The plot shows 10Hz data from a maneuver with 9 oscillations.*

White Noise

As mentioned above white noise is present in every kind of data system. The following sections will show how this noise contribution can be detected and quantified for a specific unit and how this error propagates through the data processing.

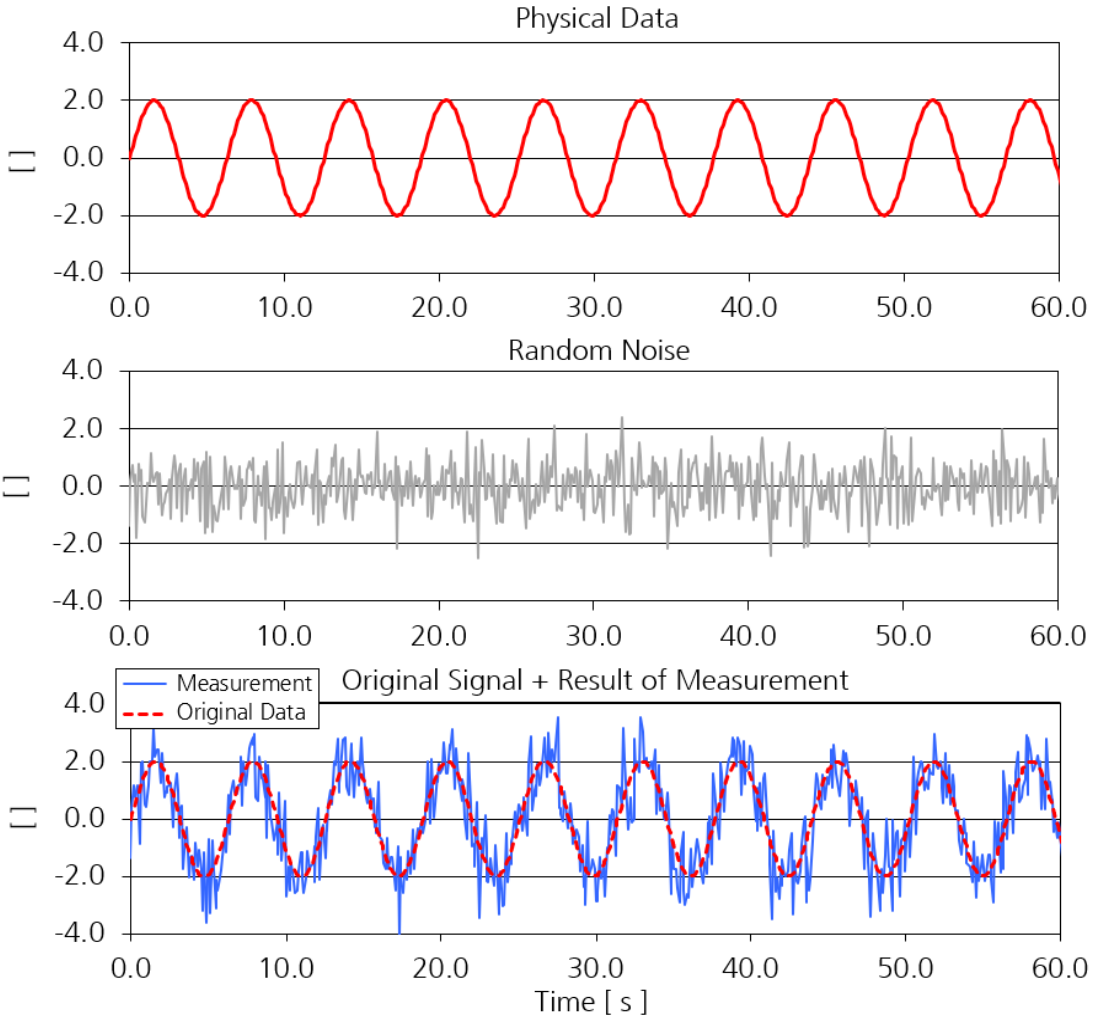

Figure 7*: Test signal for the investigation of the white noise effects on real data. The data index n in the formulas below is scaled according to the 10Hz HALO standard data acquisition rate in order to achieve a realistic delay time dt in the autocovariance function. The signal consists of a sine signal with an amplitude of 2 and a frequency of 0.16Hz ($\omega = 1$). The artificial random noise was calculated from a Gaussian distribution with a standard deviation of $\sigma_{rn,s} = 0.8$. The length of the data series used for the calculations is 600 s (6000 values).*

Properties of Random Noise

In order to demonstrate the properties of this error contribution we use an artificial data ("s") time series. As one can see in Figure 7 the test data consists of a sine signal which represents the atmospheric signal and a noise contribution which is generated with the IDL RANDOMN function.
The most important property of the random signal results from the fact that the single data points are completely independent from each other. This means that there is absolutely no correlation between adjacent data points and that no structure can be detected in the data. This property can be visualized by mathematical tools like the autocovariance function or the power spectrum of the respective time series.

Random Error Investigation: Autocorrelation and Power Spectrum

Every data time series $s(t)$ can be represented as the sum of the mean value $\bar{s}$ of the data and a temporal variability $s'(t)$ around this value:

$$s(\mathrm{t}) = \bar{s} + s'(t) \qquad \textbf{Equation 1}$$

In our case a time series consists of discrete values according to the sampling process inside a real data acquisition. Equation 1 can then be written as

$$s(i) = \bar{s} + s'(i), \qquad \mathrm{i} = 1,..\mathrm{m} \qquad \textbf{Equation 2}$$

The mean value of the time series is calculated according to

$$\overline{s(i)} = \frac{1}{m}\sum_{i=1}^{m} s(i) = \bar{s} \quad since \quad \bar{s'} = \frac{1}{m}\sum_{i=1}^{m} s'(i) = 0 \qquad \textbf{Equation 3}$$

The variability of $s'(i)$ is described by two units: The **variance** σ_s^2 represents the average squared deviations of a time series from the mean value of the data, while

the **standard deviation** σ_s is the square root of that number and can be seen as the mean width of the data "scatter" around the mean value.

$$\sigma_s^2 = \frac{1}{m}\sum_{i=1}^{m} s'^2(i) \qquad \textbf{Equation 4}$$

For the test data in Figure 7 the standard deviation of the random noise contribution is $\sigma_{rn,s} = 0.8$ which corresponds to a variance of $\sigma_{rn,s}^2 = 0.64$.
In case of random noise there is absolutely no correlation between single data points and no systematic structures can be observed in the time series. This can be checked by multiplying the time series $s(i)$ with a copy of itself which has been shifted by one index, i.e. $s(i-1)$. For a sine signal it is obvious that this product will be almost identical to $sin^2(i)$ because $sin(i)$ and $sin(i+1)$ are always very close to each other. In other words: two adjacent data points are always strongly correlated due to the sine function.
This is completely different for the random noise where such a correlation does not exist. Therefore, the product $s(i) \cdot s(i+1)$ must also be completely random: a single data point has absolutely no relation to its neighbour. As a consequence, the mean of the product of the 2 shifted time series must be zero.
For of the random noise contribution to the above test data we find that $\overline{s^2(i)} = 0.625$ and $\overline{s(i) \cdot s(i-1)} = -0.016$. In case of the "clean" sine signal these values are 2.000 and 1.990 respectively.
The **autocovariance function** (ACV) is used to systematically investigate this behaviour. It is defined as

$$ACV_s(n) = \overline{s'(i) \cdot s'(i+n)} = \frac{1}{m}\sum_{i=1}^{m} s'(i) \cdot s'(i+n) \qquad \textbf{Equation 5}$$

From Equation 5 it is obvious that $ACV_s(0)$ is identical to the variance σ_s^2:

$$ACV_s(0) = \overline{s'(i) \cdot s'(i)} = \frac{1}{m}\sum_{i=1}^{m} s'^2(i) = \sigma_s^2$$ **Equation 6**

The ACV helps to find out whether the data points of a time series are correlated between each other. It can quantify:

- How strong this correlation is (by comparing it to the variance of the original time series at n=0)
- Over which typical time the data is correlated with itself

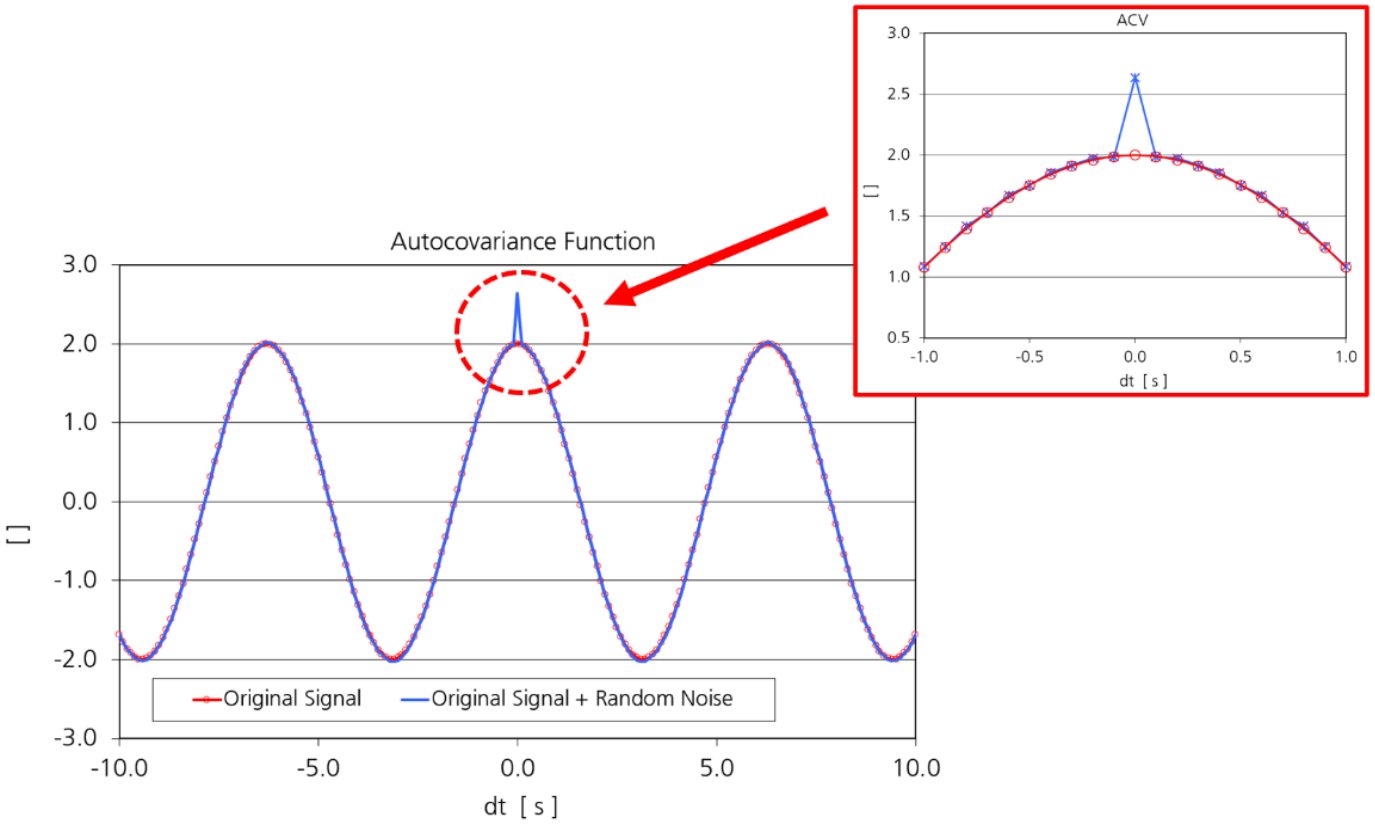

Figure 8*: Autocovariance of the test signal. The plot shows the strong correlation in the time series caused by the artificial sine signal. This correlation is still completely visible in the presence of white noise. At dt=0 one can see the "white noise peak" which results from the uncorrelated error contribution in the signal at dt=0.*

Figure 8 shows the ACV for the test signal and compares it with the (noise free) original sine data. From the plot we see that:

- A systematic correlation is given over a very long delay time dt which extends far beyond the shown plot window. This is clear, because the main signal follows an exact sine shape.
- The correlation changes between 2 (perfectly correlated signals: $sin^2(t)$) and -2 (anti-correlated signals: $-sin^2(t)$). The correlation depends on the value of dt, which can be seen as a phase shift of the second sine function in Equation 5.
- The ACVs of the original data and the "noisy" signal are almost identical with an exception at dt=0
- The ACV of the noisy signal shows a sharp peak at $dt = 0$. It is immediately clear, that this additional peak must represent the white noise contribution which vanishes otherwise i.e. for $dt \neq 0$.

Assuming that the signal variability $s'(i)$ contains contributions from the "real" (physical) data ($s_{data}'(i)$) as well as from random noise ($s_{rn}'(i)$), i.e.

$$s'(i) = s'_{data}(i) + s'_{rn}(i) \qquad \textbf{Equation 7}$$

the total variance of the time series σ_s^2 can be calculated as

$$
\begin{aligned}
&\sigma_s^2 \\
&= \overline{s'^2(\iota)} \\
&= \overline{(s'_{data}(\iota) + s'_{rn}(\iota))^2} \\
&= \overline{{s'_{data}}^2(\iota) + 2 \cdot s'_{data}(\iota) \cdot s'_{rn}(\iota) + {s'_{rn}}^2(\iota)} \\
&= \overline{{s'_{data}}^2(\iota)} + \overline{{s'_{rn}}^2(\iota)} \qquad (since\ \overline{s'_{data}(\iota)} = \overline{s'_{rn}(\iota)} = 0) \\
&= \sigma_{rn,s}^2 + \sigma_{data,s}^2 \\
&= ACV_s(0)
\end{aligned}
$$

Equation 8

Equation 8 proves that the value of $ACV_s(0)$ which corresponds to the overall data variance σ_s^2 is the sum of the variances of the true signal $\sigma_{data,s}^2$ and the random noise $\sigma_{rn,s}^2$. Therefore, the ACV can be used to determine these two units by interpolating the ACV at $dt = 0$. However, in most cases it is sufficient to determine the difference between $ACV_s(0)$ and $ACV_s(1)$:

$$
\begin{aligned}
\sigma_{rn,s}^2 &= ACV_s(0) - ACV_s(1) \\
\sigma_{data,s}^2 &= ACV_s(1)
\end{aligned}
$$

Equation 9

In case of the test function we find $ACV_s(0) = 2.637$ and $ACV_s(1) = 1.986$ which corresponds to $\sigma_{data,s} = 1.41$ and $\sigma_{rn,s} = 0.81$.

The ACV can be normalized with the data signal variance $\sigma_{data,s}^2$ of the time series. The result is called the **autocorrelation function** (ACF).

$$
ACF_s(n) = \frac{1}{\sigma_{data,s}^2} \cdot \overline{s'(\iota) \cdot s'(\iota + n)}
$$

Equation 10

With the exception of the white noise peak the ACF has a data range between 1 (perfectly correlated at dt=0) to -1 (anticorrelated) which makes this function a useful tool for correlation analyses.

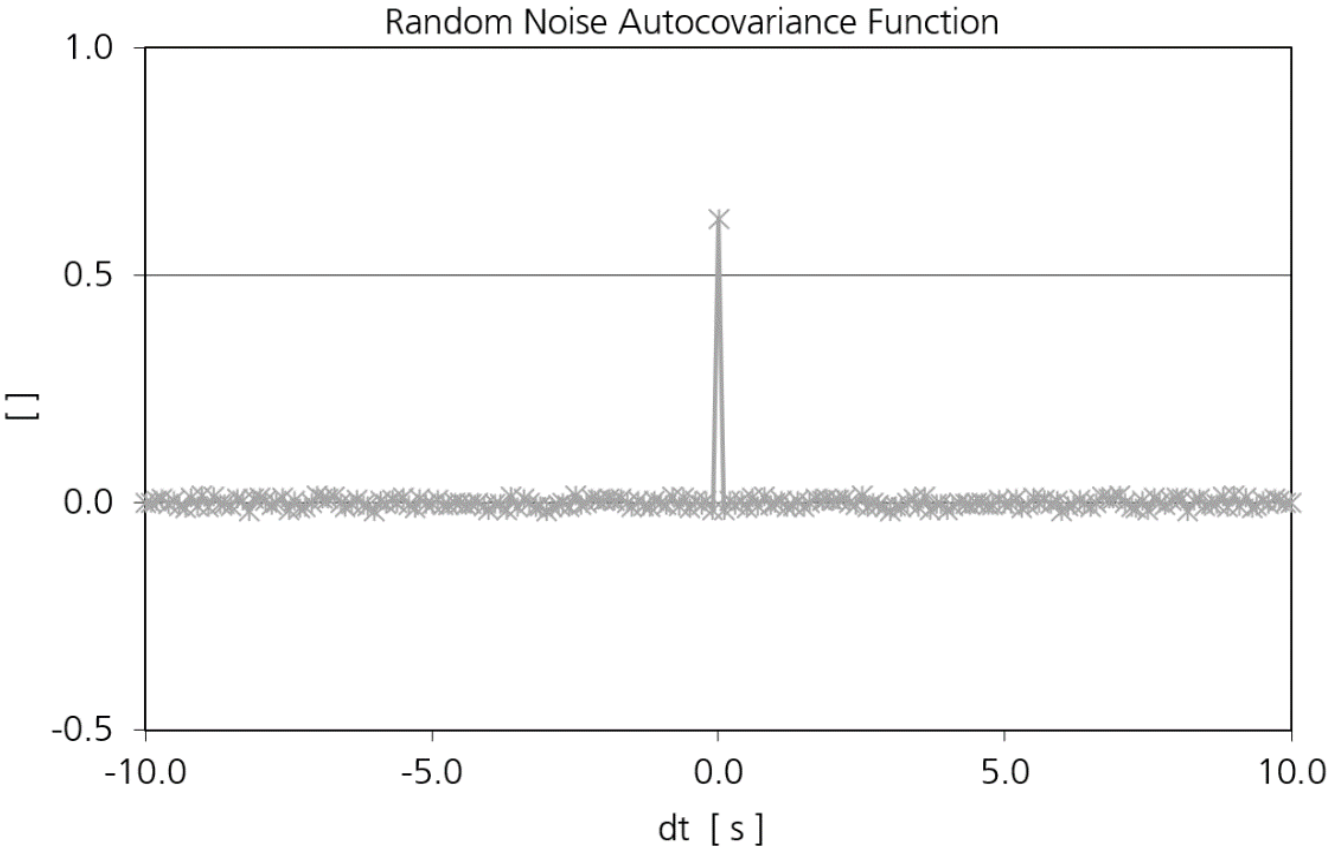

Figure 9*: Autocovariance Function of the random noise used for the generation of the test signal. With the exception of the white noise peak at dt=0 the ACV is zero. The height of the peak is identical to the random noise variance of 0.64.*

Figure 9 shows the ACV of the noise contribution to the test signal. As expected the function is zero with the exception of the white noise peak at dt=0. The height of this peak represents the variance of the white noise.

Another tool to investigate the properties of time series is the **power spectrum** which can be calculated from the data by means of a Fast Fourier Transform (FFT). Figure 10 shows the result for the test signal.

As already mentioned above random noise does not show any systematic structure in the time series. Therefore, no specific frequency contributions to the signal can be detected. As a consequence, the noise power spectrum is represented by a horizontal line. The contribution from all frequencies are equal, the spectrum is **white**.

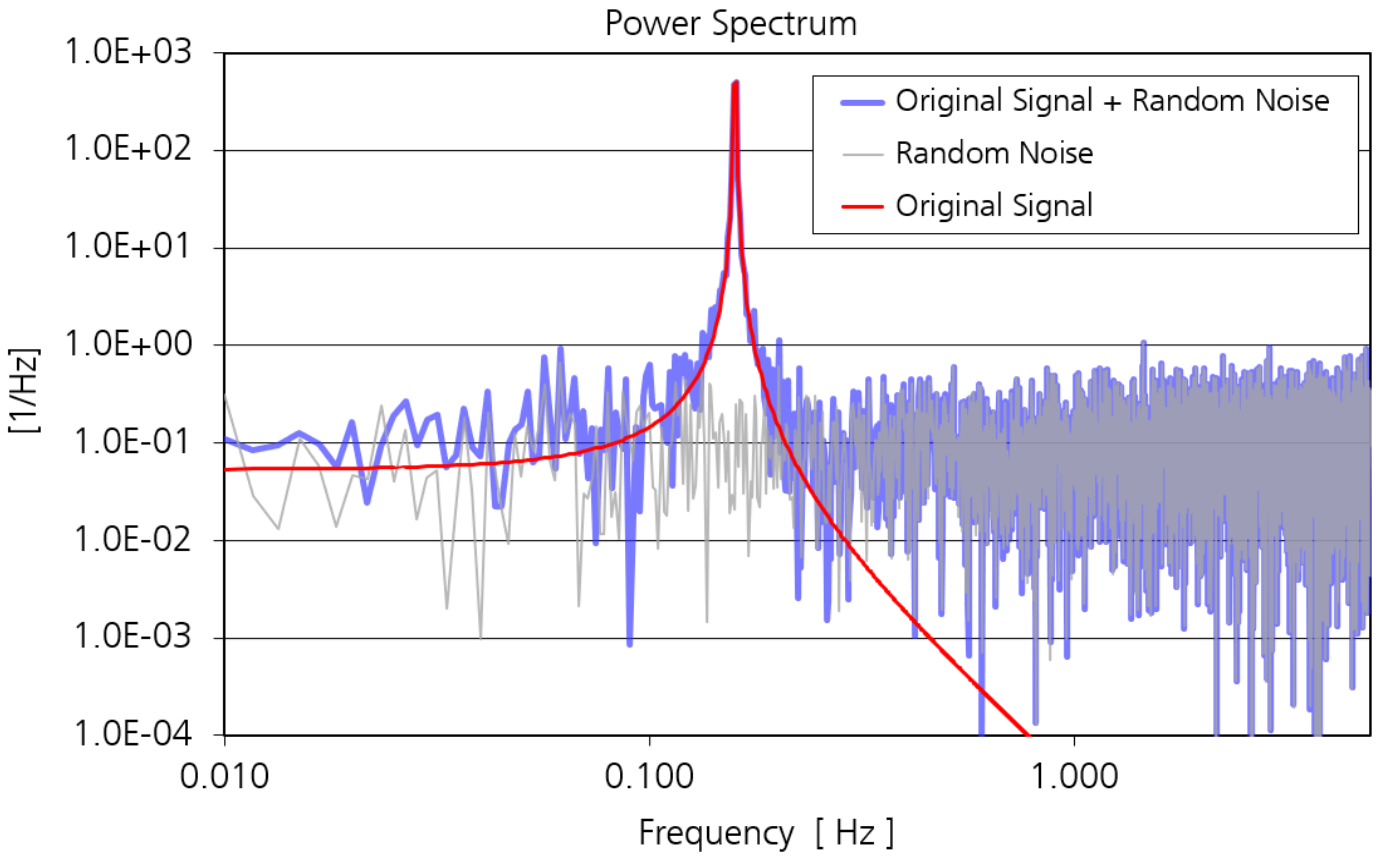

Figure 10*: Power spectra for the test signal, the original signal and the white noise contribution. Please note that both axes show a logarithmic scaling. Therefore, the plot shows some minor effects caused by the limited length of the test signal.*

The level of this horizontal line is a measure for the amount of noise and the integral over the noise power spectrum yields the white noise variance $\sigma_{rn,s}^2$. For the combination of data signal and noise in the test data this noise level is maintained and still visible in the spectrum. However, the frequency of the sine signal peaks out of the spectrum by several orders of magnitude. In this case the integral over the spectrum (i.e. the area under the curve in Figure 10) stands for the overall signal variance $\sigma_s^2 = \sigma_{rn,s}^2 + \sigma_{data,s}^2$.

It turns out that it is much more convenient to use the ACV than the spectrum if one wants to determine the signal variance and to distinguish between the main contributions to this value. On the other hand, the power spectrum helps to

understand the structure of a signal and to identify the dimension (frequency) of dominant features in the time series.

Example: Real Aircraft Data

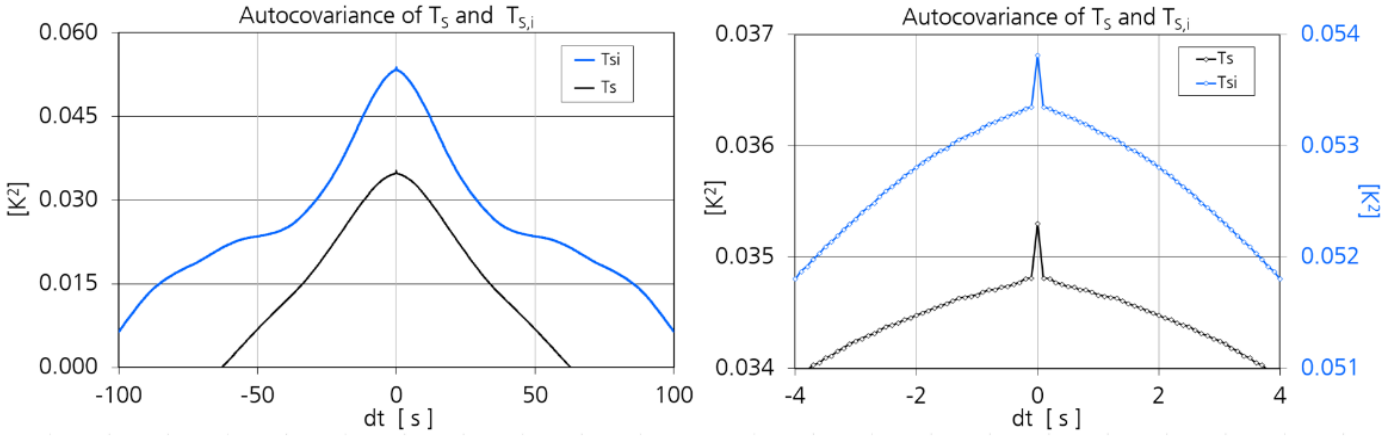

Figure 11*: Autocovariance Function of the aircraft data shown in Figure 4. The right plot shows the white noise peaks in the data.*

Figure 11 shows the Autocovariance function for the time series of Figure 4. As one can see the white noise peak in the primary and secondary data is rather small, the standard deviation which was calculated according to Equation 9 yields $\sigma_{rn,T_{S,i},orig} = 0.022K$ and $\sigma_{rn,T_S,orig} = 0.022K$. We can therefore state that the precision of the BAHAMAS Temperature measurement is very good.
This is also proved by the fact that no other primary data time series from this data set shows a detectable white noise peak on this flight leg.
From Figure 11 it becomes obvious that the random noise signal in the raw data propagated almost unchanged through the complete data processing and that no significant impact of the data processing on the white noise amplitude can be observed.
The different shape of the ACV functions in Figure 11 is due to the impact of the above mentioned aerodynamic parameters on the measurement: The shape of the ACV for $T_{S,i}$ is almost identical to the ACV for the aircraft True Air Speed (TAS) as one can see from Figure 19. As pointed out above these features are completely removed during the calculation of T_S.

Effect of Additional Input Errors on Secondary Data

In order to visualize the random error propagation for more complicated calculations artificial white noise with an amplitude of $\sigma_{rn,P_{S,i}}$=100Pa is added to the primary data time series of the indicated static Pressure $p_{S,i}$. The noise was generated with the IDL RANDOMN function and added to the original $p_{S,i}$ time series. The result is shown in Figure 12

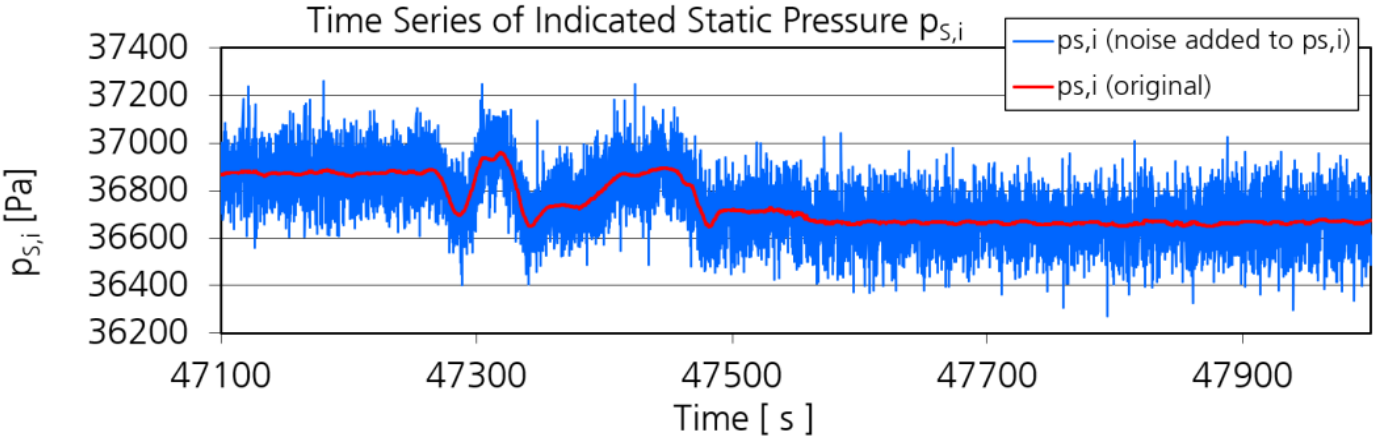

Figure 12*: Static pressure primary data before/after artificial white noise is added to the time series. The random noise amplitude is 100Pa.*

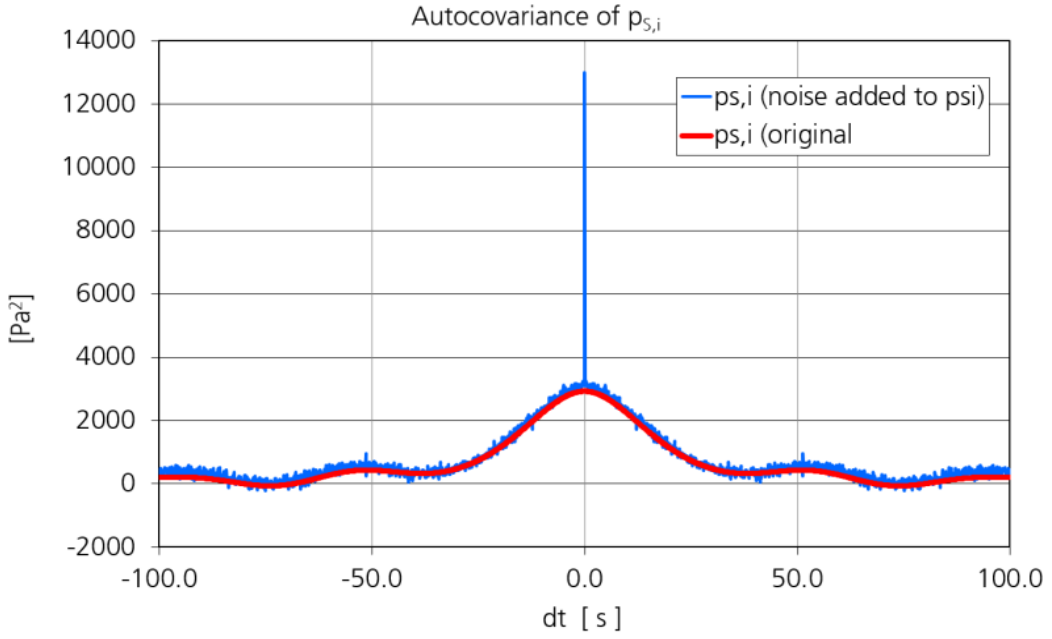

Figure 13*: Autocovariance Function of the indicated static pressure $p_{S,i}$ (primary data) before/after artificial white noise is added to the time series.*

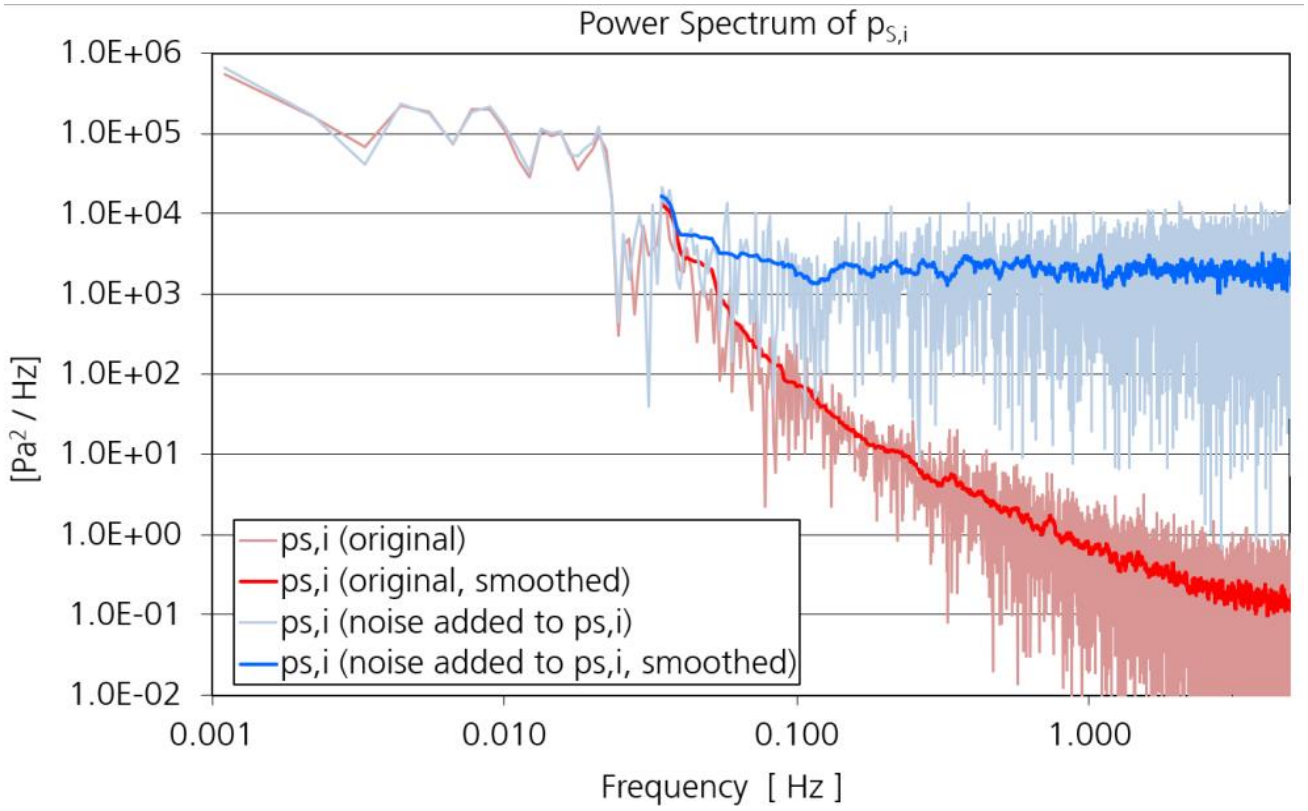

Figure 14*: Power spectrum of the indicated static pressure $p_{S,i}$ before/after artificial white noise is added to the time series.*

The artificial white noise leads to a significant white noise peak in the ACV of $p_{S,i}$ as one can see from Figure 13.
The height of the white noise peak is found to be 9750 Pa² which gives $\sigma_{rn,P_{S,i}}$= 98.7 Pa. This value corresponds well with the white noise amplitude which was chosen in the noise generation. The comparison of the power spectra in Figure 14 clearly shows the flat (white) noise contribution which exceeds/eliminates the structure from the original time series at higher frequencies.

White Noise Propagation in Data Processing

In order to investigate the impact of the increased white noise level of $p_{S,i}$ on secondary data a complete data processing run is performed with RAMSES using the modified $p_{S,i}$ data. Figure 15 shows the comparison between the time series of the static air temperature T_S which were calculated with and without the artificial noise contribution.

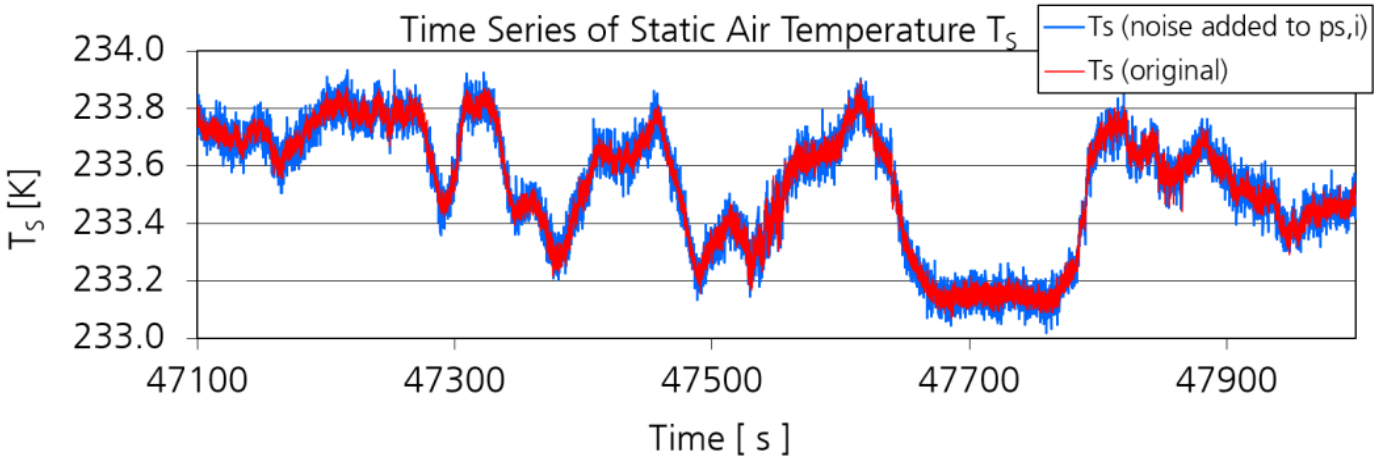

Figure 15*: Time series of static air temperature T_S before/after artificial white noise was added to the indicated static pressure $p_{S,i}$.*

It is obvious that the T_S noise level increases as there is more random noise in the T_S data processing. Figure 3 shows where $p_{S,i}$ is used in the processing of temperature data.

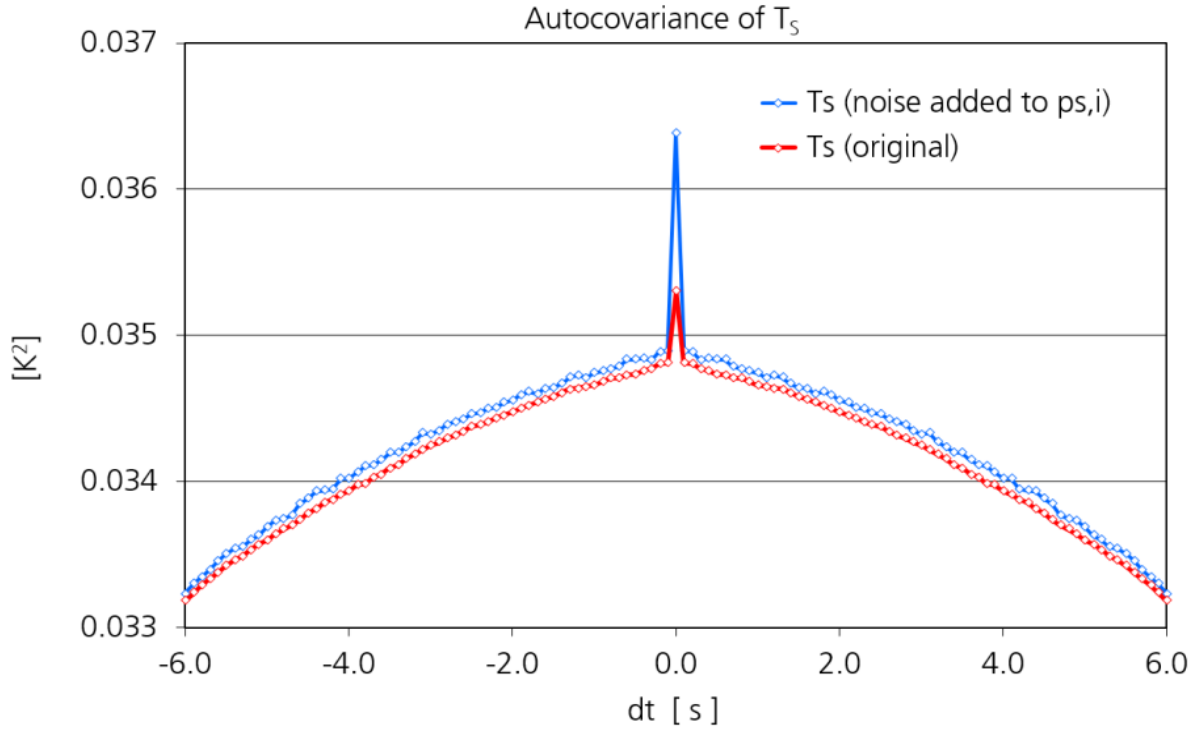

Figure 16*: Autocovariance function of static air temperature T_S before/after artificial white noise was added to the indicated static pressure $p_{S,i}$*

The ACV analysis helps to quantify the increase of σ_{rn,T_S}. Figure 16 shows the comparison of the ACV for T_S with/without the artificial random noise contribution. From the plot we find the total white noise error of T_s for the modified data set to be

$$\sigma_{rn,T_S,mod} = \sqrt{ACV_{T_S,mod}(0) - ACV_{T_S,mod}(1)} = 0.039K$$

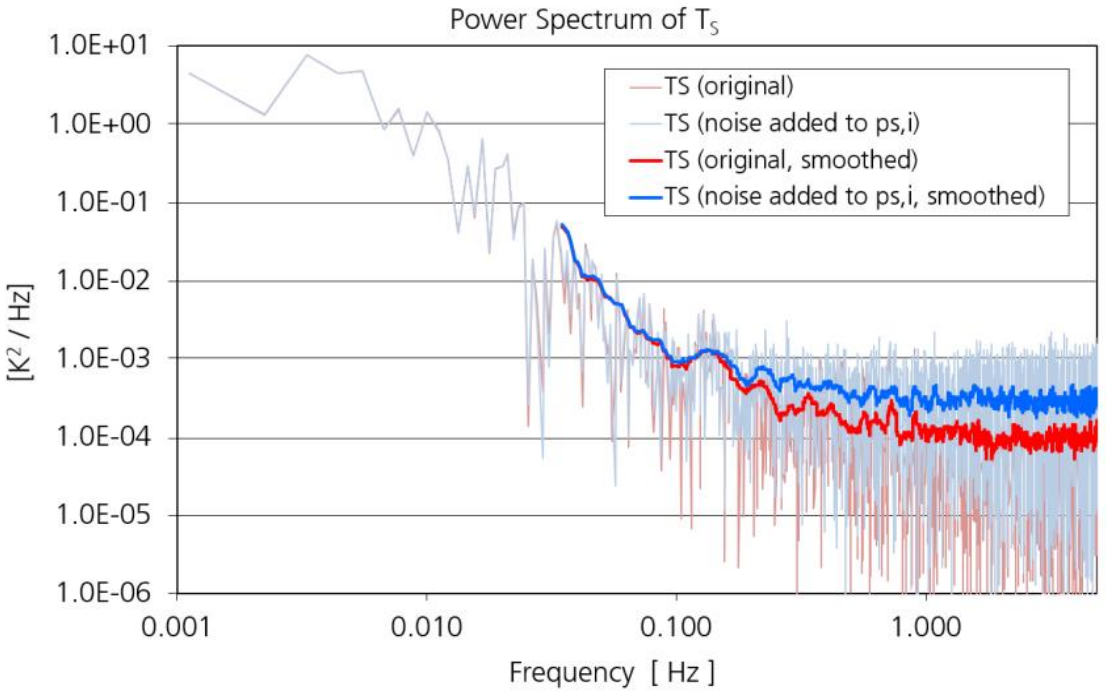

Figure 17*: Power spectrum of static air temperature T_S before/after artificial white noise was added to the indicated static pressure $p_{S,i}$.*

This value is significantly larger than the standard deviation of $\sigma_{rn,T_S,orig} = 0.022K$ which was determined above from the original time series. The power spectrum of the T_S data with the different noise contributions can be seen in Figure 17. One can see that the additional white noise contribution in $p_{S,i}$ results in an increased level of white noise in the spectrum.

Since RAMSES processes the data point by point and since no averaging or "temporal smearing" of data takes place by any processing step it is immediately clear that every white noise contribution to a BAHAMAS raw data time series will

remain "random" during the complete data processing. This means that the noise contribution to a single data point of any secondary data time series will always be completely uncorrelated with any other noise value from this time series.
According to Equation 8 this means that the total white noise variance of a secondary unit (S) will always represent the sum of random error variances which can be attributed to the different raw data inputs (i) which get involved in the calculation of S:

$$\sigma^2_{rn,S,total} = \sum_{i\ (all\ prim.\ data\ sources)} \sigma^2_{rn,S,i} \qquad \textbf{Equation 11}$$

For the above case we can therefore write

$$\sigma^2_{rn,T_S,total} = \sigma^2_{rn,T_S,T_{S,i}} + \sigma^2_{rn,T_S,p_{S,i}}$$

which allows for the determination of the impact of the additional white noise in $p_{S,i}$ on the calculated static pressure T_S:

$$\sigma_{rn,T_S,p_{S,i}} = \sqrt{\sigma^2_{rn,T_S,total} - \sigma^2_{rn,T_S,T_{S,i}}} = \sqrt{\sigma^2_{rn,T_S,mod} - \sigma^2_{rn,T_S,orig}} = 0.032K$$

This means that a 100Pa white noise contribution to $p_{S,i}$ results in a 0.032K random error in the final T_S data time series during this flight leg
A second example shows impact of white noise on a unit which is subject to a more complicated data processing.

The True Air Speed (TAS) is the aircraft speed relatively to the air at rest. It is calculated from secondary pressure and temperature data (p_S, qc and T_S) according to

$$\mathrm{TAS} = \sqrt{C_2 \cdot T_s \cdot \left[\left(1 + \frac{\mathrm{qc}}{p_s}\right)^{\mathrm{C_1}} - 1\right]}$$ **Equation 12**

where

$C_1 = \frac{\kappa - 1}{\kappa}$, $C_2 = 2 \cdot \frac{\mathrm{R}}{\mathrm{C_1}}$

p_s is the static pressure

qc is the dynamic (impact) pressure

κ is the adiabatic index

R the universal gas constant

T_S is the static air temperature

Please note that p_s and qc in Equation 12 represent data that was subject to major aerodynamic corrections which concern the static source error and flow angle dependencies.

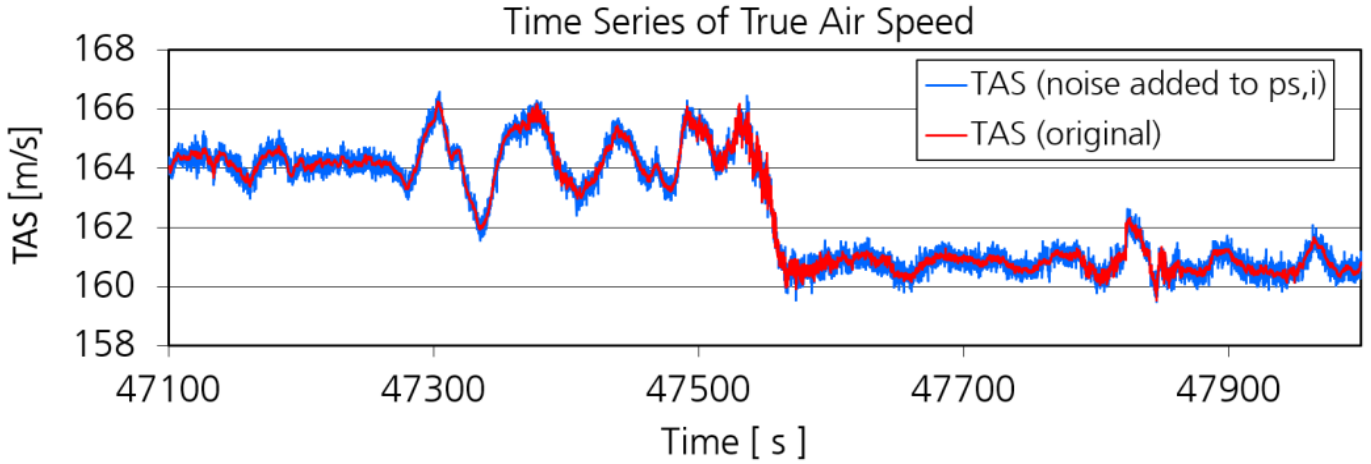

Figure 18*: Time series of True Air Speed (TAS) before/after artificial white noise was added to the indicated static pressure $p_{s,i}$.*

Figure 18 shows the TAS time series for the same time interval as Figure 4 and Figure 15. One can see, that the additional white noise in $p_{s,i}$ results in increased random noise in TAS. The question whether the original ("real") random noise in $T_{S,i}$ also has an impact on TAS is answered by the comparison of the ACVs

before/after the artificial white noise was added to the data. This comparison is shown in Figure 19. The plot on the left side shows the same specific shape as the ACV of $T_{S,i}$ in Figure 11, which proves the strong dependency of $T_{S,i}$ on TAS caused by the aerodynamic properties of the temperature sensor housing.

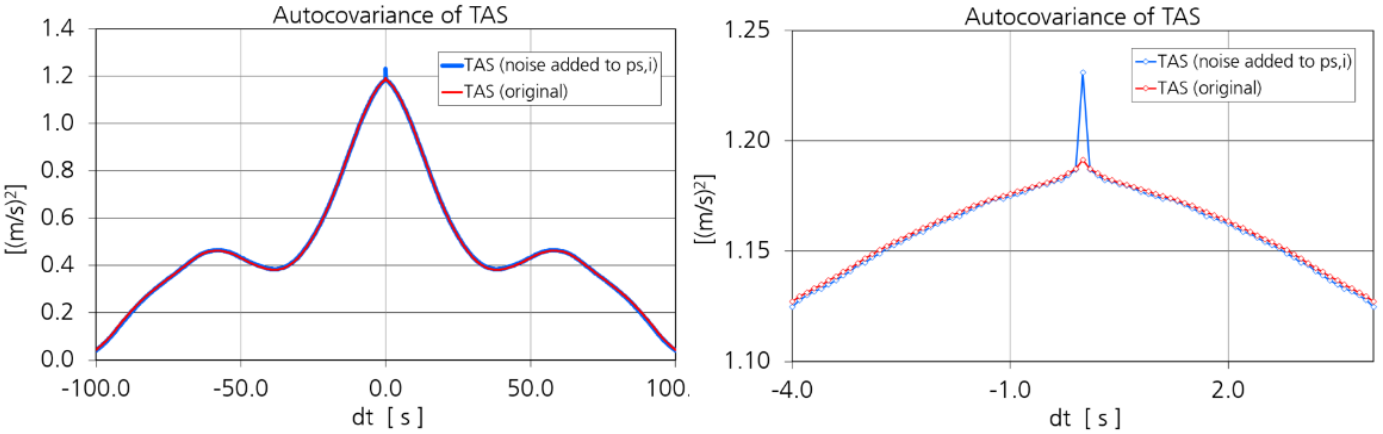

Figure 19*: Autocovariance function of True Air Speed (TAS) before/after artificial white noise was added to the indicated static pressure $p_{S,i}$*

On the right-hand side of Figure 19 one can see that the original ACV of TAS shows only a very small white noise peak which corresponds to

$$\sigma_{rn,TAS,T_{S,i}} = \sqrt{ACV_{TAS,orig}(0) - ACV_{TAS,orig}(1)} = 0.065\ \mathrm{m/s}$$

The modified random error of $p_{S,i}$ results in a total TAS white noise of

$$\sigma_{rn,TAS,mod} = \sqrt{ACV_{TAS,mod}(0) - ACV_{TAS,mod}(1)} = 0.209\ m/s$$

This means that the effect of a 100Pa noise contribution in $p_{S,i}$ on TAS can be determined to be

$$\sigma_{rn,TAS,p_{S,i}} = \sqrt{\sigma^2_{rn,TAS,mod} - \sigma^2_{rn,TAS,T_{S,i}}} = 0.199\ m/s$$

Figure 20 shows the TAS power spectra before/after the artificial white noise was added to the $p_{S,i}$ data time series

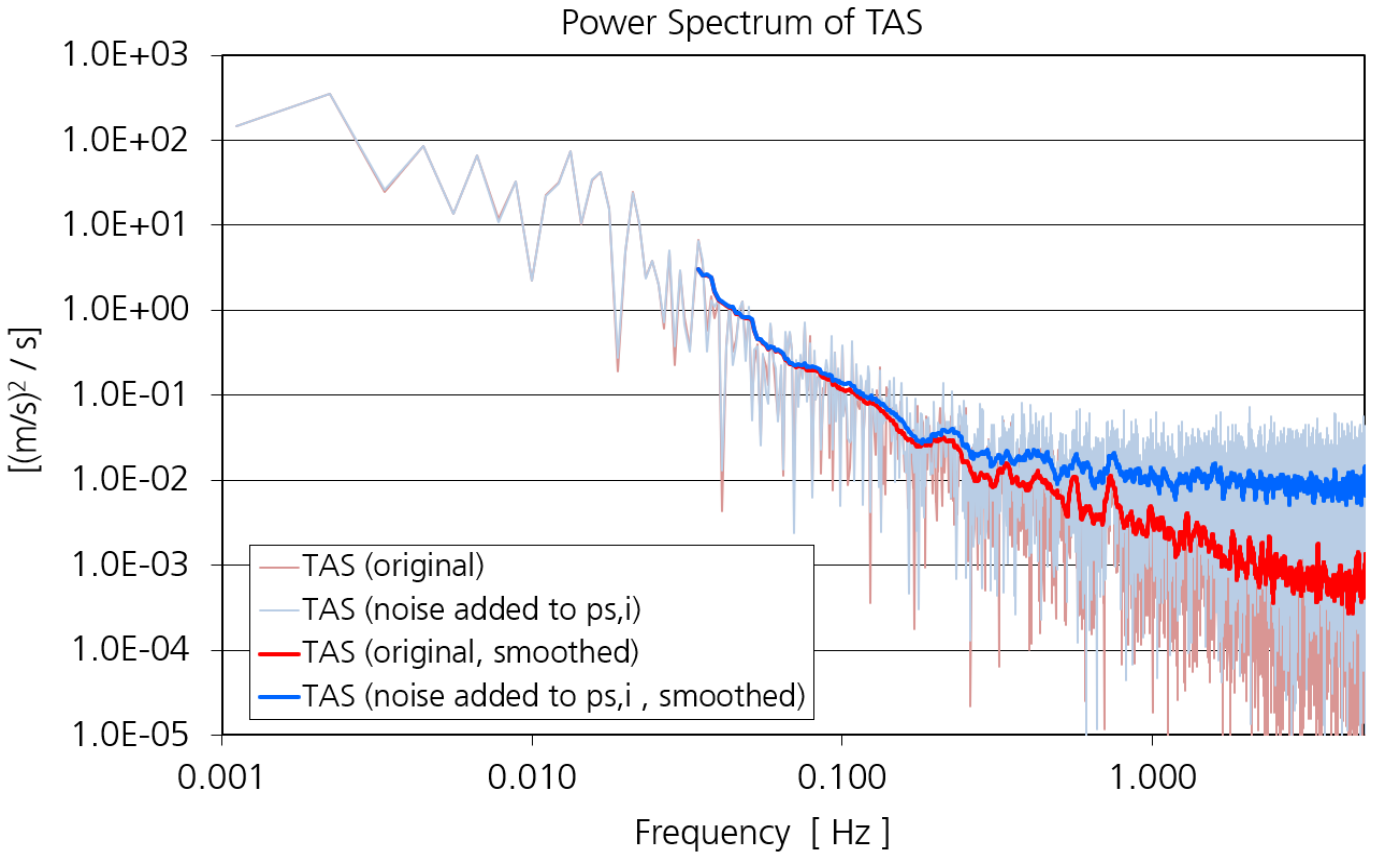

Figure 20*: Power spectrum of True Air Speed (TAS) before/after artificial white noise was added to the indicated static pressure $p_{S,i}$*

This analysis demonstrates how random error contributions from the primary/raw data propagate through the data processing and lead to respective white noise in the final secondary units where it can be determined by means of ACV. The last example also shows that the error propagation is influenced by the data processing scheme. The influence of $T_{S,i}$ on TAS is very small because Equation 12 uses the absolute Temperature. In this case a random error contribution of 0.022K will not show a significant impact on the result. On the other hand, the white noise of $T_{S,i}$ is found in the same order of magnitude in T_S, since these units are directly correlated with each other.

Systematic Errors

The second error contribution to experimental data concerns systematic deviations of measurement data from reality due to "errors" in

- the sensors
- the data acquisition
- the data processing

These errors are not random but a result of systematic effects which can in principle be explained, parameterized and corrected for.
However, in most cases such a correction is not possible, because the necessary input for an error determination/correction does not exist. Furthermore, the respective deviations from the "real" data cannot be detected directly in the data and - depending on the unit - they are very difficult to determine.

A very simple but only qualitative way to detect major systematic errors in the data is the check whether a measurement result is "plausible": a direct correlation of wind data with aircraft flight parameters like speed or attitude is very unlikely and a mean vertical wind speed other than zero over a longer time interval indicates problems with this measurement. Very "uncommon" humidity values for a specific region of the atmosphere or a relative humidity far above 100% indicate that the determination of this unit might be erroneous.
However, it is usually not clear which step of the measurement chain is concerned: a malfunction at the sensor itself, a drift effect of an electronic component, an erroneous calibration (scaling) in the laboratory or a wrong secondary data parameter which was used in the data processing?
The only way to determine systematic errors directly from the flight data is to compare the measurement with independent reference data. However, for aircraft measurements of meteorological parameters it is sometimes very difficult to obtain an independent and accurate reference from another source.

Possible methods to detect systematic errors in the data are:

- cross checks with data from other airborne platforms, instruments or independent evaluation methods and data sources:
    - in flight:
        - comparison of aircraft data with model calculations [5], [10]
        - comparison of aircraft data with radiosonde data
        - comparison of data which was determined by different data evaluation methods: wind triangle <-> exact wind calculation, vertical velocity from meteorological data <-> from GPS
        - comparison of data from redundant instrumentation. This requires multiple humidity, pressure and temperature sensors as part of the original data system
        - comparison of data with the aircraft avionic system, i.e. the aircraft Air Data System (ADS)
        - application of inflight calibration routines based on maneuvers or special flight patterns
        - tower fly-by experiments for comparison with ground-based measurements
        - intercomparison flights with other (research) aircraft [13]
    - on ground:
        - calibration cross checks between different organizations or laboratories using a common test sensor
        - comparison of software algorithms and parameterizations with other aircraft operators
- periodic calibration of aircraft sensors in order to detect drift effects, aging and other changes of sensor properties
- periodic calibration of the reference sensors from the calibration testbeds which are used for the aircraft instrumentation. This calibration must be performed by an external calibration laboratory which is traceable to national standards

- laboratory testing of sensors for environmental dependencies using an environmental simulation chamber

Some possible error sources are explained in the following sections.

Sensor

The measurement of any unit is always based on a physical principle. Some examples:

- a pressure measurement usually monitors the deformation of a membrane which is exposed to different air pressure on each side
- temperature is based on the change of resistivity of a thin Platinum wire which is exposed to the air flow
- humidity measures the loss of laser light intensity by absorption or the change of the dielectric constant of a thin film of polymer

These physical effects have to be converted into an electronic signal which is forwarded to the data acquisition.

Some of these measurement principles show dependencies to other parameters or are sensitive to external factors: the elasticity coefficient of the pressure membrane is temperature dependent, the Platinum wire of a temperature sensor collects dirt on its surface or is deformed by the air flow leading to a changed resistance, lasers are subject to aging effects concerning their spectral properties or output power, laser mirrors degrade over time and humidity can condense and evaporate inside the measurement cell. All these factors will cause measurement errors, drift effects or a dependence of the sensor output on environmental conditions. Furthermore, the sensor signal conditioning will always generate additional uncertainties caused by temperature effects in the electronics or aging of electronic components. It is difficult to quantify these error sources separately, but periodic calibration of a sensor and testing in an environmental simulation chamber helps to determine the sum of these effects.

An experienced sensor operator is sometimes able to detect some of these effects during data processing and to trigger a respective calibration or investigation.

Calibration

Calibration is necessary to correlate the sensor output to a real physical unit by comparing the output signal of an instrument with a precise reference measurement of the respective unit. Frequent calibration is the key to achieve optimum accuracy beyond the specified values for a specific sensor because it can compensate effects like non-linearity or offset in the sensor output. Periodic calibrations will also help to detect and eliminate long term drift effects of an instrument.

The accuracy of a calibration is mainly determined by the reference sensor which itself requires a primary calibration from an official calibration laboratory (in Germany: Deutscher Kalibrierdienst, DKD) that can be traced to national standards from the national metrology institute (like the "Physikalisch Technische Bundesanstalt, PTB" in Brunswick, Germany).

The experimental setup which is used for the calibration causes additional uncertainties in the result: spatial inhomogeneities of the probe volume of a temperature calibration (liquid bath) in which temperature sensors are calibrated, the accuracy of the multimeter which is used for the resistance measurement of temperature sensors, the precision in the determination of the height difference between a sensor and the reference instrument in a pressure calibration or the quality of the pressure measurement which is used to determine water vapor mixing ratio from the dewpoint which is determined by the humidity reference sensor. Therefore, any calibration requires a detailed and precise analysis of the total accuracy which must include all possible error sources that have an impact on this result.

The complete calibration of an analogue sensor must include the data acquisition i.e. the accuracy of the analog to digital conversion (ADC) inside the data system.

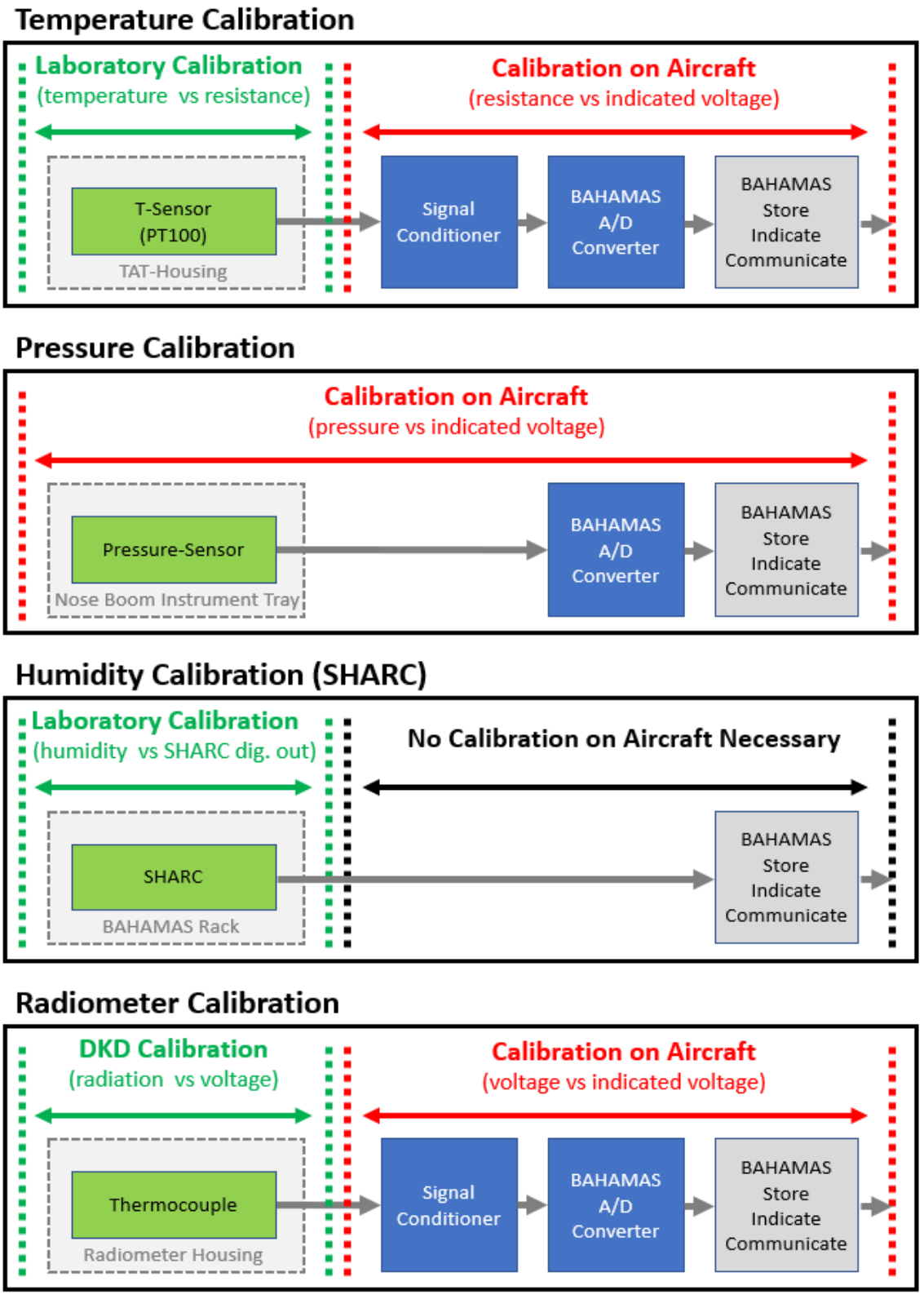

Figure 21: ***Different calibration procedures for sensors on HALO. For all analogue sensors the process has to include the data acquisition. In some cases, the calibration is performed as a two-step process.***

Therefore, if the calibration of a sensor cannot be performed directly at the aircraft the complete sensor calibration becomes sometimes a two-step process as shown in Figure 21.
However, if the sensor is an autonomous instrument which includes the digitization of the data the calibration can be performed completely in the laboratory. This is the case for the HALO water vapor sensor SHARC.

Data Processing

The stored raw data from the data acquisition is subject to an excessive data processing in order to determine the desired secondary data for scientific applications. The processing contains physical and mathematical formulas as well as parameterizations which were obtained from experimental data like wind tunnel testing or aircraft inflight calibrations. These dependencies are never error free as can be seen in the scatter of the experimental data which was used for these parameterizations. Examples are the inflight flow angle and pressure calibrations of the aircraft air data sensor [6], [7], [1] or the correction terms for recovery factor and anti-ice effects of the Total Air Temperature (TAT) housing which is used for the temperature measurement [8].
Other uncertainties are caused by the error contribution from the humidity data in the air density calculation and by the question how this calculation is performed if no humidity measurement is available. It is also important to decide which formula is used in the calculation of the water vapor saturation pressure and whether this value is related to water or ice.

Error Investigation: Error Propagation Calculation

As pointed out above systematic errors cannot be determined directly from the data of a measurement. An error analysis requires knowledge about all input errors for a measurement in order to determine their impact on the final result. The determination of this impact is called “error propagation calculation”.
If we assume that the result “S” of a measurement depends on a number of n input parameters x_i ($i = 0,1,..n$):

$$S = S(x_1, x_2, x_3, \dots, x_n)$$ **Equation 13**

and that an input parameter x_i is subject to a systematic error of σ_{x_i} a classical error propagation calculation estimates the impact of this error on the final result according to:

$$\sigma_S = \sqrt{\sum_i \left(\left(\frac{\partial S}{\partial x_i} \right)_{x_1, x_2, .., x_n} \right)^2 \cdot {\sigma_{x_i}}^2}$$ **Equation 14**

Where $\frac{\partial S}{\partial x_i}$ is the partial derivative of S with respect to x_i. According to Equation 14 the dependency of S on x_i is approximated by a linear relation which is then used to propagate the original error of x_i into S. This method is well established and robust. It works as long as the derivative of S with respect to any input parameter x_i can be determined.

However, the processing of aircraft data is rather complex. From Figure 2 and Figure 3 one can see that it consists of many processing steps including several matrix operations and complex formulas.

For this reason, a complete "traditional" error propagation calculation is usually not possible and error analyses of aircraft meteorological data typically represent rough estimations only. These estimates are usually based on significant simplifications of the data processing and ignore large portions of the real workflow.

In this work we propose a new method which applies true error propagation to the data. The method considers the complete data processing scheme and includes all known error sources.

True Error Propagation: White Noise Method

Basic Idea

In the above chapter on white noise we have learned that this kind of error propagates through the complete data processing scheme without losing its random character as long as no "temporal smearing" of data takes place. All original data processing steps are applied to the random error contributions of a specific unit. As long as there is no direct correlation between the different error input signals these white noise time series will contribute independently to the total random error of a secondary data unit according to Equation 11.
Therefore, the resulting white noise peak in the secondary data represents the superposition of the independent random error input signals from all raw data sources - properly scaled by the standard aircraft data processing.

The idea behind the new error propagation method is **to use artificial white noise as a "carrier" to propagate the amplitudes of systematic errors through the complete data processing into the secondary units**. This procedure ensures that the error values are handled like the real data and that they can be found properly scaled in the result of the data processing. The method was subject to a German patent in 2005 [4].

The procedure is similar to the above example where we used artificial white noise to demonstrate the impact of static pressure random noise on TAS:

1. An artificial random signal is generated at the exact location in the data processing where systematic errors get into the data. Examples are the scaling of raw data with the coefficients from the calibration at the beginning of the processing or the application of aerodynamic parameterizations in the calculation of flow parameters in the wind vector calculation.

2. The random signal amplitude is scaled with the standard deviation of the respective error.
3. The result is added to the original time series and the standard data processing continues.
4. At the end of the data processing an ACV analysis performed for the secondary units of interest. The white noise peak will deliver a total error which represents the superposition of all systematic errors which were added during the data processing.

Figure 22 visualizes the complete procedure. Due to the random character of the noise signal the method shows some similarities to a traditional Monte-Carlo simulation. The main difference is that the random data is applied "on the fly" directly to time series of experimental data.

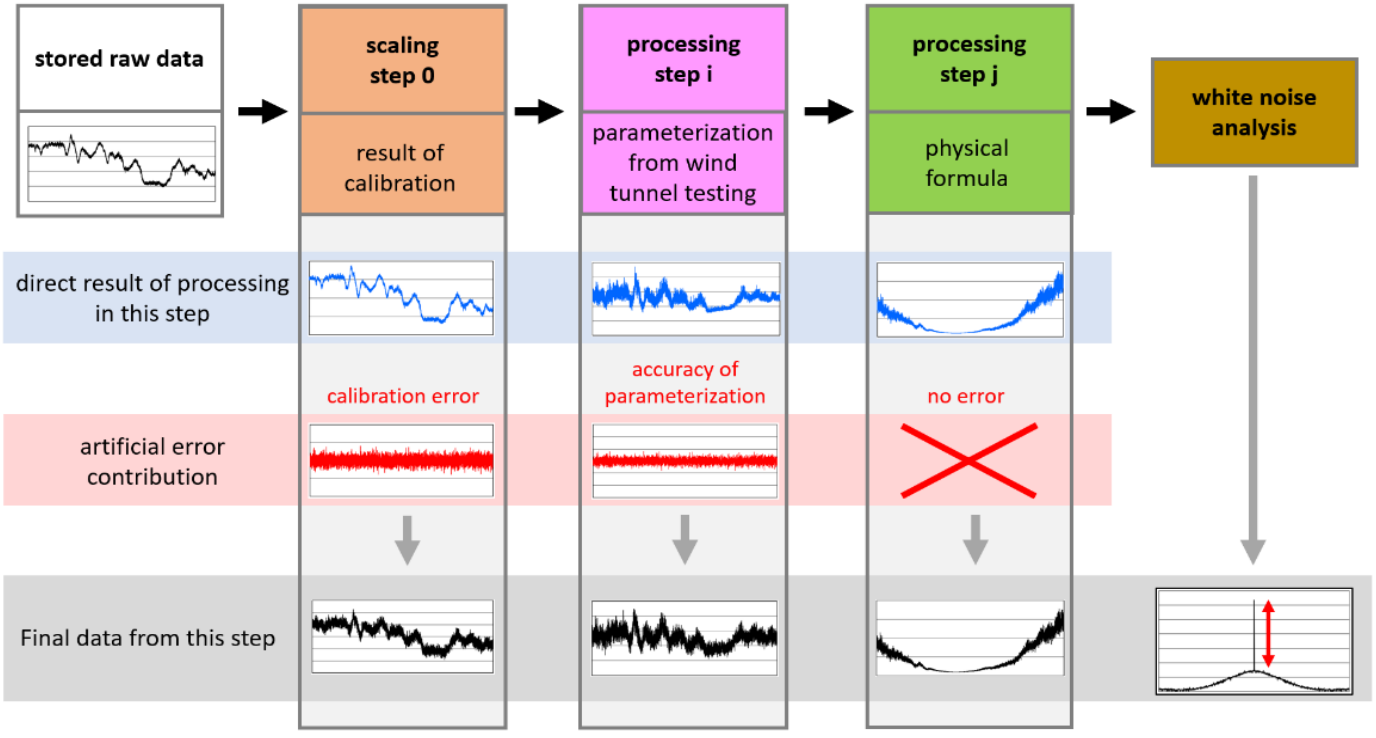

Figure 22*: Functional principle of the white noise error propagation method.*

The proposed error propagation method is based on some assumptions

- The error which is detected in the secondary data always represents the sum of the original random noise in the data and the contribution from systematic error sources. In principle it is possible to separate these two errors by comparing the data processing results before/after the application of the artificial random signal. However, this total error describes best the overall uncertainty of the final data.
- The method will not work properly when the data processing includes any kind of averaging or smoothing of data. In this case the white noise peak in the ACV will vanish and appear as a broadened maximum.
- The random signal contributions to the data must be completely independent from each other. The input to the IDL RANDOMN function contains a SEED value. This value allows (if chosen identically) to exactly reproduce a random signal. Different SEED values lead to completely independent random number arrays. Therefore, each error contribution has to use a separate SEED value. There is one exception in the HALO data from this rule which is explained below.
- The determination of the total error for a certain unit by means of the ACV requires data from a time interval of an adequate length. The error specification always refers to this interval. In order to get representative values for specific flight conditions, it is desirable that this interval is chosen for a time where the flight parameters do not change too much.

Possible Error Parameterizations

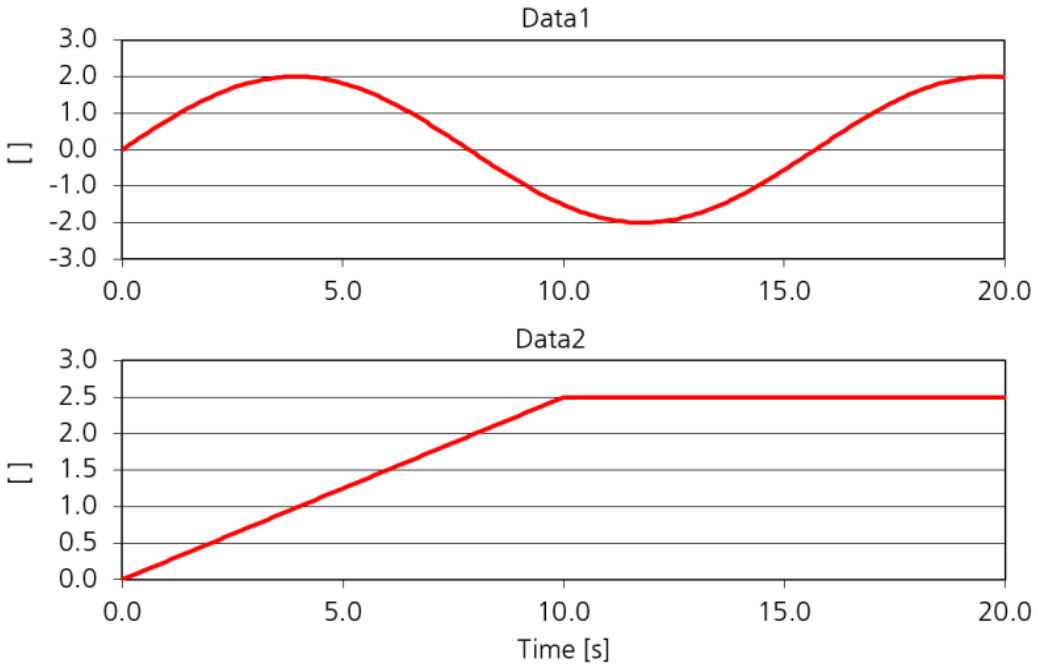

Figure 23*: Data time series used to demonstrate the different error models*

The amplitude of the artificial white noise which is added to the original signal represents the error of this specific unit. The determination of this scaling parameter depends on the kind of error which is considered. Based on the two test time series shown in Figure 23 we want to present the different error models which are used in the HALO error propagation calculation.

Absolute Error

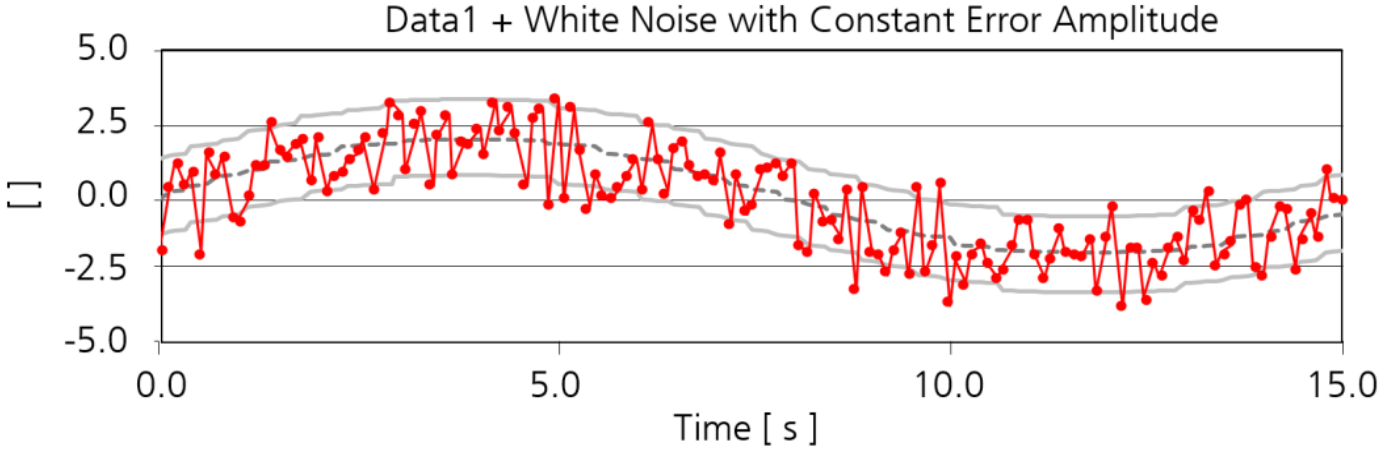

Figure 24*: Data1 + white noise contribution based on a constant error amplitude.*

If the error of a time series s_i is described by an absolute number $A_{s_{i0}}$ the random noise signal has to be scaled with a fixed amplitude $A_{s_{i0}}$ which is constant over the complete length of the time series.

$$s_{i,rn} = s_i + A_{s_{i0}} \cdot RANDOMN(Seed_i, m)$$

The resulting signal for the test data1 is shown Figure 24. An example for this kind of error on HALO is the result of a temperature calibration. In this case the error is mainly defined by the accuracy of the reference thermometer as determined by the DKD calibration which is a fixed value.

Relative Error

Sometimes the error is expressed as a fraction of the measured value. In this case the error is a relative error and the random signal has to be scaled with the original signal s_i and the relative error Amplitude A_{s_i}

$$s_{i,rn} = s_i + A_{s_i} \cdot s_i \cdot RANDOMN(Seed_i, m)$$

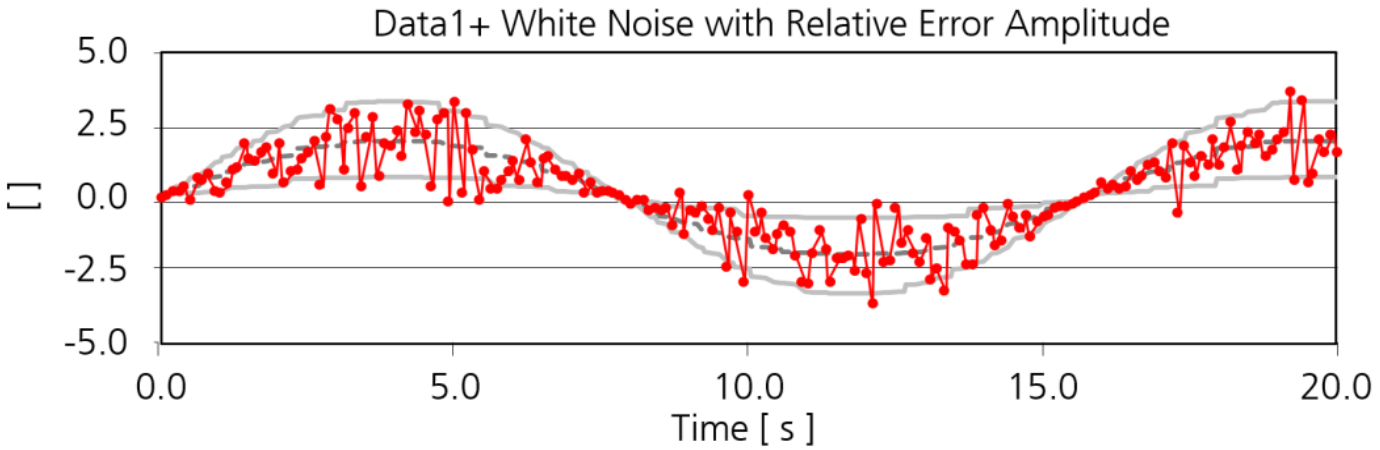

Figure 25*: Data1 + white noise contribution based on a variable error amplitude which is proportional to the original data (relative error).*

Figure 25 shows how the resulting signal. In case of the calibration of the SHARC humidity sensor on HALO the error is mainly given by the accuracy of the

calibration testbed HYGROSTAR which is expressed in a percentage of the measured value.

Error Dependence on Other Parameters

Sometimes the error of a measurement s_i is expressed as a function of another parameter $f(s_k)$.
In this case the random error signal must be scaled with this function:

$$s_{i,rn} = s_i + A_{s_i s_k} \cdot f(s_k) \cdot RANDOMN(Seed_i, m)$$

Figure 26 shows for the above test signals how the random error amplitude is determined in this case.

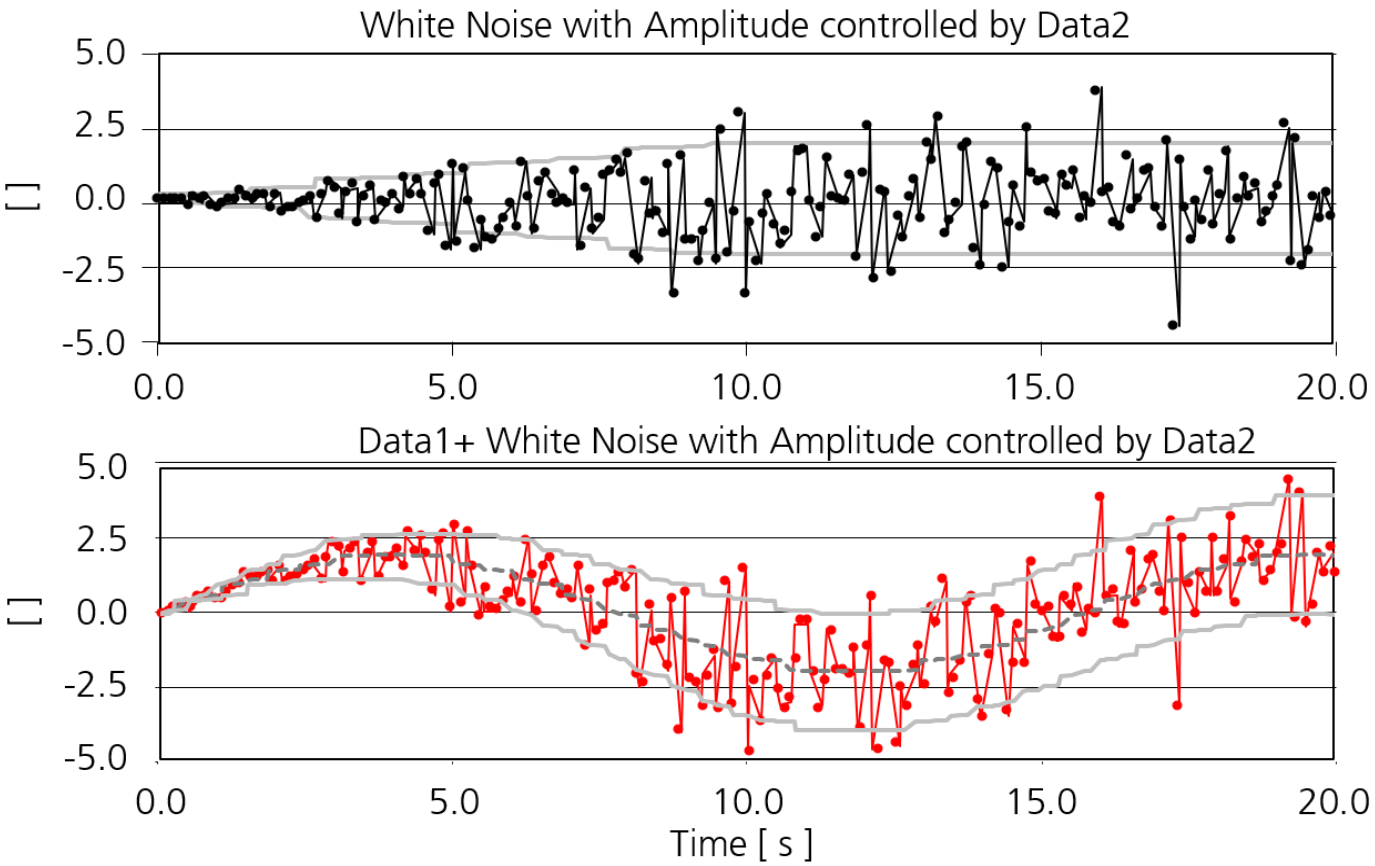

Figure 26*: Data1 + white noise contribution based on an error amplitude which is a function of another parameter (data2). The upper plot shows the white noise contribution only.*

An example for this kind of error is the uncertainty of the anti-ice correction for a temperature sensor which is located in a TAT housing. The required correction term was determined by wind tunnel tests and parameterized as a function of the Mach Number M_C. The respective uncertainty for this correction is also a function of M_C.

Correlated Errors

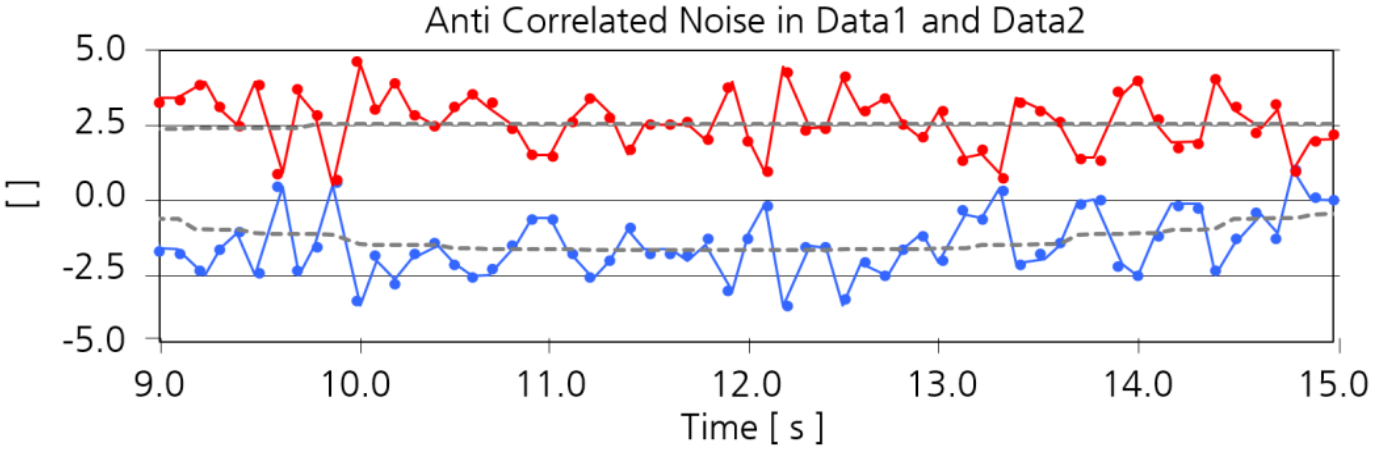

Figure 27*: Data1 and data2 + white noise contributions which are (anti-) correlated (same value but opposite sign).*

Sometimes a certain error source directly influences two different units in a correlated fashion. An example is the static source error correction of the HALO pressure measurement. This correction is added to the indicated dynamic pressure as measured by the nose boom but subtracted from the indicated static pressure [6]. Therefore, any error in this unit will always act in a correlated way on these two units. For a proper error analysis this relation must be considered:

$$s_{i,rn} = s_i + A_{s_{i,k}} \cdot RANDOMN(Seed_{i,k}, m)$$
$$s_{k,rn} = s_k - A_{s_{i,k}} \cdot RANDOMN(Seed_{i,k}, m)$$

Figure 27 shows how the random error time series look like for this case.

Implementation in RAMSES-II

The error propagation method was implemented in RAMSES-II by additional software modules in the standard processing algorithm which are activated when the program is operated in the "error mode" as one can see in Figure 28. This status is indicated by a global parameter which is checked by every routine. The random time series generation takes place at the locations in the program where the error occurs, the required error amplitude parameter is provided by a global structure which contains the different error contributions (amplitude, seed value, sign).

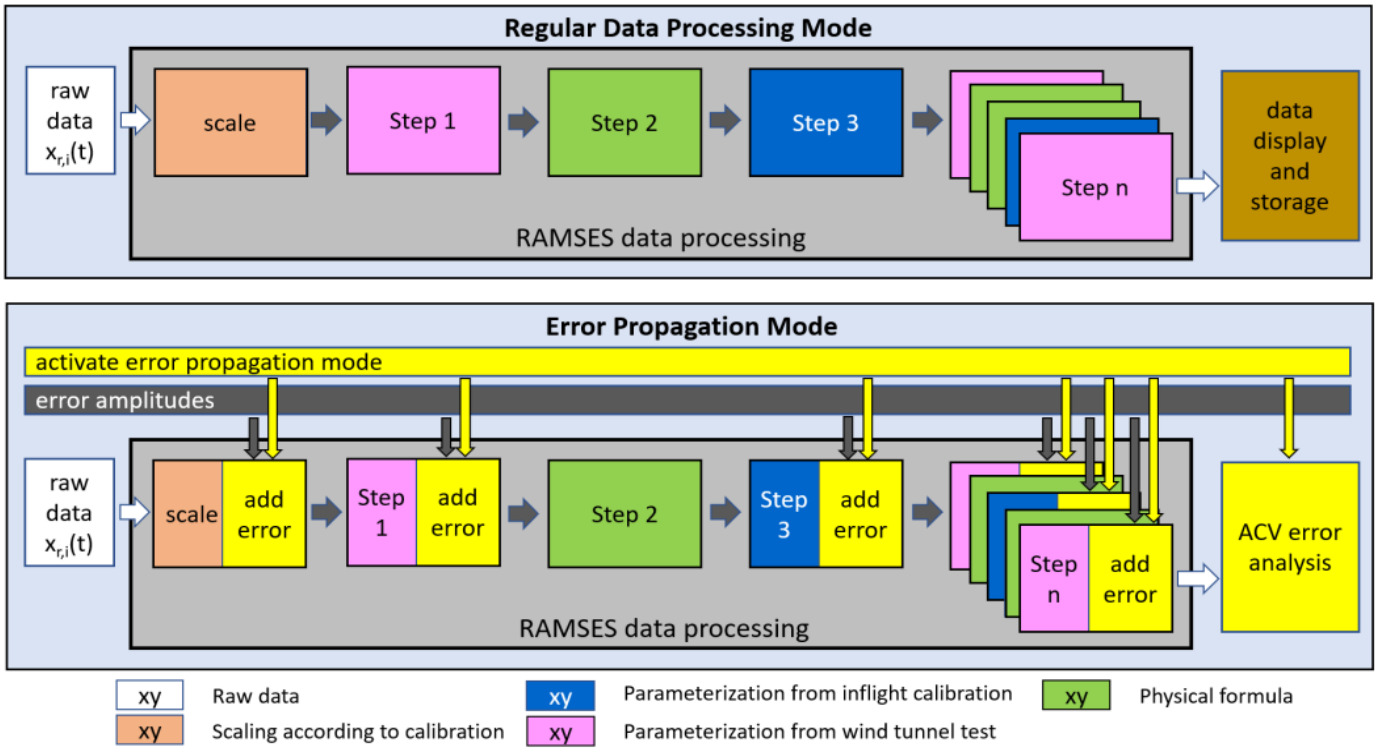

Figure 28*: Implementation of error propagation in RAMSES-II. In the "error propagation mode" the program adds random noise contributions throughout the data processing and finishes with an ACV analysis of the secondary data time series for a selected time interval of the flight.*

The final determination of the total error from the result of the data processing is achieved by means of the ACV. The desired total error value was determined

similar to Equation 9 i.e. by the simple difference of $ACV_s(0)$ and $ACV_s(2)$ (which turns out to be more representative/stable than $ACV_s(1)$). The error evaluation starts with an overview plot of the flight in which the program operator can mark the time interval of interest by a simple mouse click.

By changing the input error configuration file is also possible to separately switch different error sources on and off. This allows to analyze the impact of a single error source on the final result.

Error Sources for HALO Aircraft Data

Before the determination of errors with the new method can be performed it is necessary to determine realistic inputs for the different error sources. The following chapter evaluates the respective data. All errors which are listed in the following represent **1 σ values**.

Sensor/Instrument Errors

Pressure Sensors

Unit concerned:

Primary data:

- indicated static pressure ($p_{S,i}$)
- indicated dynamic pressure (qc_i)
- indicated α and β differential pressures ($dp_{\alpha,i}$, $dp_{\beta,i}$)
- pressure at capacitive humidity measurement (p_{hum})
- pressure inside SHARC measurement volume (p_{SHARC})

Error determined by:

Pressure calibration. The accuracy is mainly limited by the reference instrument, a Ruska 7750i Air Data Test Set (ADTS) [12] which shown in Figure 29. The accuracy of this transfer standard can be seen in Figure 30.

Figure 29: ***The pressure transfer standard Ruska 7750i which is used for all pressure calibrations of the HALO nose boom sensors.***

Additional minor contributions to this error concern changing environmental conditions during the calibration, the precision of the pressure control during readout, pressure sensor random output and the accuracy of the "zeroing procedure" during the initialisation of the ADTS.

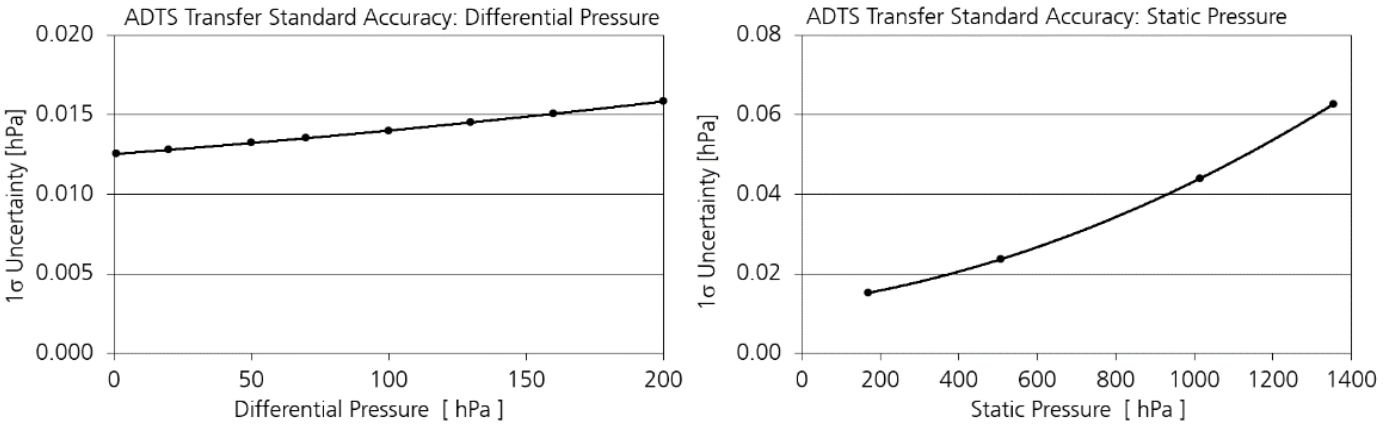

Figure 30: ***Accuracy of the pressure transfer standard Ruska 7750i from [12]. The plot shows the 1σ combined uncertainty of linearity, hysteresis, repeatability, thermal effects one-year drift stability and the uncertainty in the primary standard, which includes the uncertainty from the national standard.***

A complete calibration of all pressure sensor of the nose boom is performed before every HALO campaign directly at the aircraft as a one step process which includes the complete BAHAMAS data acquisition.
The result of a nose boom static pressure calibration on HALO can be seen in [6] while [7] shows the result from a calibration of the angle of attack differential pressure sensor.

The temperature sensitivity of the pressure sensors was tested in an environmental simulation chamber in the Flight Experiment Facility which is shown in Figure 31. The Test Facility covers a temperature range between -70°C and +180°C and a pressure between 1 hPa and 1000 hPa for a test volume of 0.8 x 0.8 x 0.75 m^3 which corresponds to approx. 500 l.

Figure 31: ***Environmental simulation chamber.***

Error value

The accuracy of the pressure calibration and the influence of temperature on the pressure sensor is estimated as an absolute error with an amplitude of

- 8 Pa for the indicated static pressure ($p_{S,i}$)
- 6 Pa for the indicated dynamic pressure (qc_i)
- 5 Pa for the indicated α and β differential pressures ($dp_{\alpha,i}$, $dp_{\beta,i}$)
- 10 Pa for the pressure at the capacitive humidity measurement (p_{hum})
- 8 Pa for the pressure inside the SHARC measurement volume (p_{SHARC})

Error Application:

The error contribution from the sensor calibration is added to the time series directly after the scaling of data before the actual data processing starts (Procedure init_noise in tools.pro)

Temperature Sensors

Unit concerned:

Primary data:

- indicated temperature of PT100 temperature sensors in TAT housings ($T_{s,i}$)
- Temperature at capacitive humidity measurement (T_{hum})
- Temperature inside SHARC measurement volume (T_{SHARC})

Error determined by:

Temperature calibration. A temperature sensor calibration is performed before every HALO campaign.

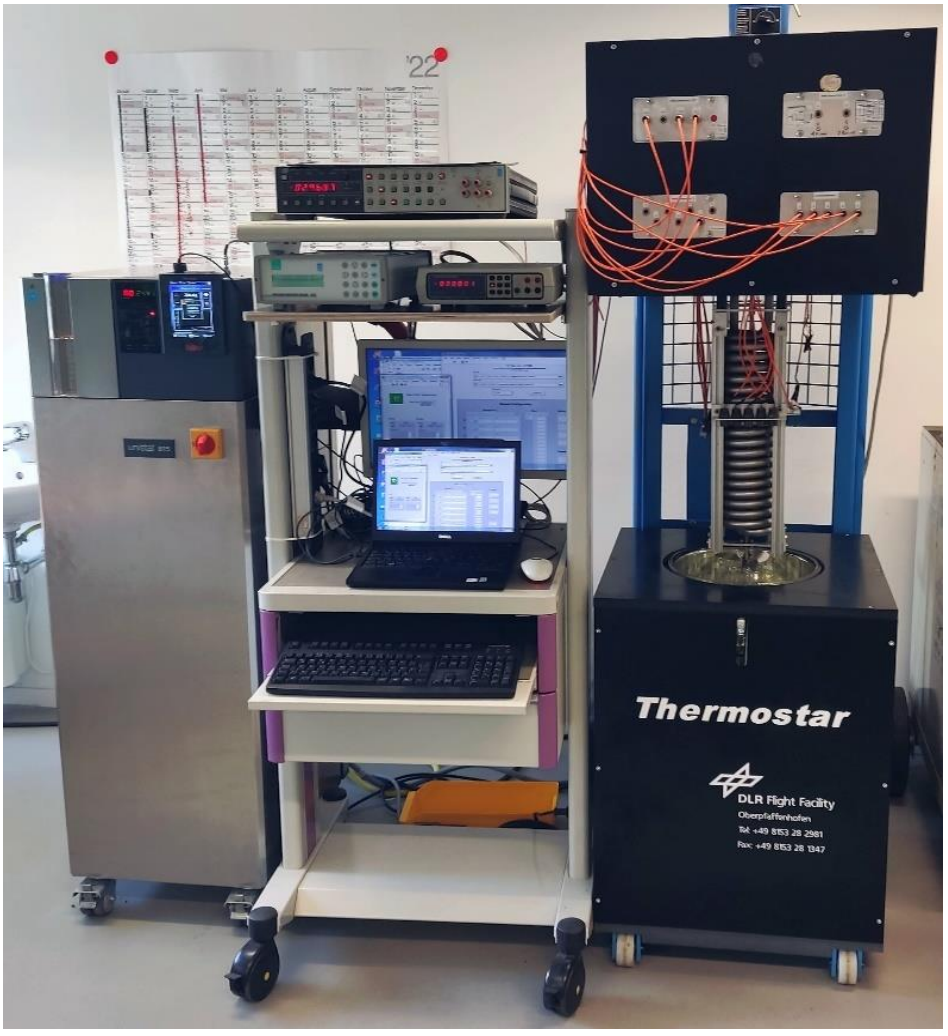

Figure 32: ***Temperature calibration testbed THERMOSTAR.***

Temperature calibration is performed as a 2-step process with a laboratory calibration of the sensor itself (temperature vs. resistance) and a signal path calibration on the aircraft (resistance vs. voltage) which covers the Pt100 signal conditioner and the BAHAMAS data system (ADC) according to Figure 21. The laboratory calibration uses the THERMOSTAR calibration bench which was developed by DLR Flight Experiments. It is shown Figure 32. Figure 33 shows the principle of operation.

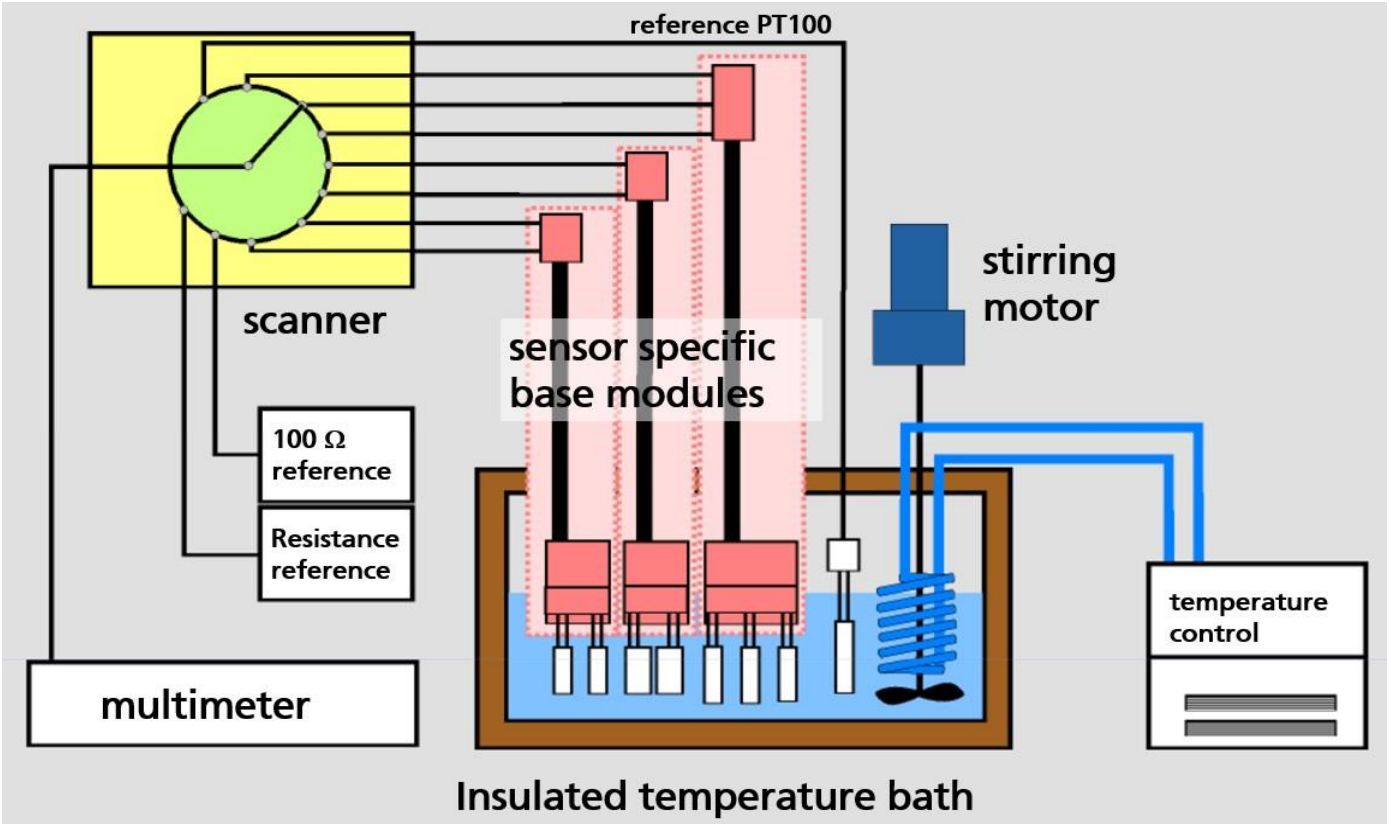

Figure 33: ***Temperature calibration testbed THERMOSTAR: principle of operation***

The laboratory calibration of the sensors is based on a stirred immersion bath with a high precision quartz PT100 sensor as reference (Heraeus PW-EZ 100). The Heraeus PW-EZ 100 is a high precision ultra-stable secondary standard PRT that is calibrated against primary standards on a regular base. The resistance of the device under test (DUT) and the PW-EZ 100 are measured with an 81/2 digits

multimeter HP 3455A and compared to a programmable high precision resistance decade Burster 1427. The decade is again calibrated on a regular base against national standards and is also used as the reference for the signal path calibration on the aircraft. The temperature of the calibration bath is controlled by a Huber Unistat 815w from -80°C to +50°C with a stability of a few mK. The system is fully automated and computer controlled.
The overall accuracy of the whole measurement chain from sensor to the data acquisition system includes temporal and spatial stability of the bath, accuracy and aging of the reference PRT, accuracy of the decade, contact voltages, variance and accuracy of DUT reading as well as the accuracy of the data fit. The two-step temperature calibration on HALO achieves a typical accuracy of 40 mK for the sensor calibration (first step) and about 30 mK for the data acquisition calibration (second step).

Error value

The total accuracy of the temperature calibration is estimated as an absolute error with an amplitude of 0.1K. This value contains the temperature sensitivity of the sensor signal conditioner on the aircraft. This error specification is the same for all temperature sensors on HALO.

Error Application:

The error contribution from the sensor calibration is added to the data directly after the scaling of data before the actual data processing starts. (Procedure init_noise in tools.pro)

Humidity Sensors

Unit concerned:

Primary data:

- SHARC mixing ratio

Error determined by:

Humidity calibration. A complete humidity sensor calibration is performed before every HALO campaign in the laboratory as a one step process which includes the complete SHARC data acquisition.

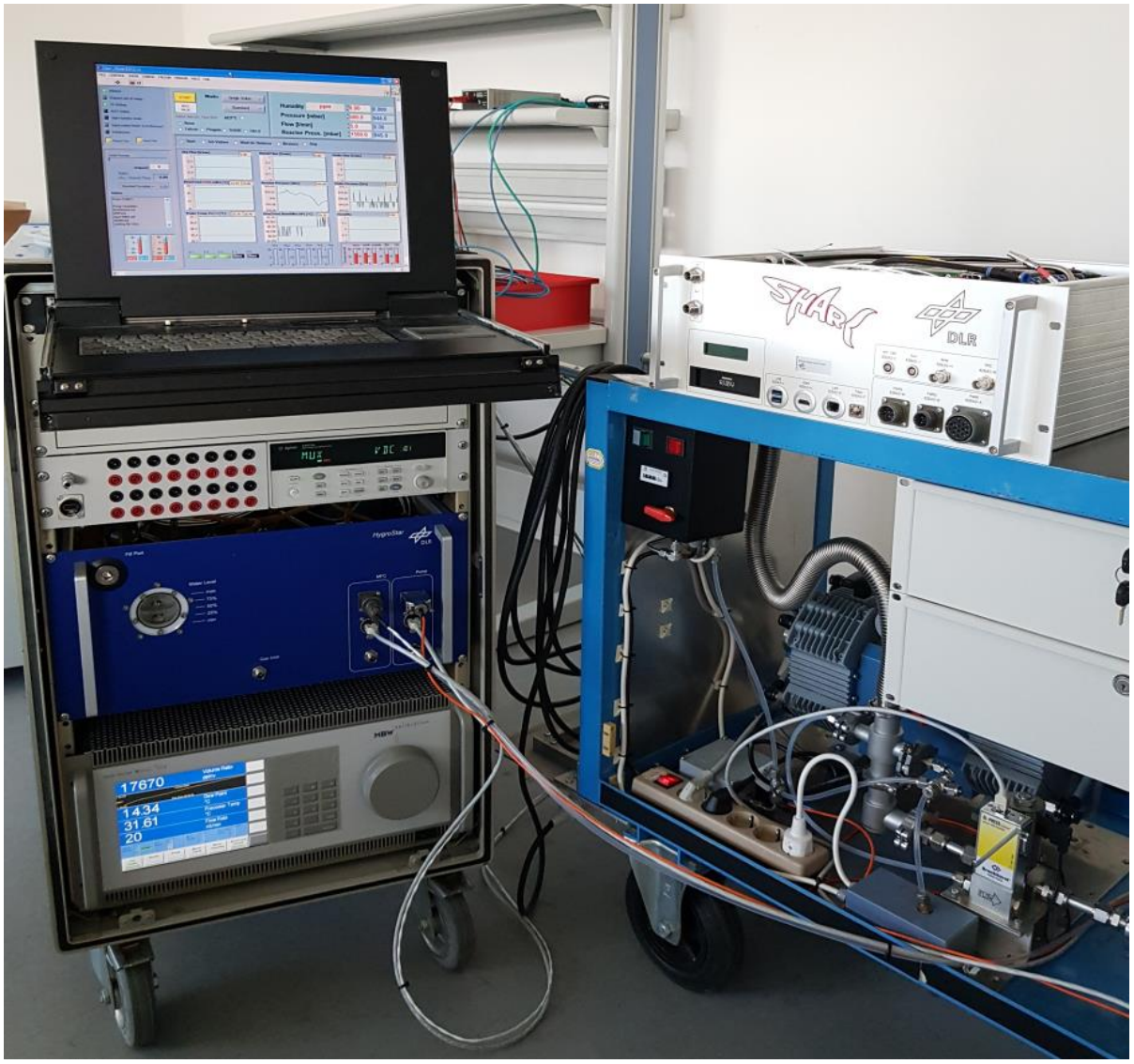

Figure 34: ***Humidity calibration testbed HYGROSTAR.***

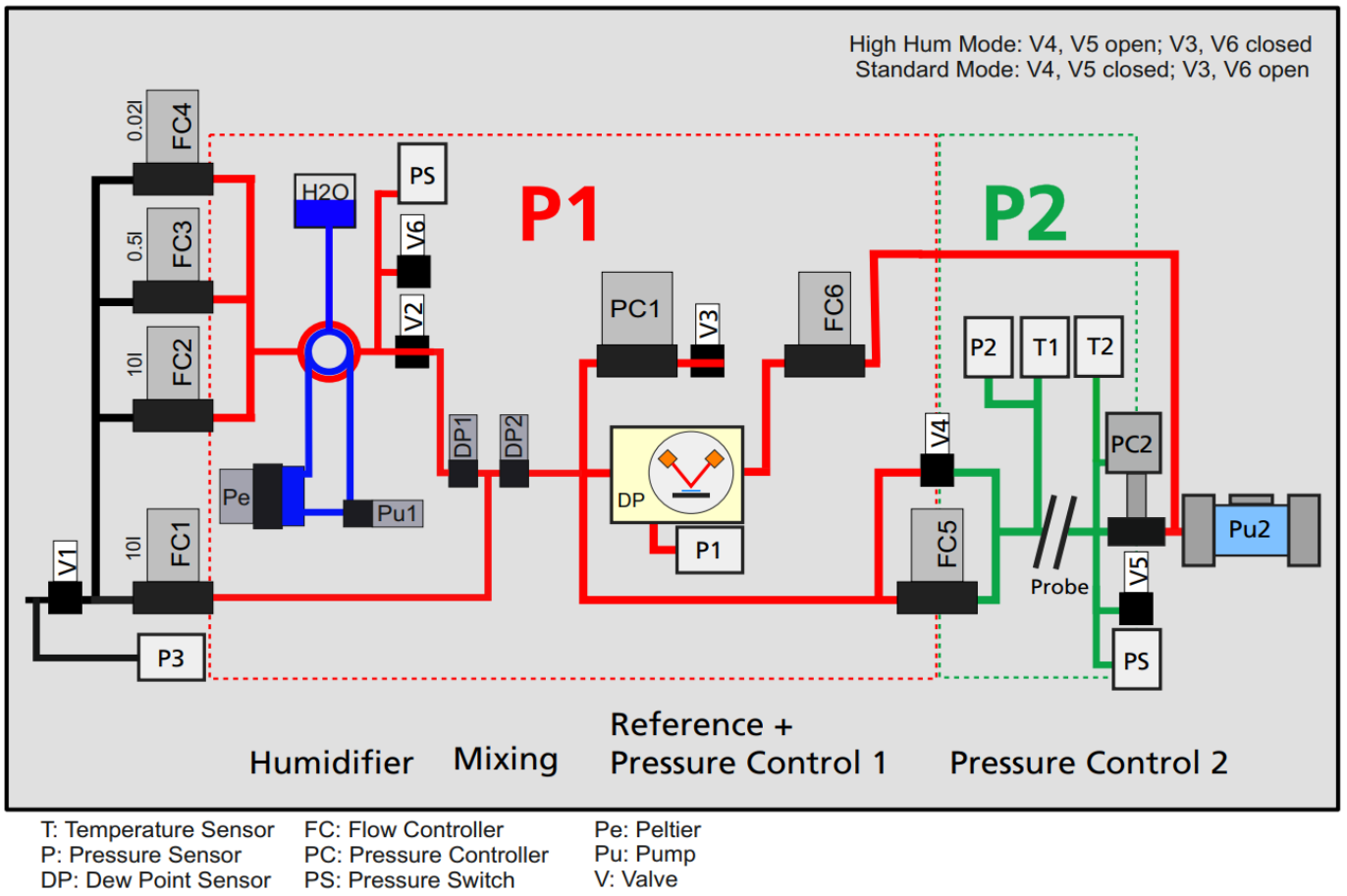

Figure 35: ***Humidity calibration testbed HYGROSTAR: principle of operation.***

The humidity calibration uses the HGROSTAR calibration bench which is also a complete DLR-FX development. The calibration setup is shown in Figure 34. Figure 35 visualizes the principle of operation.

The humidity calibration is based on the mixing of a wet and a dry air flow by electronic flow controllers (FC1 – FC4 in Figure 35) and the simultaneous measurement of the resulting humidity with a reference dew point hygrometer (MBW 373 LX) as the transfer standard with an accuracy of 2-3% in mixing ratio or 0.3K in dew point. Dry synthetic air from a standard 200l gas bottle is used as 'carrier' gas which is humidified by a Nafion permeation tube. The wide range of reachable humidity levels is achieved by combining several flow controllers with different ranges and a two-pressure system which separately controls the pressure inside the mixing and reference unit as well as of the device under test (DUT). To

avoid condensation inside the system the DUT pressure, temperature, flow and humidity are continuously monitored by the software. The system is fully computer controlled and runs autonomously. The calibration bench allows to simulate the whole troposphere and lower stratosphere regarding humidity (2..30000 ppmv) and pressure (1300..150 hPa).

Error value

The accuracy of the SHARC humidity measurement is estimated as a relative error of 5% with a lower limit of 1ppm.

Error Application:

The error contribution from the sensor calibration is added to the data in the humidity calculation procedures (Procedure scale_humvai in aircraft.pro and calc_sharc2 in aircraft.pro)

Attitude and Speed Measurement

Unit concerned:

BAHAMAS contains an experimental Inertial Reference System (IRS) AEROconrol III which is manufactured by the Ingenieur-Gesellschaft für Interfaces (IGI) in Kreuztal/Germany [3]. The system consists of a compact Inertial Measurement Unit (IMU-IIe) and a Sensor Management Unit (SMU) which contains the GNSS receiver. The required GNSS antennae are installed on the HALO upper fuselage. The SMU is part of the main BAHAMAS data acquisition system in the aircraft cabin. The IMU-IIe sensor head is certified for temperatures down to -55°C and altitudes of 55,000ft and located very close to the nose boom [7].

Error determined by:

The error in the speed and attitude data of the IRS is specified by the manufacturer in the technical description of the system and displayed in Table 1.

Position [m]	0.05
Velocity [m/s]	0.005
Roll/Pitch [deg]	0.003
True Heading [deg]	0.007
Max. data rate [Hz]	400

Table 1: ***Performance of the AEROcontrol-III experimental IRS onboard HALO. The specified accuracies refer to postprocessed data.***

Calibration and functional tests are performed regularly to ensure the proper performance of the system and to detect any degradation of instrument components. Furthermore, the postprocessing applies sensible quality checks to the data which helps to detect technical problems very early.

In the past there was an ongoing discussion about the error specification for the heading data and possible problems of the Kalman filter especially for long

straight flight legs with no turns. Turns are important for the filter to work properly and to minimize the heading errors. The system performance stated in Table 1 was only demonstrated for typical earth observation flight patterns which contain many heading changes. Therefore, HALO was upgraded in 2022 with a dual antenna GNSS option which provides an independent heading reference for the post processing.

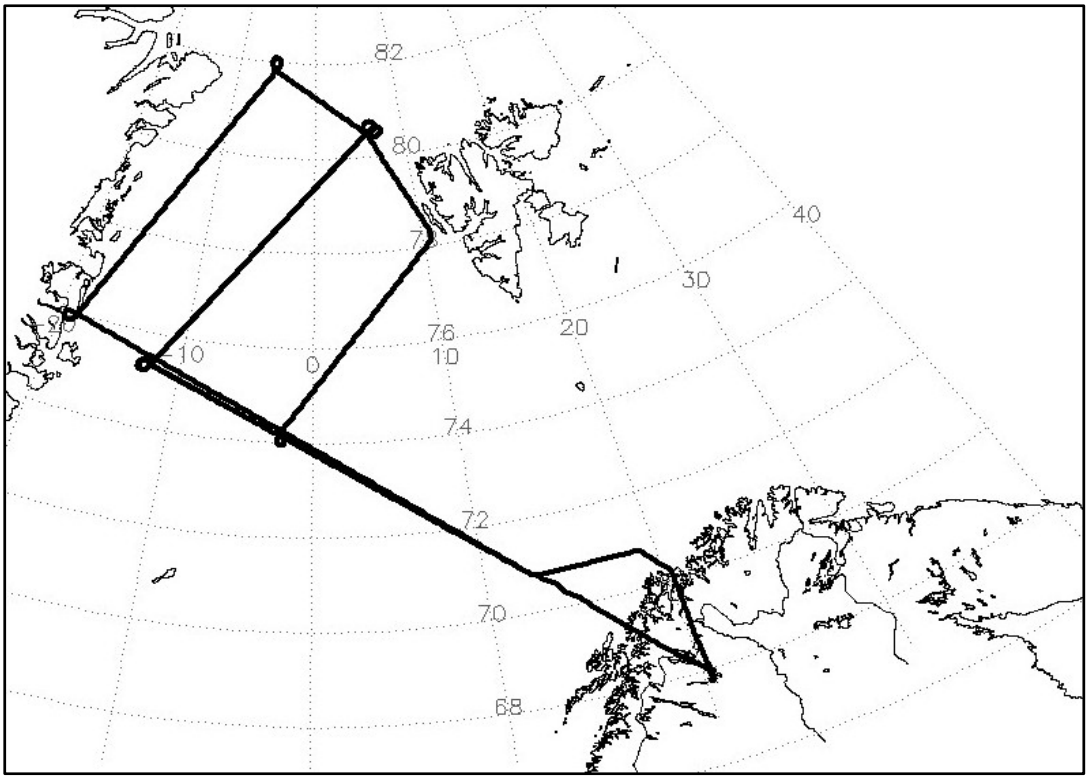

Figure 36: ***Aircraft flight track for the research flight #7 of the (AC)³ campaign.***

As an example, we present data from a flight of the (AC)³ campaign [9] which took place in Kiruna, Sweden, in March and April 2022. Figure 36 shows the flight track of a 9-hour mission flight from March 20th 2022. As one can see the flight focused on a North Atlantic region between Iceland and Greenland. It contained long flight legs with constant heading and only a few turns between them. Figure 37 compares the different heading data from BAHAMAS with a reference value which was calculated from the IGI data by using the new GNSS dual antenna heading reference.

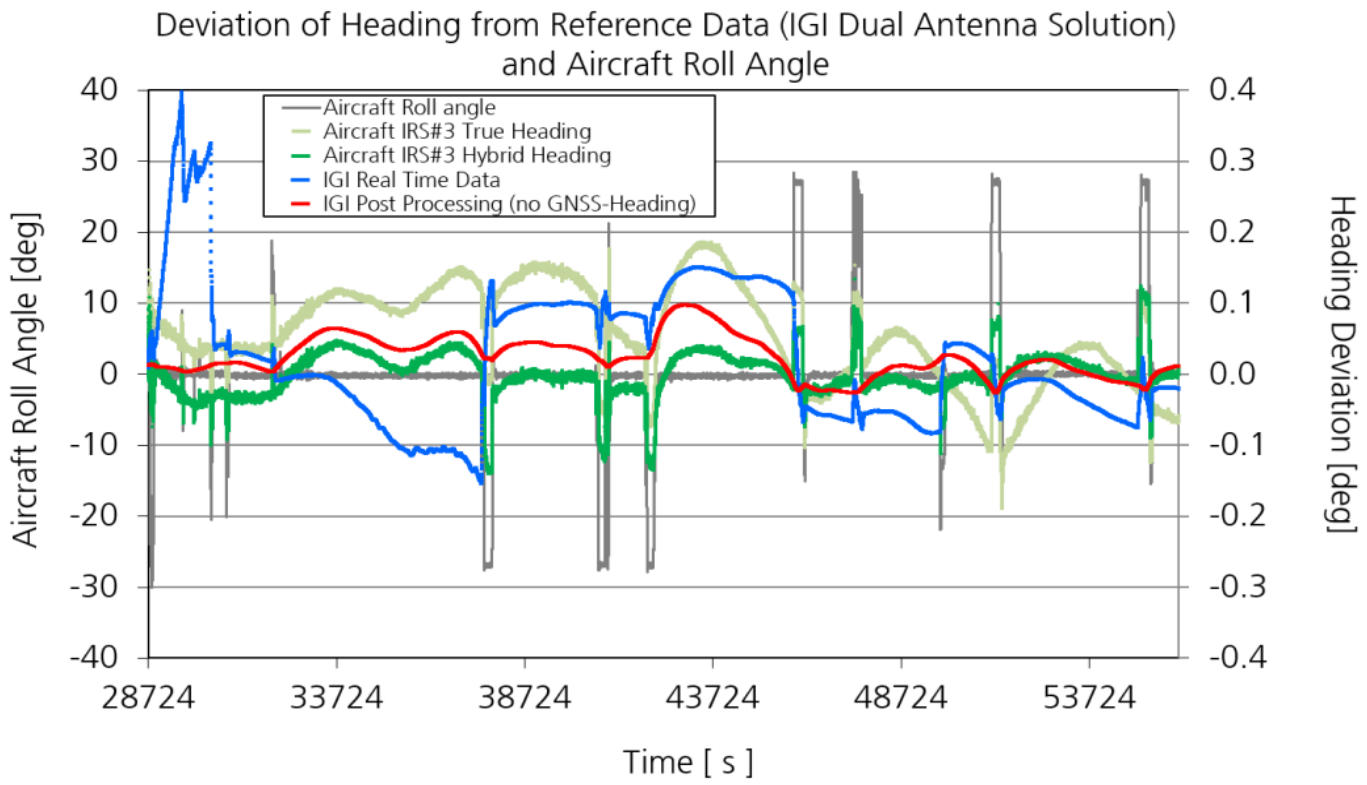

Figure 37: ***Deviation of the different aircraft heading data sources from the reference value of the IGI IRS-system which was post processed using a GNSS heading reference from the dual antenna system on HALO. The data set represents the complete flight pattern shown in Figure 36. The roll angle is plotted in order to indicate turns in the aircraft track.***

The different heading data shown in Figure 37 are

- the real time heading data from the IGI system which is available during flight and which is not subject to any kind of post processing
- the IGI data which was subject to a "standard" post processing which did not use the GNSS dual antenna heading information
- the heading which is provided by one of the three standard aircraft IRS systems (true heading)
- the hybrid heading from the same aircraft IRS which is subject to an online Kalman filter

As one can see the observed deviations from the reference heading are significant. Especially the standard IGI post processing solution shows relatively large

deviations (of up to 0.1°) from the reference data which clearly exceed the error limits from Table 1. The analysis of other (AC)[3] flights confirmed this observation. The aircraft standard IRS is equipped with very accurate sensors (ring laser gyros und Q-flex quartz accelerometers) and uses a real time Kalman Filter which provides an excellent heading information (but worse timing characteristics than the IGI system). Figure 37 suggests that the IGI post processing solution which is based on the GNSS-heading reference can be seen as the best reference data.

We can therefore conclude that the official IGI performance data in Table 1 can only be achieved for flights with many heading changes and that long straight flight legs require the additional GNSS heading reference which can only be provided by using a dual antenna configuration, i.e. the errors stated in Table 1 are valid for this configuration only.

Error value

The accuracy of the above listed IRS units is given by absolute values according to Table 1. From this table the accuracy of the rotational rates is estimated to be 0.005°/s.

Error Application:

The error contribution from the sensor calibration is added to the data directly after the scaling of data before the actual data processing starts. (Procedure init_noise in tools.pro)

Processing/Parameterization Errors

Pressure: Static Source Error

Unit concerned:

Indicated static ($p_{S,i}$) and dynamic (qc_i) pressure

Error determined by:

The static source error (SEE) was determined during an inflight calibration experiment with a Trailing Cone. The error is parameterized as a function of the indicated Mach number. The complete experiment and the respective data are subject to a separate report [6]. Figure 38 shows the result and the error of the SSE correction.

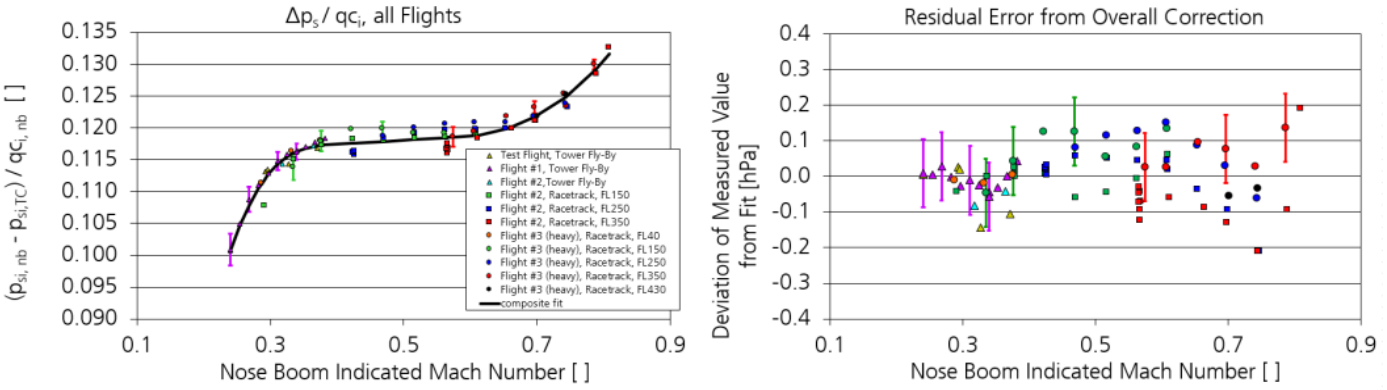

Figure 38: ***Result of the Static Source Error calibration on HALO from [6]. The data was acquired with a Trailing Cone***

The static source error determination assumes a constant total pressure in the aircraft environment. Therefore, the SSE is applied with a negative sign to the indicated static pressure $p_{S,i}$ and added as a positive value to the dynamic pressure qc_i. This means that a systematic error of the SSE always acts in a correlated way on these two pressure values.

Error value

The uncertainty of the SSE correction was determined in [6] with an absolute value of 8Pa.

Error Application:

The noise is added during the static source error correction (Procedure press_corr in aircraft.pro) as a correlated random noise to the indicated values of static and dynamic pressure.

Pressure: Flow Angle Dependence

Unit concerned:

The indicated values of the static ($p_{S,i}$) and dynamic (qc_i) pressure are subject to a set of corrections which include static source error and additional aerodynamical effects. The flow angle dependence is one of these corrections and acts on an already corrected value of $p_{S,i}$ and qc_i.

Error determined by:

The dependence of the static pressure measurement on the flow angles was investigated during the inflight calibration of the nose boom mounted airflow sensor on HALO which is described in [7]. Figure 39 shows the result from this experiment for the angle of sideslip.
Please note that the dependence of static pressure on the angle of attack is already contained in the static source error correction as explained in [7].

Error value

The accuracy of the static flow angle pressure correction is described by an absolute value of 8 Pa according to [7]. The noise signal is applied as a correlated random noise to the indicated values of static and dynamic pressure.

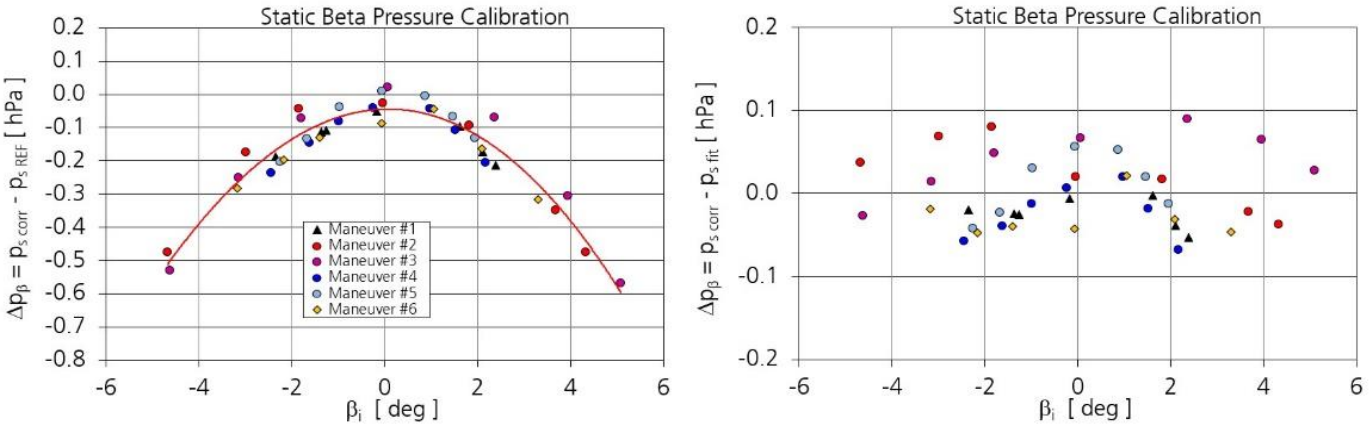

Figure 39: *Beta: flow angle static pressure correction* from [7].

Error Application:

The noise is added during the pressure correction routine which applies the different aerodynamic corrections to $p_{S,i}$ and qc_i. (Procedure press_corr in aircraft.pro).

Flow Angle

Unit concerned:

The true flow angles "angle of attack" α and "angle of sideslip" β are calculated from their indicated values α_i and β_i.

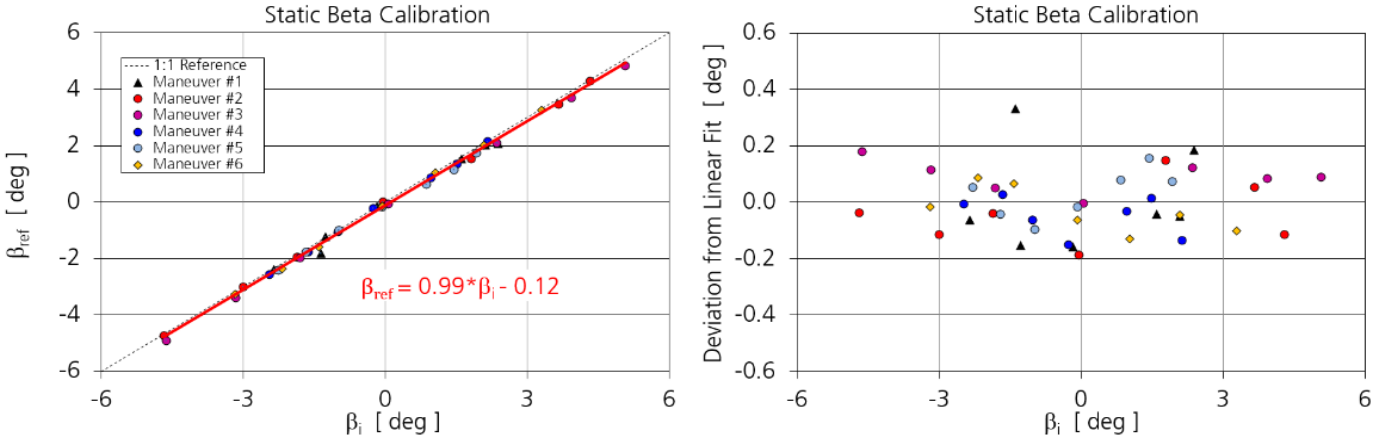

Figure 40: *Beta: Result of static flow angle calibration from* [7].

Error determined by:

The scaling of β is based on the results of an inflight calibration which is described in [7]. Figure 40 shows the result from this report.

The calculation of α from α_i is subject to a procedure which is described in detail in [7]. Two inflight calibration techniques are available for this calculation:

- the static α calibration from regular flight data
- the dynamic offset calibration

Figure 41 shows the result from these two techniques for a single HALO flight.

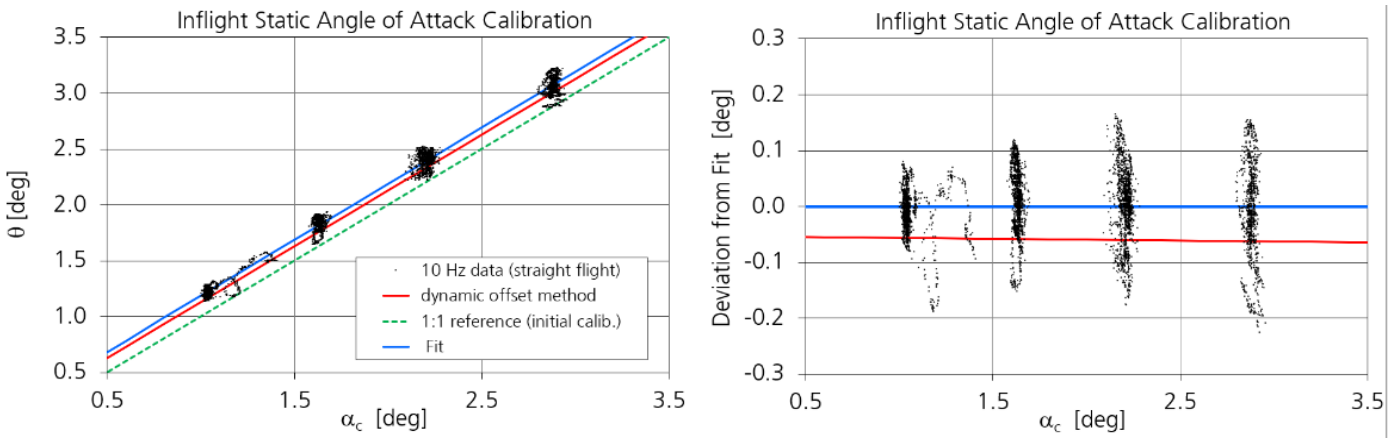

Figure 41: *Alpha: Static calibration and dynamic offset calibration from regular flight data from* [7].

Error value

The error in the scaling of β is described by an absolute value of 0.11° according to [7].

The estimation of the α calibration error is based on many years of experience in the processing of HALO data. Both evaluation techniques are applied to each flight and the final data processing is always based on a "best choice" between these two methods. The parameters found in the fit and in the α offset method are stored in a data base in order to determine the variability of these values and to check for drift effects or "conspicuous" results. Based on these statistics the error

of the static α calibration from regular flight data is estimated to be 0.08° and chosen to be identical for the dynamic offset calibration method (best choice).
Please note that the indicated flow angle values are already subject to the random noise contribution from the pressure sensors which are used to determine the indicated values.

Error Application:
The error signal is applied to the processed values of α and β after the scaling.
The random noise is added after the flow angles are calculated from their indicated values (Procedure calc_alpha_beta in aircraft.pro)

Flow Angle Dynamic Correction

Unit concerned:
The indicated flow angles at the 5-hole probe are subject to a correction which is based on an inflight calibration procedure that applies dynamic yaw and pitch maneuvers to the aircraft. Possible systematic errors concern the two correction factors k_α and k_β for the indicated flow angles as well as the determination of a unit called the "trimmed alpha" ($\alpha_{i,trim}$).

Error determined by:
The flow angle dynamic correction was determined by inflight calibration using dynamic maneuvers. The exact procedure and the respective results for HALO are described in [7].
The respective data processing corrects the deviations of the indicated flow angles α_i and β_i from their "typical" values which are 0 for β_i and a value called trimmed alpha ($\alpha_{i,trim}$) for α_i. These deviations are corrected with the two calibration factors k_α and k_β which are parameterized as a function of the indicated Mach number M_{Ci}. Systematic errors in this correction concern the values of k_α and k_β as well as the accuracy in the determination of $\alpha_{i,trim}$.
If the correction is not applied the error analysis has to estimate the resulting uncertainty.

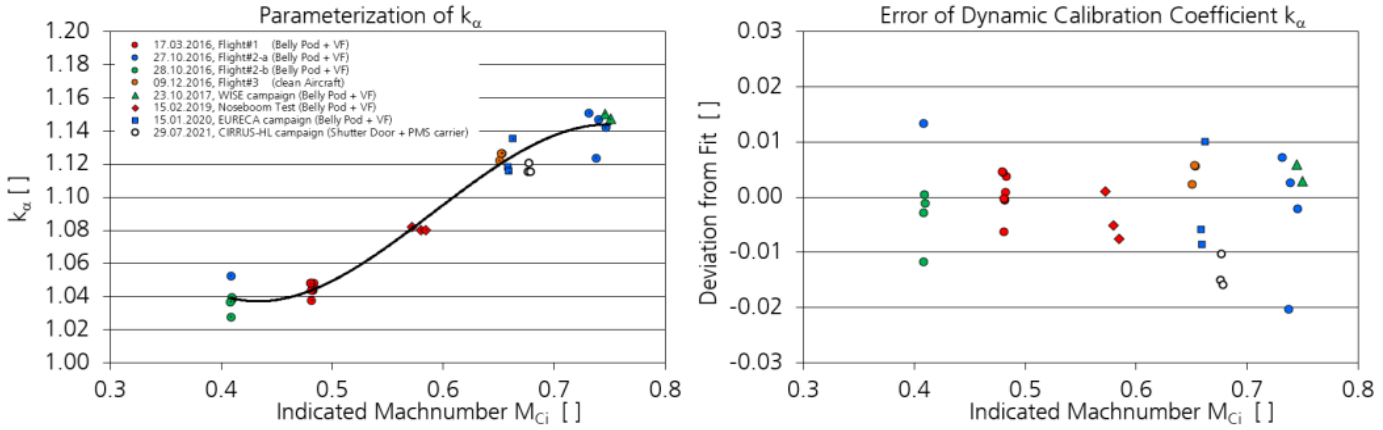

Figure 42: *Correction factor k_α for the dynamic angle of attack correction from* [7].

Error value

The assumed error due to the dynamic calibration depends on the applied data calculation scheme:

1. no dynamic correction is applied. This is in general the case for standard data processing with 10Hz, since it is impossible to determine a trimmed alpha $\alpha_{i,trim}$ along the complete length of a flight. In this case the error amplitudes are determined according to:
   - $(k_\beta - 1) \cdot \beta_{i,S}$ where $\beta_{i,S}$ is the indicated angle of sideslip which is smoothed over some seconds.
   - $(k_\alpha - 1) \cdot (\alpha_{i,S} - \alpha_{i,trim,tc})$ where $\alpha_{i,S}$ is the smoothed indicated angle of attack and $\alpha_{i,trim,tc}$ a parameterized value for the trimmed angle of attack from trailing cone flight data.
2. the dynamic correction is applied: In this case the uncertainties of the correction factors are determined from Figure 42 and Figure 43 as absolute errors:
   - k_β : 0.006
   - k_α : 0.007

In this case an additional error for the uncertainty in the determination of $\alpha_{i,trim}$ from qc_i has to be considered. It is estimated as a relative error of 5%.

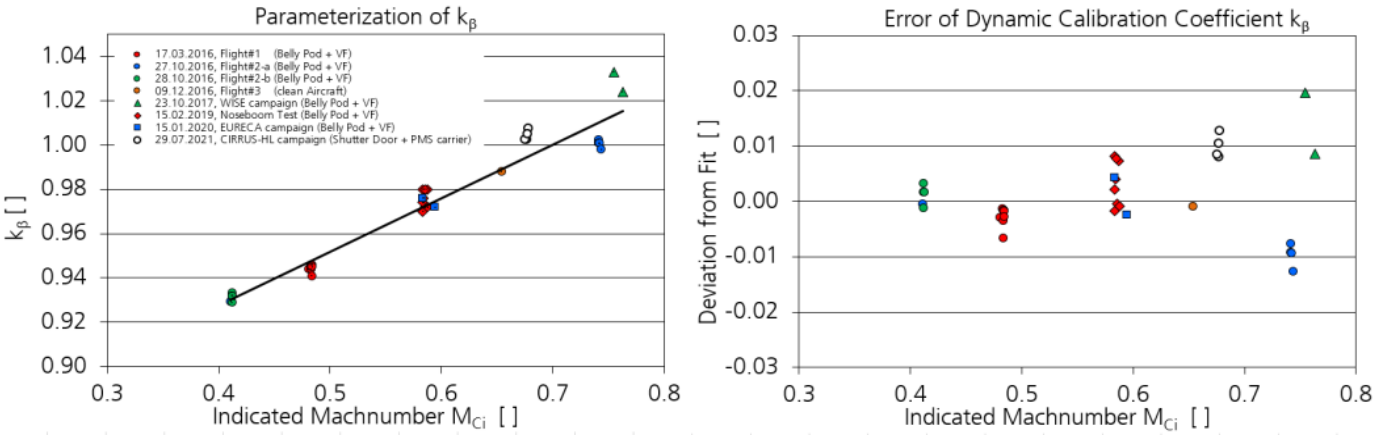

Figure 43: *Correction factor k_β for the dynamic angle of sideslip correction from* [7]

Error Application:

1. The error is applied directly after the calculation of the indicated flow angles before any other processing step is applied to the data (Procedure calc_alpha_beta in aircraft.pro)
2. The errors of k_α and k_β and $\alpha_{i,trim}$ are applied directly to these units during the correction process. (Procedure calc_alpha_beta in aircraft.pro)

Pressure: Flow Angle Dynamic Pressure Correction

Unit concerned:

Indicated static ($p_{S,i}$) and dynamic (qc_i) pressure during the pressure correction process.

Error determined by:

The respective error was determined by inflight calibration using dynamic maneuvers. The exact procedure and the respective results for HALO are described in [7].

Error value

The natural variability of α is largest inside a turbulent boundary layer. For the example of a boundary layer flight presented in [7] (EMeRGe intercomparison flight, 13.07.2017) we find a standard deviation of 0.6° for α_i and β_i. According to Figure 44 and Figure 45 this corresponds to a static pressure uncertainty of

- 5 Pa from α -variations
- 3 Pa from β - variations

Error Application:

The noise is added during the pressure correction routine which applies the different aerodynamic corrections to $p_{S,i}$ and qc_i. (Procedure press_corr in aircraft.pro).

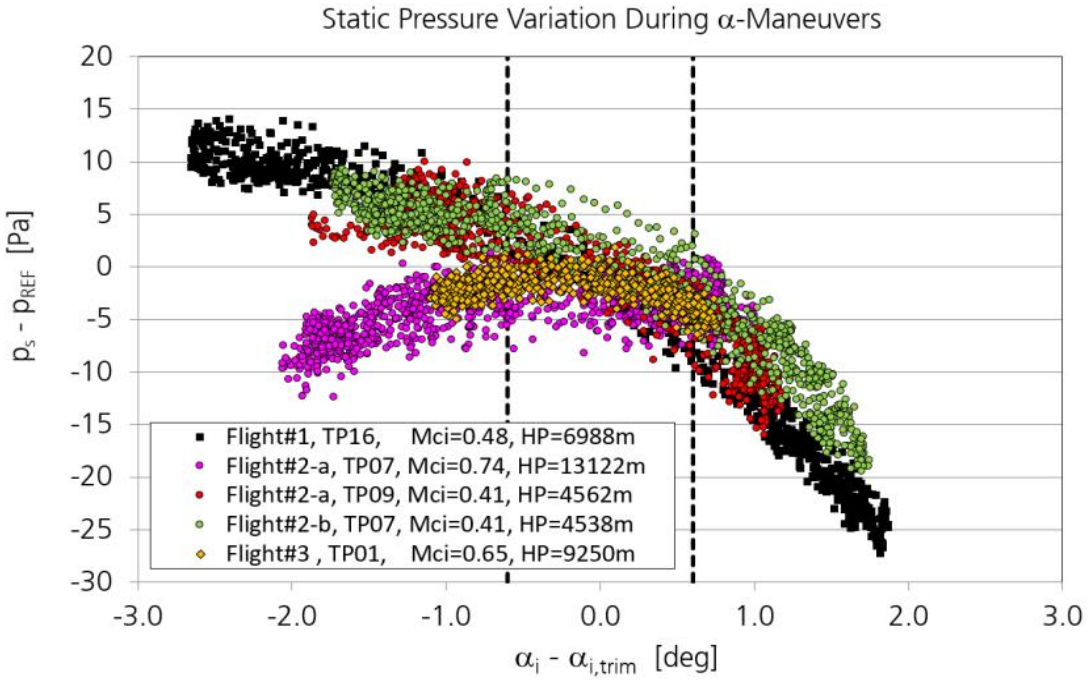

Figure 44: *Static Pressure dynamic flow angle correction from* [7] for angle of attack α. *The dashed lines indicate the typical data range of α_i caused by wind fluctuations during a flight in a turbulent boundary layer.*

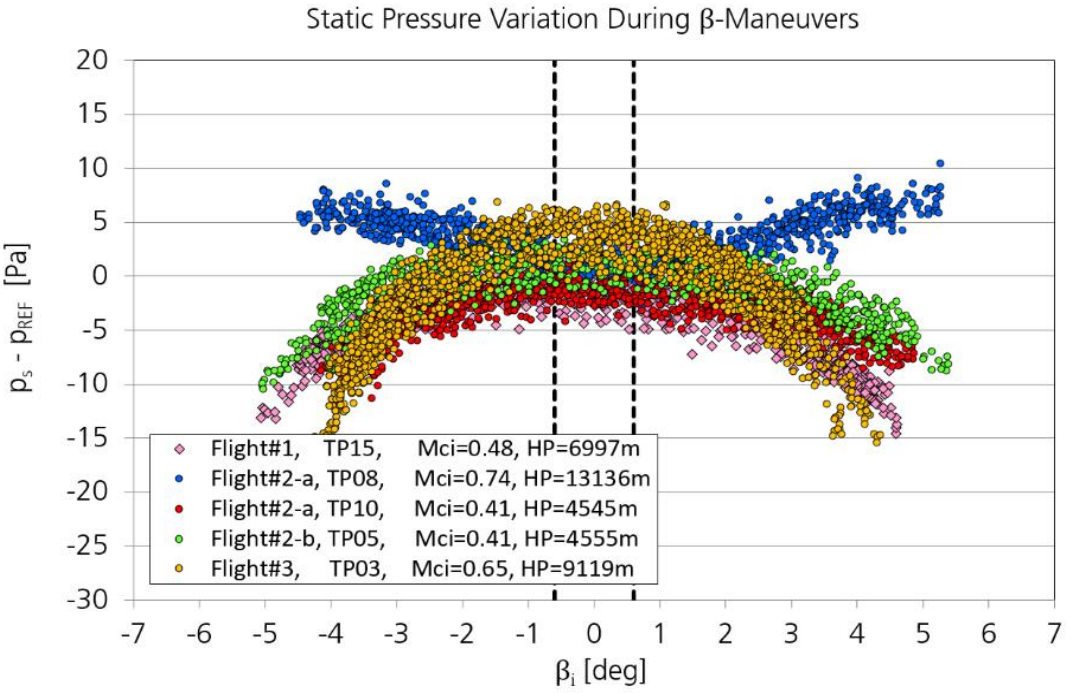

Figure 45: ***Static Pressure dynamic flow angle correction from*** **[7] for angle of sideslip β.** ***The dashed lines indicate the typical data range of β_i caused by wind fluctuations during a flight in a turbulent boundary layer.***

Temperature: Recovery Correction and Deicing Error

Unit concerned:

The indicated temperature $T_{S,i}$ in a Total Air Temperature (TAT) housing is subject to two corrections which concern

1. the deviation of this temperature from the theoretical TAT ("recovery correction") and
2. the influence of the heating element inside the housing on the temperature measurement (the element prevents icing effects on the housing).

Error determined by:

The TAT housings which are used on HALO are known as Rosemount Type BW 102 (Later: Goodrich Aerospace, today Collins Aerospace). They were subject to excessive wind tunnel testing by the manufacturer. The results from these experiments and the aerodynamical corrections which are necessary to determine

the static air temperature from the indicated temperature data are documented in the a report which is provided by the manufacturer [8].
According to this document the static temperature T_S is calculated according to:

$$\frac{T_r}{T_S} = 1 + \mathrm{r} \cdot \left(\frac{\gamma-1}{2}\right) \cdot {M_C}^2 \qquad \textbf{Equation 15}$$

with
r : recovery factor
γ : ratio of specific heats
T_r : recovery temperature

The recovery temperature T_r is the "adiabatic value of local air temperature on each portion of the aircraft surface due to incomplete recovery of the kinetic energy". It is related to the measured temperature $T_m (= T_{S,i})$ which is "the actual temperature as measured, which differs from T_r because of heat transfer effects due to imposed environments". One of these effects is the deicing error.

As shown in [8] the recovery factor is given by:

$$r = 1 - \eta \cdot \left[1 + \frac{2}{(\gamma - 1) \cdot {M_C}^2}\right] \qquad \textbf{Equation 16}$$

with
η : recovery correction

From Equation 15 and Equation 16 we find

$$T_S = \frac{T_r}{(1 - \eta) \cdot \left[1 + \frac{\gamma - 1}{2} \cdot {M_C}^2\right]} \qquad \textbf{Equation 17}$$

The recovery correction η has to be determined by wind tunnel experiments. The results from these tests are also provided by [8]. Figure 46 shows the results.

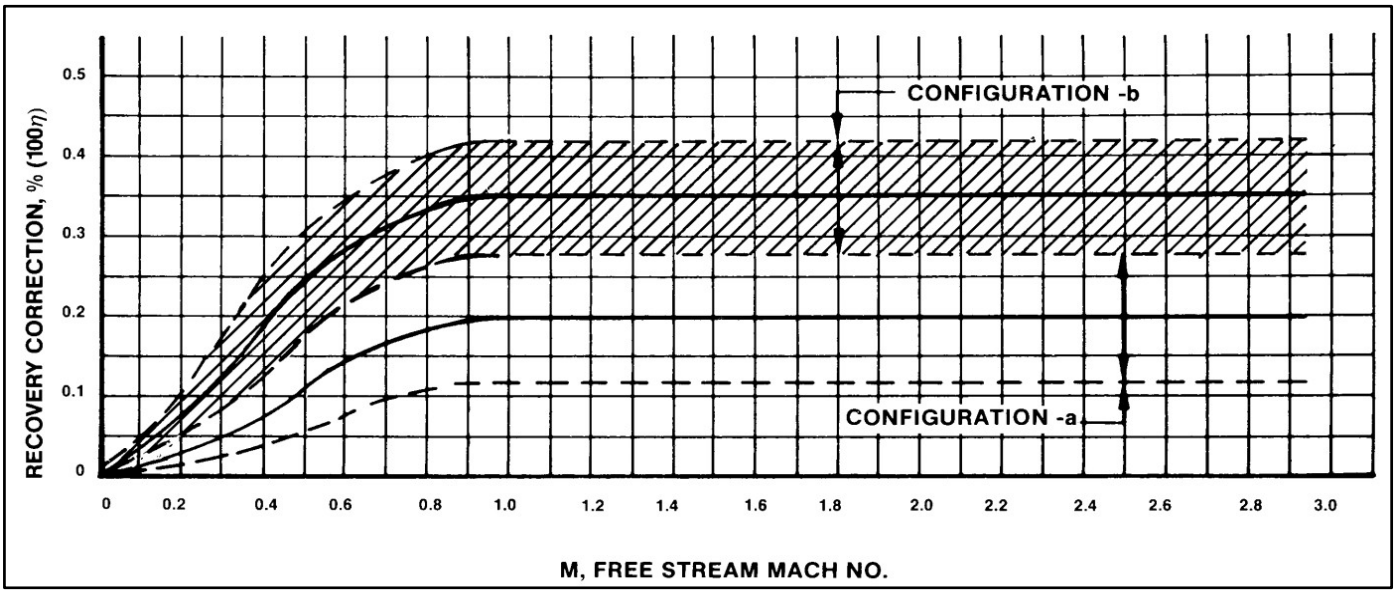

Figure 46: ***Recovery correction η with error bars from wind tunnel data (Model 102, configuration b) from [8].***

The relation between T_r and $T_{S,i}$ is described by the deicing correction which is a function of the parameter Z that can be calculated according to:

$$Z = M_{C,1} \cdot \frac{\rho_1}{\rho_0}$$ **Equation 18**

with
$M_{C,1}$: Mach number at sensor inlet
ρ_0 : air density at standard conditions
ρ_1 : air density at sensor inlet

Since air density and Mach number cannot be measured at the sensor inlet during flight the parameter Z is calculated from the free stream values.

The deicing correction itself was determined by wind tunnel testing. The result and the respective error bars can be seen in Figure 47 which is taken from [8].

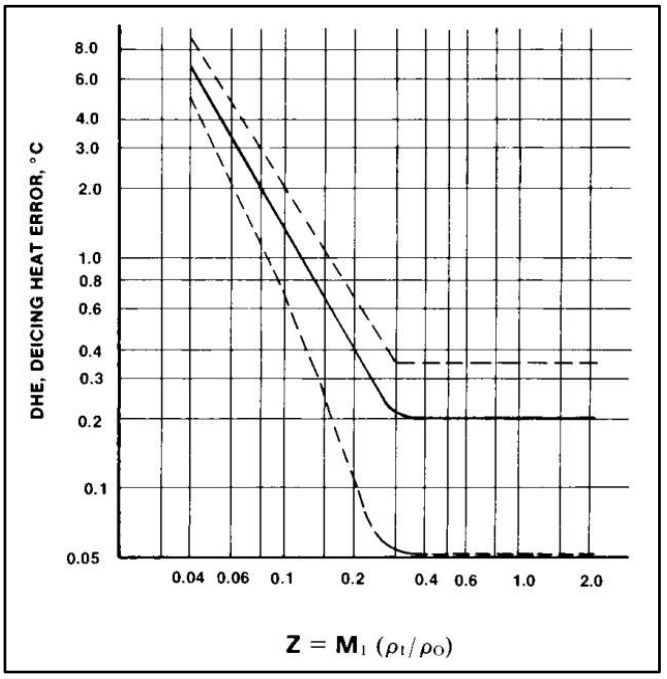

Figure 47: ***Deicing heat errors for Model 102 sensors with error bars (Model 102, single mandrel construction) from [8].***

Error value

The error bars used for the recovery correction η and the deicing correction are taken directly from the plots in Figure 46 and Figure 47.

It is clear that these error values also have to cover the known variability in:

- the shape of the TAT housings within the manufacturing tolerances. These differences become obvious when comparing single housings with each other.
- the design of the temperature sensor itself which concerns the heat shield and the sensor element shape. Different sensor designs have been available by the manufacturer in the past.
- the power consumption of the deicing heater element and the exact location of this element in the housing

Therefore, the above errors of the temperature measurement represent a worst-case scenario. First inflight investigations of the deicing effect on HALO indicate that the real values are smaller than the numbers presented in the TAT report.
One way to obtain smaller errors for a single housing would be an individual determination of both effects either in a wind tunnel or by inflight trials. Both possibilities are presently discussed. The effect of a smaller error is also addressed in the final error analysis.

Error Application:
The error is applied in the routine which calculates T_S from $T_{S,i}$ and performs the deice correction (Procedure temp_corr in aircraft.pro).

Sensor Random Noise

A "natural" error contribution to the measured basic data on HALO is the random noise which generated by the different BAHAMAS sensors and the data acquisition. For the proposed error propagation method this error is automatically contained in the final error which is determined by the ACV. We conclude that the final result of this error propagation method is always the combination of statistical and systematic errors.
However, as shown above the random noise is generally very small for BAHAMAS signals. Therefore, the final error mostly represents the systematic error contributions to the measurement.

Error Analysis for HALO BAHAMAS Data

As shown above most inputs to the BAHAMAS error calculation depend on flight parameters like speed and aircraft altitude as well as on atmospheric parameters like the pressure or temperature of the atmosphere around the aircraft.
In order to provide representative results, we selected three different flight scenarios which mainly differ in the aircraft altitude ("low", "mid", "high").
Additionally, we want to investigate the effect of changing error inputs caused by two different scenarios:

- The first case concerns a scenario with an improved temperature measurement where recovery correction and deice correction are better understood ("improved temperature"). In this case we assume that the respective error inputs (for recovery and anti-ice corrections) are only 50% of the present values.
- A second scenario investigates the effect of a heading information which is less accurate than the values stated in Table 1 ("bad heading"). In this case the heading error input is increased by a factor of 10.

The respective results of the error calculation are always listed in comparison with the original results ("standard") which uses the error inputs described above. The following error analysis is always based on 10Hz data and all error specifications represent $1\,\sigma$ data.
The error investigation was performed for a research flight from the CAFE-EU campaign which took place on June 9th 2020 above southern France and Spain. The flight covered a lot of different flight states with respect to aircraft altitude and speed. Figure 48 shows the aircraft flight track while Figure 49 plots the most important flight parameters and the selected time intervals for the error analysis.
The result of the error calculation for the different flight scenarios is displayed in Table 2, Table 3 and Table 4.
The "standard" error analysis assumes that the aircraft heading data is the result of post processed IGI data which uses a GNSS Heading reference from a dual antenna configuration and that the accuracies stated in Table 1 are valid.

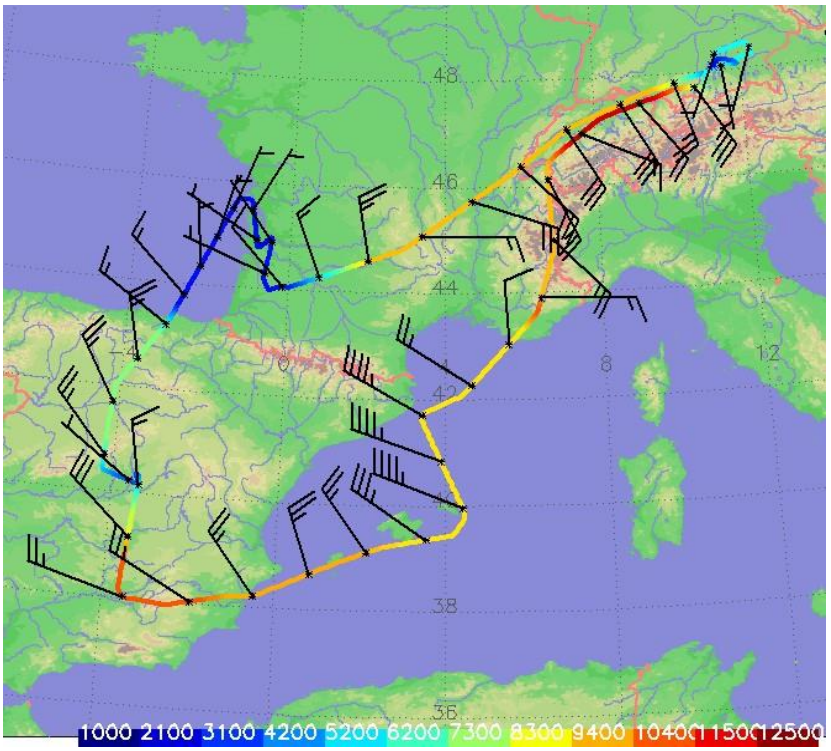

Figure 48: ***Flight track for the CAFÉ-EU flight from June 9th 2020.***

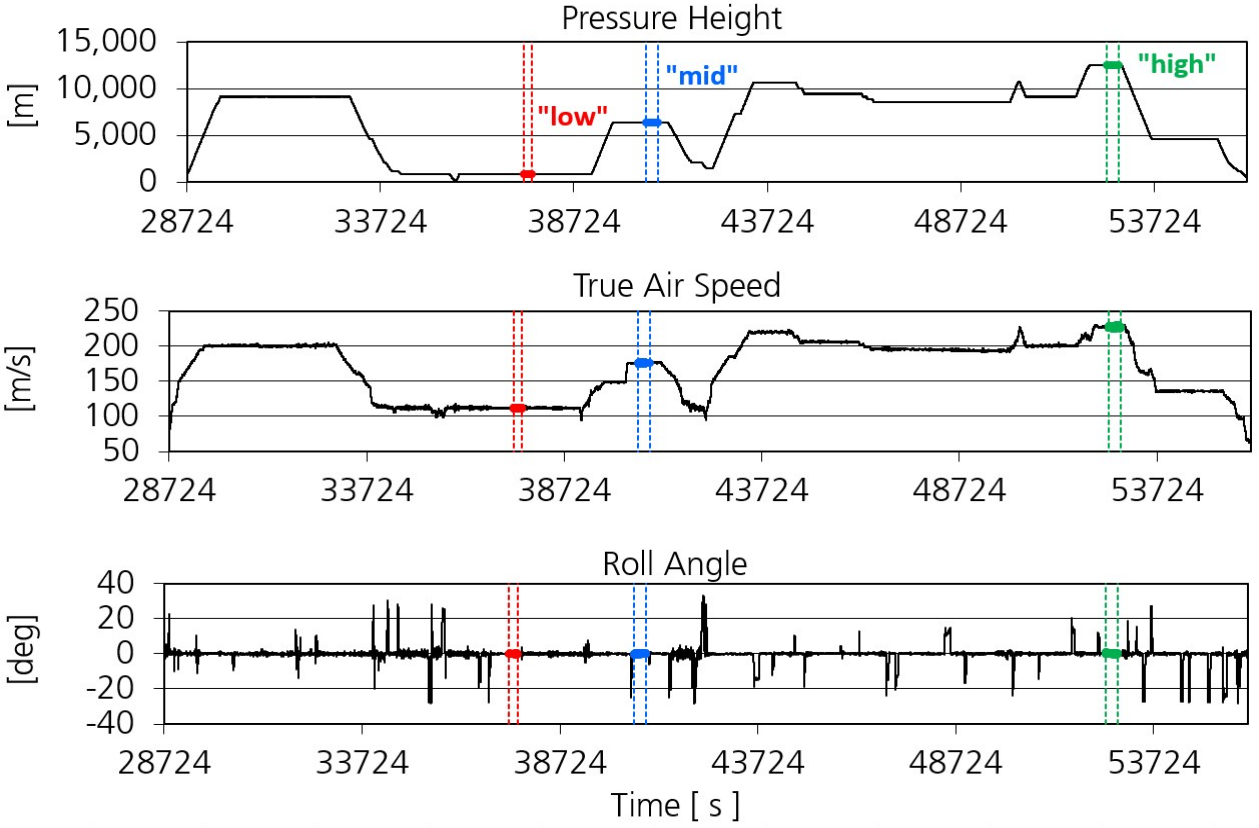

Figure 49: ***Overview on the CAFÉ-EU flight from June 9th 2020 with the selected time intervals ("low", "mid", "high") for the error analysis.***

Low Altitude

"Low Altitude"	Unit	Mean Value	standard error input		"improved temperature"		"bad-heading"	
			Absolute Error	Relative Error [%]	Absolute Error	Change of Absolute Error [%]	Absolute Error	Change of Absolute Error [%]
Static Pressure	hPa	915.27	**0.15**	0.02	0.15	0	0.15	0
Dynamic Pressure	hPa	72.48	**0.16**	0.2	0.16	0	0.16	0
Pressure Altitude	m	849.5	**1.4**	0.2	1.4	0	1.4	0
Machnumber		0.3318	**0.0004**	0.1	0.0004	0	0.0004	0
Calculated True Airspeed	m/s	112.14	**0.13**	0.1	**0.13**	-3	0.14	0
Angle of Attack	deg	3.83	**0.09**	2.3	0.09	0	0.09	0
Angle of Sideslip	deg	0.00	**0.11**	-	0.11	0	0.11	0
Static Air Temperature	°C	10.02	**0.22**	-	**0.14**	-34	0.26	0
Static Air Temperature (#2)	°C	10.02	**0.21**	-	**0.14**	-35	0.25	0
Total Air Temperature	°C	16.26	**0.22**	-	**0.14**	-34	0.26	0
Potential Temperature	°C	17.28	**0.22**	-	**0.15**	-34	0.26	0
Virtual Potential Temperature	°C	18.45	**0.23**	-	**0.16**	-31	0.27	0
Virtual Temperature	°C	11.17	**0.23**	-	**0.16**	-31	0.27	0
Wind Vector East Component	m/s	-1.37	**0.21**	15.1	0.21	0	**0.24**	15
Wind Vector North Component	m/s	-4.21	**0.16**	3.7	0.15	-2	**0.17**	7
Wind Vector Vertical Component	m/s	0.35	**0.17**	-	0.17	0	**0.17**	0
Horizontal Windspeed	m/s	4.44	**0.14**	3.1	0.13	-3	**0.14**	1
Horizontal Wind Direction	deg	17.86	**2.90**	-	2.90	0	**3.39**	17
H2O Mass Mixing Ratio	kg/kg	0.00670	**0.00034**	5.1	0.00034	0	0.00034	0
Rel. Humidity (with resp. to water)	%	79.0	**4.1**	5.2	**4.0**	-2	4.2	0
Absolute Humidity	kg/m^3	0.00747	**0.00038**	5.1	0.00038	0	0.00038	0
Dewpoint Temperature	°C	6.5	**0.7**	-	0.7	0	0.7	0

Table 2: ***Result of HALO error propagation calculation for the "low altitude" flight leg of the CAFÉ-EU flight from June 9th 2020 (10:23:54-10:27:28 UTC). The error analysis also shows the impact of the "improved temperature" and "bad heading" scenarios. The mean aircraft heading during this leg is 205.5°. The presented accuracies represent 1 σ errors.***

Mid Altitude

"Mid Altitude"	Unit	Mean Value	standard error input		"improved temperature"		"bad-heading"	
			Absolute Error	Relative Error [%]	Absolute Error	Change of Absolute Error [%]	Absolute Error	Change of Absolute Error [%]
Static Pressure	hPa	447.65	**0.15**	0.03	0.15	0	0.15	0
Dynamic Pressure	hPa	104.81	**0.15**	0.1	0.15	0	0.15	0
Pressure Altitude	m	6381.5	**2.4**	0.0	2.4	0	2.4	0
Machnumber		0.5565	**0.0004**	0.1	0.0004	0	0.0004	0
Calculated True Airspeed	m/s	176.24	**0.15**	0.1	**0.14**	-9	0.15	0
Angle of Attack	deg	2.19	**0.08**	3.6	0.08	0	0.08	0
Angle of Sideslip	deg	-0.03	**0.11**	-	0.11	0	0.11	0
Static Air Temperature	°C	-23.69	**0.24**	-	**0.15**	-38	0.24	0
Static Air Temperature (#2)	°C	-23.68	**0.24**	-	**0.15**	-39	0.24	0
Total Air Temperature	°C	-8.23	**0.26**	-	**0.16**	-39	0.26	0
Potential Temperature	°C	40.71	**0.30**	-	**0.19**	-38	0.30	0
Virtual Potential Temperature	°C	40.81	**0.30**	-	**0.19**	-38	0.30	0
Virtual Temperature	°C	-23.61	**0.24**	-	**0.15**	-38	0.24	0
Wind Vector East Component	m/s	6.89	**0.34**	4.9	0.34	0	**0.40**	18
Wind Vector North Component	m/s	-11.82	**0.16**	1.4	0.15	-9	**0.16**	2
Wind Vector Vertical Component	m/s	-0.04	**0.24**	-	0.24	0	**0.24**	0
Horizontal Windspeed	m/s	13.70	**0.24**	1.8	0.24	-2	**0.28**	14
Horizontal Wind Direction	deg	329.78	**1.20**	-	1.19	-1	**1.39**	16
H2O Mass Mixing Ratio	kg/kg	0.000529	**0.000027**	5.1	0.000027	0	0.000027	0
Rel. Humidity (with resp. to water)	%	41.8	**2.4**	5.6	**2.2**	-5	2.4	0
Absolute Humidity	kg/m^3	0.000330	**0.000017**	5.1	0.000017	0	0.000017	0
Dewpoint Temperature	°C	-33.1	**0.5**	-	0.5	0	0.5	0

Table 3: ***Result of HALO error propagation calculation for the "mid altitude" flight leg of the CAFÉ-EU flight from June 9th 2020 (11:16:41-11:21:46 UTC). The error analysis also shows the impact of the "improved temperature" and "bad heading" scenarios. The mean aircraft heading during this leg is 187.4°. The presented accuracies represent 1 σ errors.***

High Altitude

"High Altitude"	Unit	Mean Value	standard error input		"improved temperature"		"bad-heading"	
			Absolute Error	Relative Error [%]	Absolute Error	Change of Absolute Error [%]	Absolute Error	Change of Absolute Error [%]
Static Pressure	hPa	178.57	**0.15**	0.1	**0.15**	0	**0.15**	0
Dynamic Pressure	hPa	81.87	**0.15**	0.2	**0.15**	0	**0.15**	0
Pressure Altitude	m	12502.8	**5.3**	0.0	**5.3**	0	**5.3**	0
Machnumber		0.7545	**0.0008**	0.1	**0.0008**	0	**0.0008**	0
Calculated True Airspeed	m/s	227.35	**0.29**	0.1	**0.25**	-8	**0.29**	0
Angle of Attack	deg	2.21	**0.15**	6.8	**0.15**	0	**0.15**	0
Angle of Sideslip	deg	0.10	**0.11**	-	**0.11**	0	**0.11**	0
Static Air Temperature	°C	-47.19	**0.39**	-	**0.22**	-38	**0.39**	0
Static Air Temperature (#2)	°C	-47.41	**0.38**	-	**0.21**	-39	**0.38**	0
Total Air Temperature	°C	-21.47	**0.43**	-	**0.23**	-40	**0.43**	0
Potential Temperature	°C	96.51	**0.63**	-	**0.35**	-40	**0.63**	0
Virtual Potential Temperature	°C	96.51	**0.63**	-	**0.35**	-40	**0.63**	0
Virtual Temperature	°C	-47.19	**0.39**	-	**0.22**	-38	**0.39**	0
Wind Vector East Component	m/s	-7.03	**0.31**	4.3	**0.26**	-7	**0.31**	3
Wind Vector North Component	m/s	8.66	**0.43**	4.9	**0.43**	0	**0.51**	19
Wind Vector Vertical Component	m/s	-0.43	**0.60**	-	**0.60**	0	**0.60**	0
Horizontal Windspeed	m/s	11.17	**0.42**	3.7	**0.41**	0	**0.49**	18
Horizontal Wind Direction	deg	140.98	**1.65**	-	**1.46**	-5	**1.75**	6
H2O Mass Mixing Ratio	kg/kg	3.05E-06	**6.38E-07**	20.9	**6.38E-07**	0	**6.38E-07**	0
Rel. Humidity (with resp. to water)	%	1.00	**0.21**	21.2	**0.21**	0	**0.21**	0
Absolute Humidity	kg/m^3	8.40E-07	**1.76E-07**	20.9	**1.76E-07**	0	**1.76E-07**	0
Dewpoint Temperature	°C	-81.7	**1.4**	-	**1.4**	0	**1.4**	0

Table 4: ***Result of HALO error propagation calculation for the "high altitude" flight leg of the CAFÉ-EU flight from June 9th 2020 (14:35:02-14:40:08 UTC). The error analysis also shows the impact of the "improved temperature" and "bad heading" scenarios. The mean aircraft heading during this leg is 74.3°. The presented accuracies represent 1 σ errors.***

Influence of Heading Relatively to Wind Direction

The determination of the wind vector from aircraft data is described in detail in [7]. It is based on two measurements:

- the motion of the airflow sensor relatively to the earth and
- the motion of the air relatively to the airflow sensor

The overall quality of this measurement depends mostly on the accuracy of the airflow vector data. The reason for this is the high accuracy of the post processed ground speed and attitude data from the experimental IRS (Table 1). This means that the airflow measurement usually limits the accuracy of an airborne wind vector measurement.

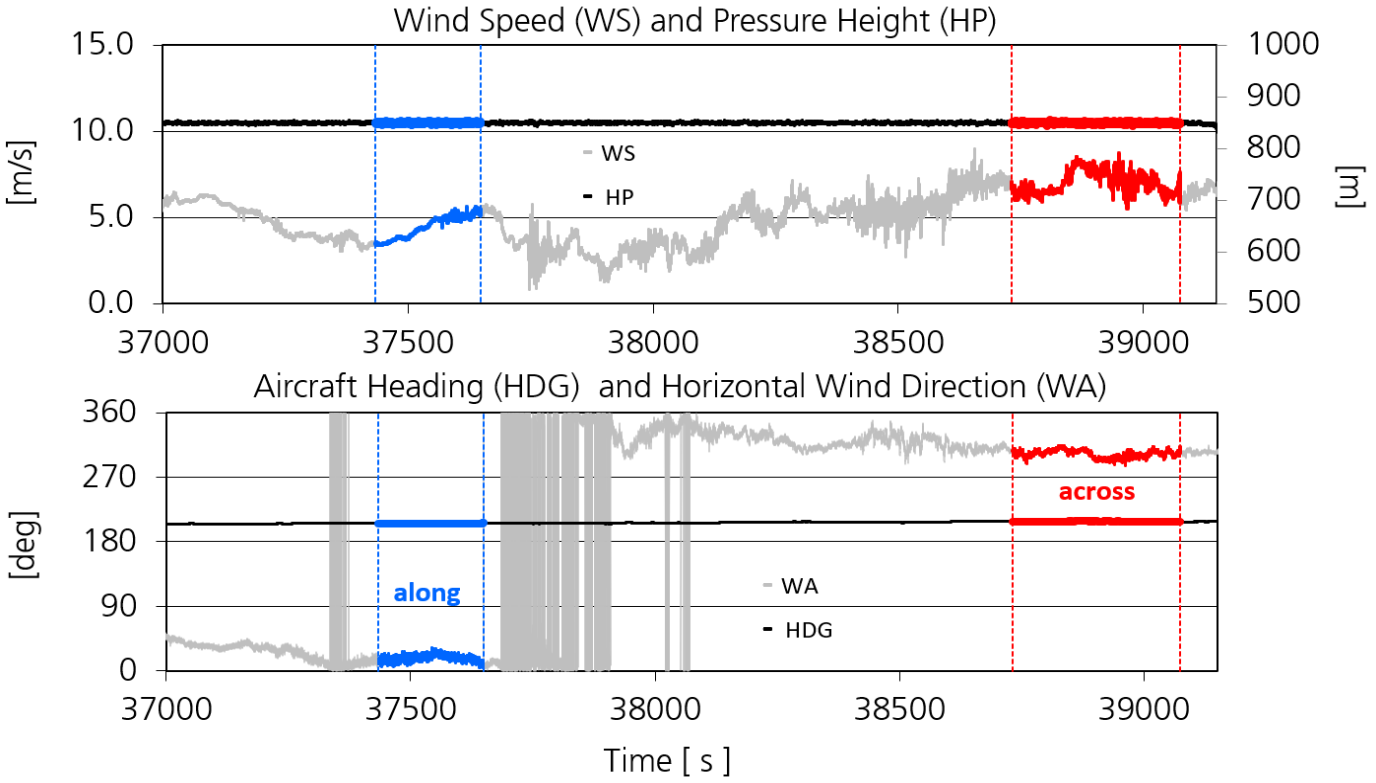

Figure 50: ***Subset of the CAFÉ-EU flight from June 9th 2020 with the selected time intervals which were used for the investigation on the influence of the relative wind direction ("along", "across" the aircraft track) on the accuracy of the wind data. The respective time intervals are 10:23:54-10:27:28 UTC (along) and 10:45:31-10:51:15 UTC (across).***

The wind direction relatively to the aircraft axis has an impact on the accuracy of the wind measurement. This can easily be explained for the horizontal wind component: If the aircraft flies along the wind direction the horizontal wind measurement is almost completely based on the true air speed determination: the difference between TAS and the ground speed is the mean wind and horizontal wind fluctuations can be seen in the dynamic pressure from the airflow sensor which points directly into the flow. For a crosswind scenario the case is different: TAS is more or less constant and the wind can be seen in the drift angle (mean wind) and the angle of sideslip (fluctuations).

Since the accuracy of angles and pressures from the airflow probe cannot be compared directly it is clear that the two scenarios must result in data with different accuracies.

The vertical wind vector is approximately given by $\mathrm{TAS} \cdot \sin(\alpha)$ where α is the angle of attack. This means that the accuracy of the vertical wind speed w is correlated with the accuracy in the determination of TAS.

In order to investigate these effects, we selected 2 time intervals from the same CAFÉ-EU flight as above. The flight data from the two intervals can be seen in Figure 50. Both time intervals are part of the lowermost flight leg in Figure 49 which was flown with constant flight altitude and speed but with different orientations relatively to the wind. The two selected time intervals represent an "along wind" (difference of heading (hdg) and wind speed (ws): hdg-ws=188°) and "cross wind" scenario (hdg-ws=-94°). The "along" wind scenario is identical to the "low" altitude interval which was analyzed in the preceding section of this document.

Table 5 compares the result of the error propagation calculation for the two relative wind orientations. The table also includes the "bad heading" case in order to demonstrate the sensitivity to this angle in the "across" wind scenario.

relative wind direction	Unit	along wind			across wind		
		standard error input		"bad heading"	standard error input		"bad heading"
		Mean Value	Absolute Error	Absolute Error	Mean Value	Absolute Error	Absolute Error
Static Pressure	hPa	915.27	**0.15**	**0.15**	915.28	**0.15**	**0.15**
Dynamic Pressure	hPa	72.48	**0.16**	**0.16**	72.47	**0.23**	**0.23**
Pressure Altitude	m	849.5	**1.4**	**1.4**	849.4	**1.4**	**1.4**
Machnumber		0.3318	**0.0004**	**0.0004**	0.3317	**0.0005**	**0.0005**
Calculated True Airspeed	m/s	112.14	**0.13**	**0.14**	111.80	**0.18**	**0.18**
Angle of Attack	deg	3.83	**0.09**	**0.09**	3.77	**0.11**	**0.11**
Angle of Sideslip	deg	0.00	**0.11**	**0.11**	-0.01	**0.13**	**0.13**
Static Air Temperature	°C	10.02	**0.22**	**0.26**	8.38	**0.22**	**0.22**
Backup of Static Air Temperature	°C	10.02	**0.21**	**0.25**	8.41	**0.23**	**0.23**
Total Air Temperature	°C	16.26	**0.22**	**0.26**	14.57	**0.23**	**0.23**
Potential Temperature	°C	17.28	**0.22**	**0.26**	15.59	**0.23**	**0.23**
Virtual Potential Temperature	°C	18.45	**0.23**	**0.27**	16.73	**0.24**	**0.24**
Virtual Temperature	°C	11.17	**0.23**	**0.27**	9.49	**0.23**	**0.23**
Wind Vector East Component	m/s	-1.37	**0.21**	**0.24**	5.91	**0.23**	**0.26**
Wind Vector North Component	m/s	-4.21	**0.16**	**0.17**	-3.75	**0.20**	**0.21**
Wind Vector Vertical Component	m/s	0.35	**0.17**	**0.17**	0.33	**0.21**	**0.21**
Horizontal Windspeed	m/s	4.44	**0.14**	**0.14**	7.02	**0.25**	**0.28**
Horizontal Wind Direction	deg	17.86	**2.90**	**3.39**	302.47	**1.51**	**1.52**
H2O Mass Mixing Ratio	kg/kg	0.00670	**0.00034**	**0.00034**	0.00654	**0.00033**	**0.00033**
Rel. Humidity (with resp. to water)	%	79.0	**4.1**	**4.2**	86.4	**4.5**	**4.5**
Absolute Humidity	kg/m^3	0.00747	**0.00038**	**0.00038**	0.00734	**0.00037**	**0.00037**
Dewpoint Temperature	°C	6.5	**0.7**	**0.7**	6.2	**0.7**	**0.7**

Table 5: ***Result of HALO error propagation calculation for the different relative wind direction scenarios ("along", "across") with respect to the aircraft axis. The mean aircraft headings during these legs are 205.5° ("along") and 208.2° ("across"). The presented accuracies represent 1 σ errors.***

Discussion

Result of error calculation

The result of the error calculations are displayed in Table 2, Table 3, Table 4 (different altitude/speed scenarios) and Table 5 (influence of wind direction). The analysis includes the impact of an improved temperature measurement and of heading data with a lower accuracy than stated in Table 1.
From the data we draw the following conclusions:

- in general, the errors increase with the flight altitude (speed) of the aircraft. This is a consequence of the error specifications:
    - an absolute error in the pressure measurement leads to an increasing relative error at lower pressures / higher altitudes.
    - For an identical wind vector larger aircraft speeds at higher altitudes (see Figure 49) will result in smaller deviations of the airflow from the main $\overrightarrow{TAS}$ direction. In this case the same absolute error in the flow angle determination will also lead to increasing errors in the wind vector measurement.
- The accuracy of the wind measurement on HALO is mainly limited by the airflow measurement with the 5-hole probe on the nose boom. This is a consequence of the extreme accuracy of the attitude and speed data from the experimental IRS. Any further improvement of wind measurements on this aircraft can only be achieved by more accurate measurements of pressure, true air speed and flow angles.
- The improved accuracy of IRS heading data which uses a GNSS heading reference from a dual antenna system represents an important contribution to the overall data quality especially during long and straight flight legs with only few turns. The error analysis for the CAFÉ-EU flight demonstrates that a heading error in the order of 0.1° will result in an increase of the absolute error for the horizontal wind of up to 20%.

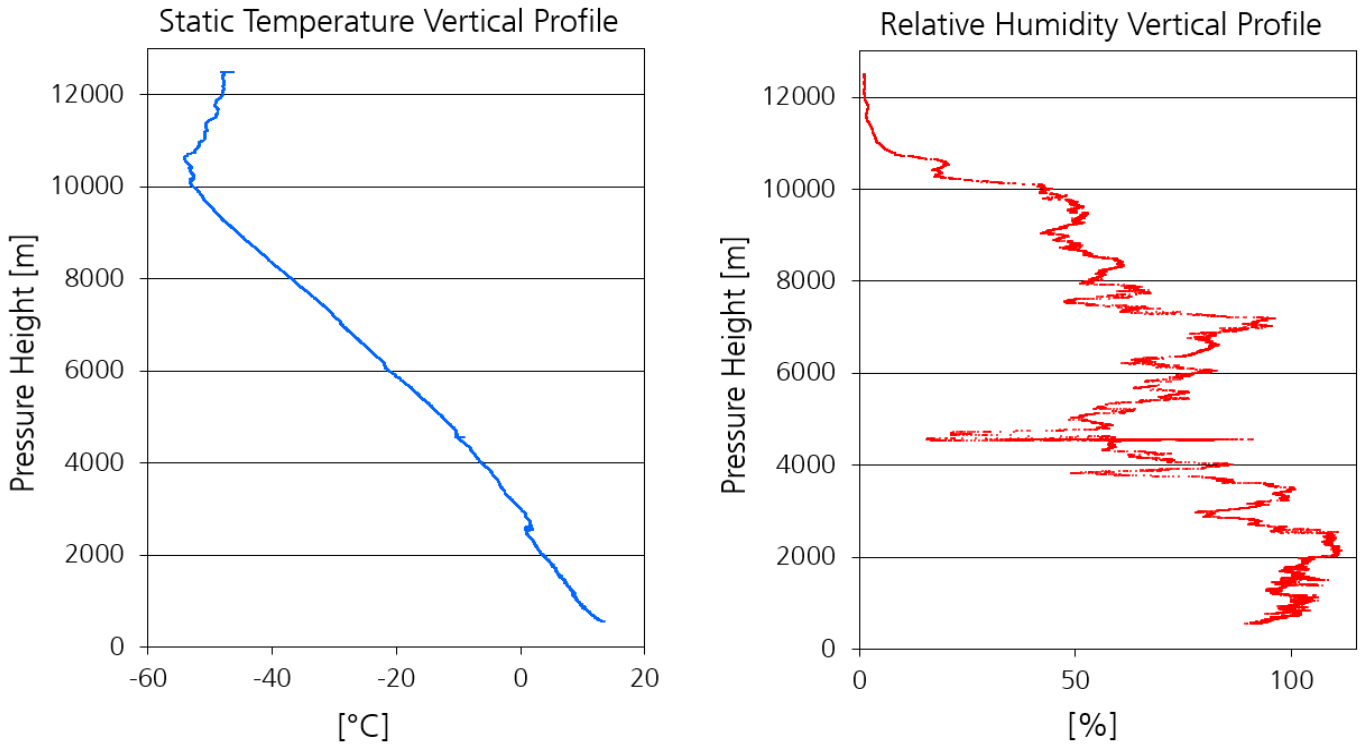

Figure 51: ***Vertical profile of static air temperature and relative humidity from the descent of the CAFÉ-EU flight from June 9th 2020. Both profiles clearly indicate that the highest leg ("high") of this flight with a pressure altitude of 12500m took place inside the stratosphere. Relative humidities above 100% at lower altitudes indicate liquid water or ice crystals which enter the instrument and evaporate.***

- The quality of horizontal wind data on HALO depends on the relative wind direction: measurements along the wind vector are more accurate than cross wind scenarios due to the high accuracy of the TAS measurement.
- Better temperature data leads to an increased accuracy of TAS. Especially for flight legs along the wind direction this automatically results in better wind data. However, the impact of "better temperature data" on relative humidity is below 10%.
- The large humidity error in the highest flight leg of the CAFÉ-EU flight is caused by the fact that this portion of the flight took place in the stratosphere where humidity is extremely low. In this case the 1ppm minimum accuracy of SHARC results in large relative errors. The increase

of static air temperature and the obvious drop of relative humidity at a pressure height of about 10km in Figure 51 clearly indicate the Tropopause at this altitude.

The errors shown in this report can be treated as "typical errors" for the respective height and speed ranges. However, a precise error analysis for a single flight requires an individual investigation due to the possible deviations from the above results caused by different

- flight conditions
- meteorological parameters
- different instrument input errors as determined by the latest calibrations

The presented error propagation and analysis method is available as a module in the RAMSES software and provides an error analysis for any short flight segment (a few minutes length) of a HALO research flight.

The data analysis also proves that the precision of HALO data is very high. The time series of primary and secondary data do not contain significant white noise contributions. This means that the secondary data time series of meteorological units still contain useful information about atmospheric structures with amplitudes below the error limits as determined by the error propagation calculation. As a consequence, a flux measurement using the Eddy Correlation Method will probably work even for small amplitudes and high frequencies. The same assumption is presumably true for studies of the atmospheric structure from almost all meteorological parameters. However, it will always be a challenge to distinguish between real atmospheric data and systematic instrument errors caused by drift effects or artificial data fluctuations from instrument electronics especially when analyzing data over longer time periods.

Possible Improvements

It is an obvious question how the quality of HALO data can be further increased. From the results above we can conclude that respective investigations have to focus on improvements in pressure, flow and temperature measurements. Possible issues concern the instrument itself (choice of sensor and location), the primary sensor calibration in the laboratory, the proper parameterization of sensor properties and the improvement of the required inflight calibration procedures and their evaluation. The preceding HALO reports [6], [7] have already addressed most of these issues and we draw the following conclusions for future improvements:

Pressure

Instrumentation

The HALO pressure measurement instrumentation is very close to an optimum: A nose boom mounted pitot static tube as part of a five-hole probe represents a very powerful sensor configuration. The boom helps to minimize the static source error as well as the static pressure dependency on flow angles. Placing the required pressure sensor right behind the flow angle sensor inside the boom reduces resonance and dampening effect to a minimum.

The accuracy of pressure sensors is critical and their sensitivity to temperature is the biggest challenge. On HALO minor optimizations of this temperature dependency are still possible. Presently, the issue is addressed in a modification of the thermal concept which includes the electronic temperature control and the overall thermal design of the sensor. However, the possible improvement will be smaller than 0.1hPa.

Primary Sensor Calibration

The Ruska 7750i Air Data Test Set still represents one of the best available pressure transfer standards. Therefore, no significant improvement can be achieved by changing this reference instrument.

Parameterizations and inflight calibration

The dominant pressure corrections in the data processing concern the static source error and the pressure dependency on flow angles. The respective flight trials are documented in [6] and [7]. The investigation has shown that the trailing cone itself is an extremely precise reference if one applies the new calibration strategies as described in the reports. Therefore, we presently do not see a better alternative to this reference.

However, improvements of the pressure corrections are possible by regularly repeating the respective calibration procedures. This helps to confirm the existing results and to acquire additional calibration data which will be used to:

- get better statistics (smaller errors) in the available calibration data
- get additional test points in the aircraft flight envelope by choosing other test points
- detect any trends and drifts in the data caused by the sensors or by different aircraft configurations

Therefore, periodic flight trials would help to achieve and maintain best data quality.

Temperature

Instrumentation

For a permanently installed and robust temperature measurement on an aircraft there is presently no alternative to the Rosemount BW102 TAT housings. Wind tunnel data from the manufacturer suggests that the "configuration B" of these housings provide the smallest errors in the data evaluation.

For the sensing elements the case is different. The original open wire PRT sensors (Pt100) are not available anymore and the operators of atmospheric research aircraft worldwide have different strategies how to replace the original instrumentation. DLR uses copies of the original sensor which are built in cooperation with an external partner. Other aircraft operators run alternative sensors like thermistors or miniature PRTs from other manufacturers. In case of

HALO there are plans to redesign the original Rosemount PRT sensor using different materials for the sensor carrier and to achieve smaller tolerances in the production.
The original Rosemount signal conditioning units are excellent. It is recommended to place them in an environment which is not exposed to extreme temperature variations in order to avoid errors from temperature dependency of the analog electronics. However, no significant error reduction (< 0.1K) is expected from these measures.

Primary Sensor Calibration

The error from the calibration of the temperature sensors with the existing calibration bath is mostly limited by the reference thermometer (transfer standard) in the bath. A weak point is the question how often the reference thermometer in the calibration bath should be calibrated by the external laboratory since the benefit from a new calibration is foiled by the danger to damage the sensitive PRT during the transport between the labs. Therefore, the calibration bath will be equipped with a tripel cell in order to get a permanent control about the absolute accuracy of this thermometer.

Parameterizations and inflight calibration

The largest contributions to the temperature measurement error are caused by the recovery and anti-ice corrections which have to be applied during the data evaluation. The respective parameterizations were determined from wind tunnel experiments by the manufacturer. The relatively large errors of these results are caused by the fact that the TAT housings and sensors show manufacturing tolerances which become visible when comparing individual housings with each other. Furthermore, there are also obvious differences between the available sensors for these housings.
Therefore, it is planned to reduce these errors in determining individual recovery and anti-ice corrections for a single housing in order to use it as an inflight reference. However, the determination of such an individual parameterization

requires a large effort. First inflight calibration experiments have shown that it is difficult to achieve the desired accuracy. For this reason, it is an ongoing discussion whether it is possible to determine such individual characterizations by wind tunnel experiments for an individual housing-sensor combination.
The achievable accuracy is estimated to be 50% of the present error bars from the manufacturer which is identical to the "improved temperature" scenario in the error determination above.

Flow

Instrumentation

Similar to the statement for the pressure measurement above we think that a unit of 5-hole probe and pressure sensors mounted on the tip of a nose boom is presently the best possible instrumentation for airflow measurements on an aircraft. The simultaneous measurement of pressure and flow at one single location ahead of the aircraft nose represents the optimum instrument configuration for this kind of measurement. The requirement for a stiff boom and aeroelastic considerations limit the maximum length of the boom which results in a still significant static source error and airflow deflection. However, we have shown in [7] that this problem can be handled with a proper inflight calibration. Therefore, we presently do not see a way to further improve this instrumentation.

There are initiatives to use optical methods for flow measurements [2] which use the Doppler-effect to determine the air speed along the line of sight. This method offers in principle many advantages when compared to the traditional method with an in-situ flow sensor. However, these initiatives still face a lot of problems and have not reached the accuracies and time resolution of a pressure-based airflow sensor yet. Especially at high altitudes it is still a challenge to achieve similar performance parameters. It will be an exciting question whether these sensors will be able to replace the traditional method in the future and which accuracies can be achieved.

Primary Sensor Calibration

Concerning the calibration of the pressure sensors which are required for the 5-hole probe the above statement on the Ruska transfer standard also applies here.

Parameterizations and inflight calibration

The proper parameterization of the necessary correction terms for the airflow measurement requires excessive inflight calibrations. As already mentioned above a periodic repetition of these experiments helps to reduce the statistical errors, to enlarge the range of available test points and to detect possible problems of the instrumentation. In case of HALO a dynamic calibration with pitch and yaw maneuvers is performed during each experiment which plans to evaluate "turbulent wind data" i.e. fast airflow measurements with increased accuracy. The evaluation of turbulence data requires the dynamic correction which is described in [7].

Summary

This report is based on two preceding publications [6], [7]. While the first two publications investigated the accuracy of pressure and flow data from the German research aircraft HALO this report uses the obtained results to determine the total accuracy of HALO data after it was processed with the RAMSES-2 software.
The work presents an innovative and complete error propagation method for aircraft data from the basic data system BAHAMAS. This method uses white noise contributions to the data time series in order to propagate the associated amplitudes through the complete processing into the final result where they can be detected and quantified by means of an the autocovariance function (ACV). The procedure can treat error contributions in the primary data as well as all other error sources along the complete data processing path. It can handle different error parameterizations like absolute errors, relative errors or errors which depend on other parameters. The method allows for error propagation investigations in very complex data evaluation schemes as long as they do not contain any kind of data averaging which would prevent the necessary ACV analysis in the result. The error determination can be performed for relatively short time intervals (<1 min) throughout a complete research flight on HALO.

The presented error propagation method offers many interesting features:

- It is possible to selectively activate single error sources in order to quantify the impact of a certain parameter on the total error.
- The method allows for the implementation of correlated errors like the static source error which applies with the same amplitude but different signs to the static and the dynamic pressures.
- The solution can handle a wide variety of error definitions like constant errors, relative errors or errors which depend on other units. However, the result always includes existing white noise in the data. In case of HALO this contribution is mostly negligible.

- The presented error propagation works even for very complex and highly non-linear processing schemes
- It does not contain any kind of simplification like the linearization of processing steps as known from the traditional error propagation calculation. Therefore, the method represents a true error propagation.
- Today, the error propagation method is established as a module in the RAMSES-2 data evaluation software. It allows to systematically analyze and provide error bars for BAHAMAS data from all future flights on HALO.

Based on this error evaluation scheme the report presents the accuracy of BAHAMAS data for some selected HALO flight scenarios. It also investigates the impact of measurement scenarios where the input errors for aircraft heading and for the temperature sensor corrections differ from the assumed standard values.

The data analysis proves that the measurement of meteorological parameters becomes more challenging with increasing aircraft altitude and speed. The investigation also showed that the quality of final data can be influenced by a proper measurement strategy. One example is the alignment of aircraft heading with the wind direction for a more accurate wind measurement.
The limiting systematic errors for basic meteorological units usually originate from the parameterization of aerodynamic corrections for primary air data. Therefore, any improvement of the data quality (accuracy) mainly depends on advancements in inflight calibration techniques and wind tunnel testing of the respective instrumentation.
However, the data analysis also indicates that there is presently only limited potential for further improvements on the accuracy of meteorological data from BAHAMAS. The report recommends three main measures:

1. Periodic repetitions of inflight calibrations in order to achieve better statistics for the parameterizations which are used by RAMSES-2 in the data processing

2. Determination of an individual anti ice and recovery correction for a single TAT + sensor combination which can then be used as a reference sensor in flight.
3. Permanent monitoring for alternative instrumentation and measurement principles with better accuracies and the potential to replace the traditional methods.

Acknowledgement

We thank the scientific community which always pushed hard for a report like that! Everybody working with experimental data needs a proper error specification but the complexity of aircraft data processing always made it difficult to provide appropriate results. Today we are happy to have this feature as a standard module in the RAMSES-2 data processing.
We thank Ulrich Schumann for his accurate and steady analysis of BAHAMAS data and all the energy he put into issues like the dual antenna option for the IGI system.
We thank the DLR-FX management which allowed us to use the little niches and free spaces in our daily work for the completion of this report. It was not easy at all to find a compromise between campaigns, the necessary "homework" and our daily tasks.
A special thank you goes to my wife Christiane who had to suffer from the stress associated with these parallel activities and my inability to sometimes ignore this work during a weekend.

.

References

[1] W.Bögel and R.Baumann, *Test and Calibration of the DLR Falcon Wind Measuring System by Maneuvers*, J. Atmos. Ocean Tech. 8, 5-18, 1991

[2] W.A. Cooper, S.M. Spuler, M. Spowart, D.H. Lenschow, and R.B. Friesen, *Calibrating airborne measurements of airspeed, pressure and temperature using a Doppler laser air-motion sensor,* Atmos. Meas. Tech., 7, 3215–3231, 2014

[3] Cramer, M., *Performance of IGI AEROcontrol-IId GPS/inertial system.* Final report, Available from: University of Stuttgart, Institute for Photogrammetry, 2001, D-70174 Stuttgart, Geschwister-Scholl-Str. 24 D, (https://www.ifp.uni-stuttgart.de/en/publications/annual_publications/)

[4] Giez, A., Zoeger, M., and Dreiling, V.: *Processed time sequence measurement data systematic error detection procedure for meteorological or other data uses autocovariance processing of additive white noise*, DE 103 40 793 B4, 2005.

[5] Andreas Giez, Christian Mallaun, Martin Zöger, Andreas Dörnbrack, and Ulrich Schumann, *Static Pressure from Aircraft Trailing-Cone Measurements and Numerical Weather-Prediction Analysis*, Journal of Aircraft Vol. 54, No. 5, 2017

[6] Andreas Giez, Martin Zöger, Volker Dreiling, Christian Mallaun, *Static Source Error Calibration of Nose Boom Mounted Air Data System on an Atmospheric Research Aircraft Using the Trailing Cone Method.* DLR-Forschungsbericht 2019-7, 2020, ISRN DLR-FB—2019-07 https://elib.dlr.de/ 145770/

[7] Andreas Giez, Christian Mallaun, Vladyslav Nenakhov, Martin Zöger, Calibration of a Nose Boom Mounted Airflow Sensor on an Atmospheric Research Aircraft by Inflight Maneuvers. DLR-Forschungsbericht 2021-17, 2021, ISRN DLR-FB—2021-17 https://elib.dlr.de/145969/

[8] Goodrich. (1975). *Total Temperature Sensors.* Technical Report 5755, Revision C, 1994, Goodrich Sensor Systems, Goodrich Cooperation, Burnsville, MN, 1976

[9] re3data.org: HALO database; editing status 2021-11-17; re3data.org - Registry of Research Data Repositories. http://doi.org/10.17616/R39Q0T last accessed: 2022-05-03bbb (check for HALO-(AC)3 Campaign)

[10] Kaufmann, Stefan und Voigt, Christiane und Heller, Romy und Jurkat-Witschas, Tina und Krämer, Martina und Rolf, Christian und Zöger, Martin und Giez, Andreas und Buchholz, Bernhard und Ebert, Volker und Thornberry, Troy und Schumann, Ulrich *Intercomparison of midlatitude tropospheric and lower-stratospheric water vapor measurements and comparison to ECMWF humidity data.* Atmospheric Chemistry and Physics (ACP), 18, Seiten 16729-16745. Copernicus Publications., 2018

[11] Krautstrunk, M. and Giez, A., *The Transition from FALCON to HALO Era Airborne Atmospheric Research*, in Atmospheric Physics - Background - Methods - Trends, U. Schumann, Editor, Springer-Verlag Berlin Heidelberg, 2012, p. 609-624, doi: 10.1007/978-3-642-30183-4_37.

[12] *RUSKA 7750i Air Data Test Set, User's Manual*, Fluke Cooperation, November 2010, Fluke Corporation, P.O. Box 9090, Everett, WA 98206-9090, U.S.A (https://eu.flukecal.com/de/literature/product-manuals/ruska-7750i-air-data-test-set-users-manual)

[13] Schumann, U., 2020 (Editor): *Measurement and model data comparisons for the HALO-FAAM formation flight during EMeRGe on 17 July 2017. DLR Forschungsbericht*, DLR-FB-2020-48, 188 pp, ISRN DLR-FB—2019-07 (2020), doi.:10.5281/zenodo.4427965 (https://zenodo.org/record/4427965)

1434-8454

ISRN DLR-FB—2022-27